Field-Effect Transistors Based on Mobile and Covalently Bound Ionophores and Photoimmobilization of Biomolecules on Polyurethane Membrane Surfaces

---

Dissertation submitted to the
Faculty of Science of the University of Neuchâtel
to obtain the degree of Doctor of Science

by

Patrick Reichmuth
Dipl. Natw. ETH Zurich

Institute of Microtechnology
University of Neuchâtel
Rue Jaquet-Droz 1
CH-2000 Neuchâtel
Switzerland

2001

"I seem to have been only like a small boy playing on the sea-shore, diverting myself in now and then finding a smoother pebble or a prettier shell than the ordinary, whilst the great ocean of truth lay all undiscovered before me."

Sir Isaac Newton (1642 - 1727)

This doctoral dissertation was carried out at the Institute of Microtechnology (IMT) at the University of Neuchâtel (Prof. de Rooij) in collaboration with the Laboratory of Organic Chemistry (Prof. E. Pretsch) of the Swiss Federal Institute of Technology in Zurich (ETHZ). The first part of this PhD thesis was performed at the ETHZ from March 1998 to August 2000 and the second part at the IMT in Neuchâtel from September 2000 to July 2001.

IMPRIMATUR POUR LA THESE

Field-Effect-Transistors Based on Mobile and Covalently Bound Ionophores and Photoimmobilization of Biomolecules on Polyurethane Membrane Surfaces

de M. Patrick Reichmuth

UNIVERSITE DE NEUCHATEL

FACULTE DES SCIENCES

La Faculté des sciences de l'Université de Neuchâtel sur le rapport des membres du jury,

Mme M. Koudelka-Hep,
MM. N. de Rooij (directeur de thèse), W. Morf,
E. Pretsch (ETH Zurich) et H. Sigrist (CSEM)

autorise l'impression de la présente thèse.

Neuchâtel, le 16 juillet 2001

Le doyen:

J.-P. Derendinger

Contents

1 Summary

The subject of the research described in the first part of this thesis is the development of a chemical sensor for ions (Chapters 3 - 5). The study was carried out at the Laboratory of Organic Chemistry of the Swiss Federal Institute of Technology in Zurich (ETHZ) in collaboration with the Sensors, Actuators, and Microsystems Laboratory of the Institute of Microtechnology (IMT) at the University of Neuchâtel. This underlies the multidisciplinary character of this research.

Ionophore-based ion-selective field-effect transistors are called CHEMFETs. These devices usually suffer from an unstable response signal. This restriction is mainly attributed to the lack of a thermodynamically well defined interfacial potential between the sensing membrane and the solid-contact. This interface includes a thin aqueous film, which must be regarded as an additional phase sensitive to sample changes. Compounds such as carbon dioxide that are able to diffuse through the membrane can cause a potential drift by altering the pH of the thin water layer and therefore interfere with the measurement of the analyte ions. In this dissertation, a novel concept using a double membrane is presented to improve the signal stability of CHEMFETs. The outer membrane in contact with the sample solution contains a mobile ammonium-selective ionophore, whereas the inner membrane incorporates the same carrier and, in addition, a covalently bound H^+-selective ionophore. The phase boundary potential between the double membrane and the water film is determined by the pH of the thin aqueous layer and counterbalances the response of the gate oxide of the field-effect transistor. Therefore, CHEMFETs of this type compensate pH changes in the inner aqueous layer.

The response mechanism of the novel double membrane was first verified by experiments performed on liquid-contacted ion-selective macroelectrodes (ISEs) and then tested with CHEMFETs. The CHEMFETs, which were covered with the double membrane, showed a Nernstian response to the activity of the analyte ion (NH_4^+) in the sample solution. Furthermore, the propagated double membrane improved the stability of CHEMFETs against interference by CO_2 and organic acids. The stabilizing effect of the double membrane on the response signal of CHEMFETs was partially limited by the pH measuring range of the inner membrane, which contained two ionophores, and by an additional potential contribution arising at the interface

between the outer and the inner membrane. Plasticized PVC membranes showed a better adhesion to the gate oxide and the encapsulation material of field-effect transistors in comparison with different polyurethane membranes.

Comprehensive studies were carried out with ISEs based on covalently bound H^+-selective ionophores and novel polyurethane membranes with "self-plasticizing" properties. The selectivities of these electrodes were comparable to the ones obtained from ISEs based on plasticized PVC matrices. However, polyurethane membranes generally exhibited a poorer selectivity with respect to hydrogen ions. Polyurethane-based sensors with covalently bound H^+-selective ionophores showed sub-Nernstian slopes caused by high membrane resistance. The addition of a plasticizer or a lipophilic salt into the membrane resulted in greatly improved slopes, as in the case of conventional PVC/DOS electrodes. The durable immobilization of the ionophores by covalent binding to the polyurethane matrix was confirmed by long-term diffusion experiments.

Chapter 6 describes the second research subject, in which biomolecules were immobilized on the surface of soft polyurethane membranes. The morphology of the polyurethane membranes was very smooth with a root-mean-square (r.m.s) roughness of about 0.7 nm. This featureless membrane surface is well suited for the covalent binding of selective recognition elements. As a prototype, a novel photoactivatable cross-linker was synthesized and covalently bound to the surface of soft polyurethane membranes. This cross-linker bears a biotin moiety, which can specifically complex a protein called streptavidin.

The surface coverage of the immobilized biomolecules was analyzed by X-ray photoelectron spectroscopy (XPS) and autoradiography using [^{35}S]-streptavidin. In general, the immobilized biomolecule layer turned out to be non-uniform. Furthermore, the immobilized biomolecules neither had an influence on the response behavior of ISEs with a Nernstian slope down to the nanomolar concentration range nor influenced the response of ISEs with a super-Nernstian behavior.

2 Introduction

Generally spoken, a chemical sensor is as a device that responds to a chemical stimulus and transmits a resulting signal. The ideal chemical sensor can be regarded as a technical analogue to the human or animal sensory system. It responds continuously to the increasing and decreasing concentration of a chemical compound, thus allowing real-time monitoring. The term "selectivity" describes quantitatively the capability to prefer target analytes and to discriminate specific background species. Ion-selective sensors based on liquid membranes are available for the analysis of the most abundant alkaline and alkaline earth metal ions as well as some heavy metal ions. These ion-selective sensors contain receptor molecules (ionophores) in their polymeric membrane, which can selectively bind guest species from the sample solution,[1] as described in Chapter 3. The most important application of these sensors is the clinical assay of K^+ and Na^+ in blood samples. Yearly well over a billion measurements with ionophore-based ion-selective electrodes (ISEs) are performed worldwide in clinical laboratories alone.[2] ISEs are also utilized in many other fields, including physiology, biology, process control, and environmental analysis.[3, 4] They thus form one of the most important groups of chemical sensors.

In contrast to ISEs, there are only a few practical applications for ionophore-based field-effect transistors (CHEMFETs). The facile miniaturization of these semiconductor devices is an advantage. The size of a tip of a classical ISE is about 10 mm, whereas the size of a CHEMFET is about 1 mm. CHEMFETs usually suffer from an unstable response signal caused by acids and bases in the sample solution, like for example carbon dioxide. In order to improve this potential instability of CHEMFETs, a novel method is propagated in this doctoral dissertation. The suitability of soft polyurethanes with "self-plasticizing" properties for sensors with a covalently bound H^+-selective ionophore[5, 6] was tested in Chapter 4 using ISEs. The modified membranes with the attached carriers were applied on CHEMFETs in order to improve the potential stability against interferents like carbon dioxide, as shown in Chapter 5. The experiments with CHEMFETs were performed at the Sensors, Actuators, and Microsystem Laboratory of the IMT in Neuchâtel. All other experiments of this thesis were carried out at the Laboratory of Organic Chemistry of the ETHZ.

Chapter 6 describes the second research subject, in which the immobilization of biomolecules on the surface of polyurethane membranes was studied. Although a great number of techniques is available to covalently bind organic compounds to various substrates in order to create selective reaction layers,[7, 8] there are comparatively few contributions in which the surface of soft polymers is modified. The present work describes initial studies of modification of polyurethane membranes by covalently attaching binding sites to their surface. A novel biotin derivative was used as a heterobifunctional cross-linker. This was photoimmobilized on a polyurethane surface. The long term aim of this study is to monitor guest molecules present in the sample solution. The guest molecules are selectively complexed by host molecules immobilized on the membrane surface. A complexation of a sample analyte with these binding sites may modulate the interfacial fluxes of specific marker ions and therefore influence the potentiometric response of ISEs. Further promising applications of selective surface modifications of polymeric membranes include the preparation of biointerfaces and bioelectronic elements.[9] Finally, Chapter 7 includes the experimental part of the whole dissertation.

References

(1) Morf, W. E. The Principles of Ion-Selective Electrodes and of Membrane Transport; Elsevier Science: New York, 1981.

(2) Bakker, E.; Bühlmann, P.; Pretsch, E. Carrier-Based Ion-Selective Electrodes and Bulk Optodes. 1. General Characteristics. Chem. Rev. **1997,** 97, 3083-3132.

(3) Cammann, K.; Galster, H. Das Arbeiten mit ionenselektiven Elektroden: eine Einfuehrung fuer Praktiker, 3rd ed.; Springer: Berlin, 1996.

(4) Spichiger-Keller, U. E. Chemical Sensors and Biosensors for Medical and Biological Applications; Wiley-VCH: Weinheim, 1998.

(5) Püntener, M., Doctoral Dissertation in Preparation, ETH, Zurich.

(6) Schöning-Hammer, A., Personal Communication, Zurich, 1998.

(7) Hermanson, G. T. Bioconjugate Techniques; Academic Press: San Diego, 1995.

(8) Cunningham, A. J. Introduction to Bioanalytical Sensors; Wiley-Interscience, 1998.

(9) Sigrist, H.; Collioud, A.; Clémence, J. F.; Gao, H.; Luginbühl, R.; Sänger, M.; Sundarababu, G. Surface Immobilization of Biomolecules by Light. Opt. Eng. **1995,** 34, 2339-2348.

3 Characteristics of Carrier-Based Ion-Selective Electrodes

3.1 Response Mechanism

The centerpiece of a carrier-based ion-selective electrode (ISE) is usually a polymeric membrane. Adding lipophilic anionic sites prevents anions from penetrating into the membrane and results in a cation-exchanger membrane. This cation permselectivity is called Donnan exclusion.[1, 2] Adding additionally an ionophore into the membrane enhances the selectivity of the sensor for a target cation.[3] The ionophore can form a reversible complex with the analyte ion in the phase boundary between membrane and solution. This selective extraction of target ions into the membrane represents the heart of the response mechanism of ISEs.[4] Herein, we focus on ISEs that contain an electrically neutral ionophore, as depicted in Figure 3.1.

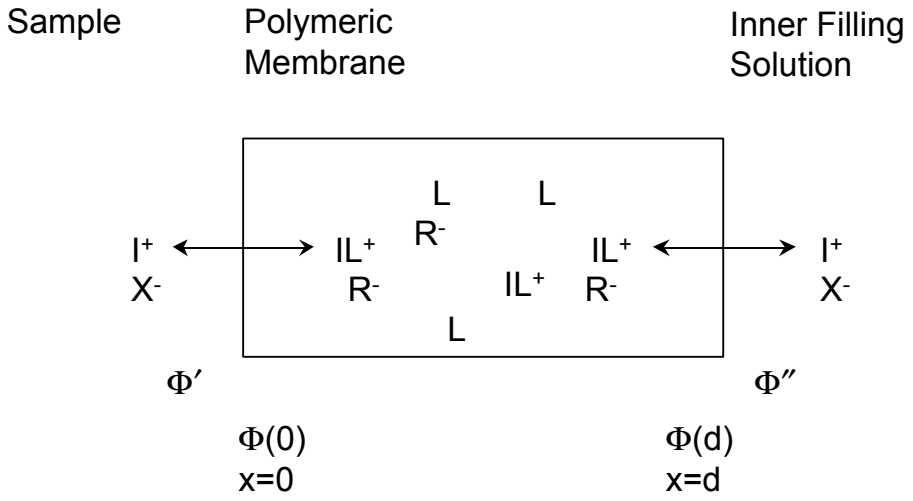

Figure 3.1 Schematic view of the equilibria between sample, ion-selective membrane, and inner filling solution for the special case of equal sample and inner electrolytes: primary ion (I^+), counterion (X^-), carrier (L), and anionic site (R^-).

We can mathematically describe the response mechanism of ISEs with the help of the following equations.[5, 6] The membrane/sample phase (′) boundary is located at x = 0, whereas the membrane/inner solution (″) interface is defined as $x = d$, as shown in Figure 3.1. We assume ion partition equlibria at the two membrane boundary surfaces initially. The total concentration $c_{i,T}$ of the free ion I^{zi} and of all its positively charged complexes at the membrane boundaries can be described as follows:

$$c_{i,T}(x=0) = K_i a_i'(aq)\Psi'^{-Z_i} \tag{3.1}$$

$$c_{i,T}(x=d) = K_i a_i''(aq)\Psi''^{-Z_i} \tag{3.2}$$

where

$$K_i = \frac{k_i}{\gamma_i(x)}\left(1 + \sum_n \beta_{iL,n} c_L^n\right) \tag{3.3}$$

$$\Psi' = e^{F(\phi(0)-\phi')/RT} \tag{3.4}$$

$$\Psi'' = e^{F(\phi(d)-\phi'')/RT} \tag{3.5}$$

Here, a'_i is the ion activity in the sample solution and a''_i is the ion activity in the inner solution. The overall partition coefficient of the indicated ion I^{zi} is K_i, which includes all effects of ion-ionophore complexation in the membrane, $\beta_{iL,n}$ is the stability constant of a given 1:n complex IL_n^{zi}, c_L is the concentration of the free ionophore L in the membrane, which is assumed to be constant, k_i is the partition coefficient of the uncomplexed ion I^{zi}, and $\gamma_{i(x)}$ is the activity coefficient of this species in the membrane. Moreover is Ψ a function of the boundary electric potentials ϕ and R,T, and F have their usual meaning. If the total concentration of anionic sites R_T is constant, the electroneutrality condition requires that:

$$\sum_i z_i c_{i,T}(x=0) = \sum_i z_i c_{i,T}(x=d) = R_T \tag{3.6}$$

Insertion of equation (3.6) into (3.1) and (3.2) leads to an implicit solution for the boundary potential function Ψ:

$$\sum_{i} z_i K_i a_i'(aq)\Psi'^{-Z_i} = \sum_{i} z_i K_i a_i'(aq)\Psi''^{-Z_i} = R_T \qquad (3.7)$$

For the sake of simplicity, interfering anions X^{Z_x} are neglected in the following treatment. The considerations are restricted to exchangeable cations of the same charge number $z_m = z$. Therefore, one obtains explicit solutions for equation (3.7):

$$\Psi'^{z} = \frac{z}{R_T}\sum_{m} K_m a_m' \qquad (3.8)$$

$$\Psi''^{z} = \frac{z}{R_T}\sum_{m} K_m a_m'' \qquad (3.9)$$

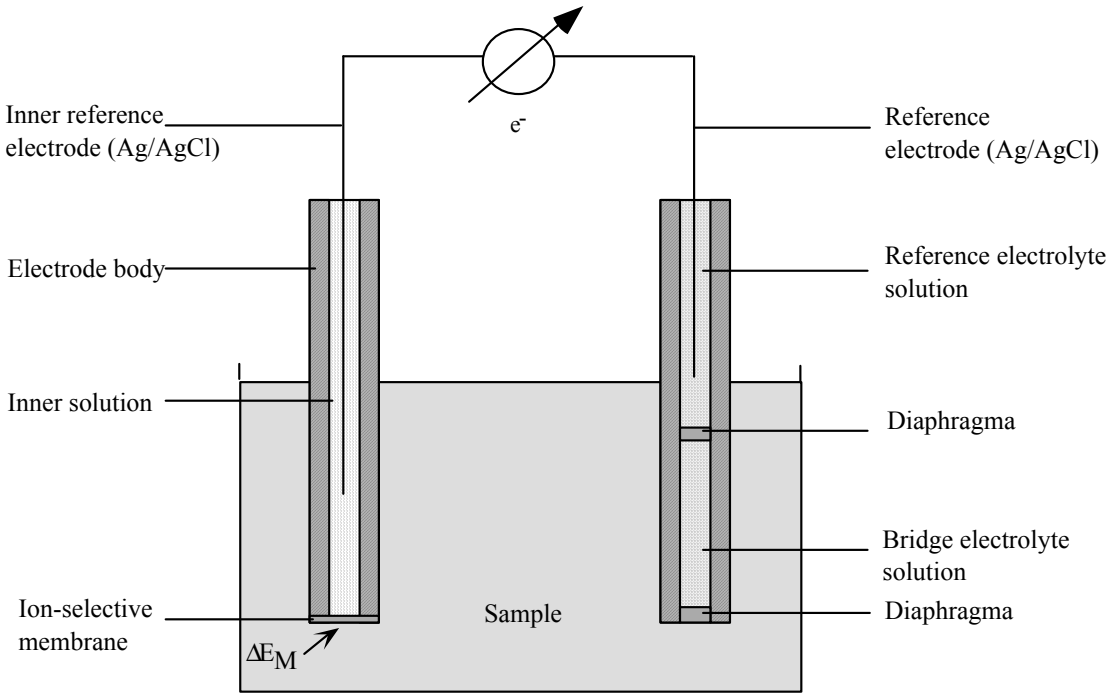

Figure 3.2 Schematic diagram of a membrane electrode measuring circuit and cell assembly.

The electromotoric force E across an ISE cell (see Figure 3.2) is the sum of all individual potential contributions:

$$E = E^0 + E_M = E^0 + \frac{RT}{F}\ln\Psi' - \frac{RT}{F}\ln\Psi'' \tag{3.10}$$

where E^0 is a reference potential summarizing all potential contributions in addition to the membrane potential E_M. The membrane-internal diffusion potential is negligible in most cases of practical relevance.[7] Hence, we assume in equation (3.10) that the membrane-internal diffusion potential is equal to zero.[8] The basic assumptions are that the mobility of all exchangeable species in the membrane can be characterized by the same diffusion coefficient, and that all sites R^- are uniformly distributed within the membrane. Thus, the response function is given by:

$$E = E^0 + \frac{RT}{zF}\ln\sum_m K_m a'_m - \frac{RT}{zF}\ln\sum_m K_m a''_m \tag{3.11}$$

Assuming that the potential at the membrane/inner filling solution interface is independent of the sample, the emf response of ISEs to different cations is described by the Nicolskii-Eisenman equation, which is the usual approximation for practical purposes:

$$E = E_{\mathrm{i}}^0 + \frac{RT}{z_{\mathrm{i}}F}\ln\left[a_{\mathrm{i}}(aq) + \sum_{\mathrm{j}} K_{\mathrm{ij}}^{\mathrm{pot}} a_{\mathrm{j}}(aq)^{z_{\mathrm{i}}/z_{\mathrm{j}}}\right] \tag{3.12}$$

where the subscripts i and j denote the primary ion I^{zi} and the interfering ion J^{zj}, a_{i}(aq) and a_{j}(aq) are the sample activities of these ions. E_{i}^0 is the standard reference potential of the electrode cell for the primary ion, and $K_{\mathrm{ij}}^{\mathrm{pot}}$ is the (Nicolskii) selectivity coefficient for the interfering ion relative to the primary ion, being defined as follows:

$$K_{ij}^{pot} = \frac{K_j}{K_i} \tag{3.13}$$

3.2 Selectivity

An ISE should measure a target ion as selectively as possible and, therefore, highly selective ISEs are characterized by values $K_{ij}^{pot} << 1$.[9] Although the Nicolskii-Eisenman equation has commonly been used for a few decades, it has a severe drawback. The equation is incorrect when two ions of different charges contribute to the emf. Sophisticated mathematical formulations of selectivities for ions with different charges were presented by Morf[6] and by Nägele.[10]

Several techniques for the determination of selectivity coefficients are known. In this work, the separate solution method (SSM) and the fixed interference method (FIM) are used. The SSM is the most popular method to determine selectivity coefficients. Both the calibration curve for the primary ion and that for an interfering ion are assumed to approximate Nernstian response. Extrapolating the potential for the primary ion (E_i) and for the interfering ion (E_j) to an activity of 1 mol L^{-1} leads to the respective standard potentials (E_i^0 and E_j^0) which are used in the following expression:

$$\log K_{ij}^{pot} = \frac{z_i F\left(E_j^0 - E_i^0\right)}{2.303RT} \tag{3.14}$$

In practice, however, many electrodes do not show a Nernstian response to the interfering ion. There are two reasons for this frequent bias.[11] First, continuous leaching of the primary ion from the electrode into to the sample solution intrudes the calibration measurement of the interfering ion. Second, the conditioning time has to be long enough to reach a steady state. ISEs are usually conditioned with a high concentration of primary ions, which can cause a non-Nernstian response to the interfering ions if the interfacial layer of the membrane contacting the sample is not fully equilibrated with the discriminated ions. Conditioning for a short time in the interfering ion solution before the respective calibration measurement is made to improve the slope of the electrode response. However, the most promising alternative

to eliminate this problem is given by the method of unbiased selectivity coefficients.[12] In this procedure, the electrodes are initially conditioned in a solution of highly discriminated ions. The most discriminated ion is measured first, and the most preferred ion at the end of the procedure. Consequently, the phase boundary layer is always conditioned with the actual measuring ion, thus resulting in Nernstian slopes and unbiased selectivity coefficients.

In the FIM, measuring a calibration curve in pure solutions of the primary ion is the first step.[11] The second primary ion calibration is done in the presence of a constant interfering ion background a_j *(BG)*. The linear response curve of the electrode as a function of the logarithm of the primary ion activity is extrapolated until, at the lower detection limit a_i *(DL)*, it intersects with the observed potential for the background alone. The Nicolskii coefficient is calculated from these two extrapolated linear segments of the calibration curve as follows:[13]

$$\log K_{ij}^{pot} = \log\left(\frac{a_i(DL)}{a_j(BG)^{z_i/z_j}}\right) \tag{3.15}$$

Taking only the ranges of the calibration curve with a Nernstian slope prevents biases from leaching primary ions. Furthermore, it is crucial that the detection limit is determined by the added interfering ion alone. This assumption has to be scrutinized by subsequent dilution of the sample with water, whereupon a Nernstian response should be observable.[11, 14]

If the electrode does not exhibit distinct ranges of Nernstian response, neither with the SSM nor with the FIM, it is better to report the full calibration curve to characterize the selectivity of the ISE.

3.3 Detection Limit

Besides the selectivity, the detection limit is one of the most important characteristics of an ISE. The upper and lower detection limits are defined by the respective inter-sections of the extrapolated linear parts of the calibration curves, as shown in Figure 3.3.[15] Recently, this definition was extended for electrodes that exhibit a super-Nernstian response.[16]

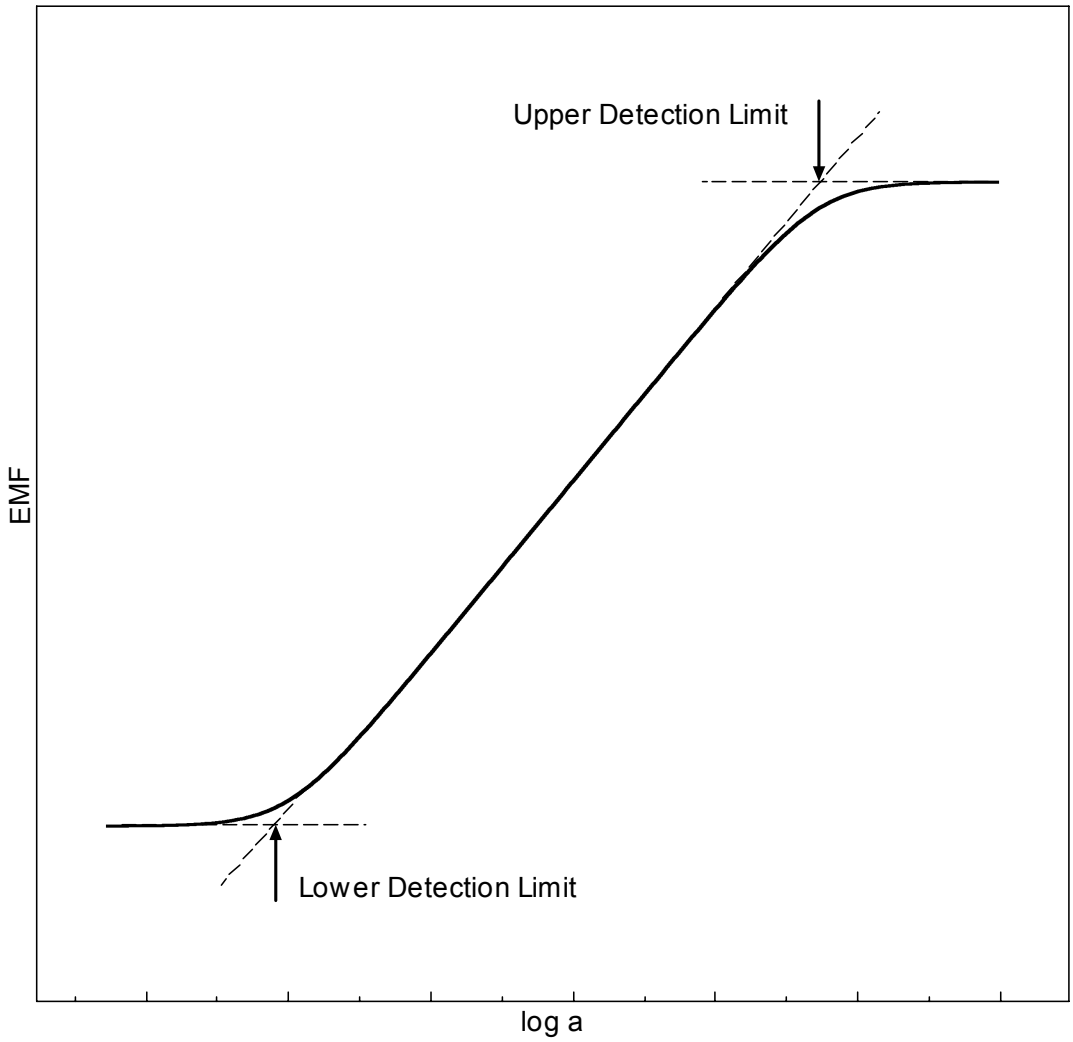

Figure 3.3 Definition of the upper and the lower detection limit of an ISE according to the IUPAC recommendations.[15]

The upper detection limit of cation-selective electrodes is caused by the interference of sample anions. When the salt concentration in the sample solution increases, interfering anions X^- enter into the membrane according to the following coextraction mechanism:

$$I^{z+}(\text{aq}) + zX^{-}(\text{aq}) + n\text{L}(\text{org}) \Leftrightarrow \text{IL}_n^{z+}(\text{org}) + zX^{-}(\text{org})$$

where *n* is a stoichiometric factor. The increased uptake of anions in the membrane causes a loss of cation permselectivity (failure of Donnan exclusion).

The reasons for the lower detection limit are either interference by competing sample cations or perturbation of the interfacial sample region by the membrane. The latter is often caused by leaching of primary ions from the membrane into the sample solution. This constant release of primary ions results in a higher effective ion activity near the membrane/sample interface, as compared with the nominal activity in the bulk sample solution.[17] Additionally, the plasticizer and the polymer matrix of the electrode membrane may also influence the lower detection limit.[18] Recently, the theoretical ultimate lower detection limit of ISEs was estimated to be 10^{-13} mol $L^{-1}$for monovalent ions, and 10^{-20} mol L^{-1} for divalent ions.[19]

3.4 Polyurethane as Polymer Matrix

ISEs often contain poly (vinyl chloride) (PVC) as polymer membrane matrix with an added plasticizer to achieve excellent selectivities and detection limits. However, the use of plasticized PVC membranes bears some problems, which are mainly caused by the outflowing plasticizer.[20] Firstly, a significant loss of plasticizer leads to a short lifetime of the sensors. Secondly, most plasticizers are toxic which makes the use of the corresponding ISEs in many clinical applications impossible. Finally, most plasticizers lead to PVC membranes that give a poor adhesion on solid surfaces in the case of solid-state membrane sensors. These inconveniences might be avoided by choosing other polymers without plasticizer. The following polymers were successfully used for ISEs and have a glass transition temperature below room temperature: polysiloxanes,[20-29] photocurable polymers,[30-32] and polyurethanes.[33-36]

In this work, polyurethanes are utilized as polymer matrix. Polyurethanes are synthetic resinous, fibrous, or elastomeric polymers that are made into foams, fibres, elastomers, and surface coatings.[37] They are formed by reaction of an alcohol with an isocyanate,[38] as shown in Figure 3.4. The polyurethanes used in this work were synthesized from a soft and a hard diol copolymer with a diisocyanate.[39] The type and the relative composition of the building blocks determine the characteristics of the

polyurethane such as phase transition temperature, mechanical properties, adhesion strength, electrical resistance, and solubility.

In the following chapters, comprehensive results of the use of polyurethanes for ISEs are presented. Among these are the applications of polyurethanes for immobilizing membrane components and for immobilizing biological molecules.

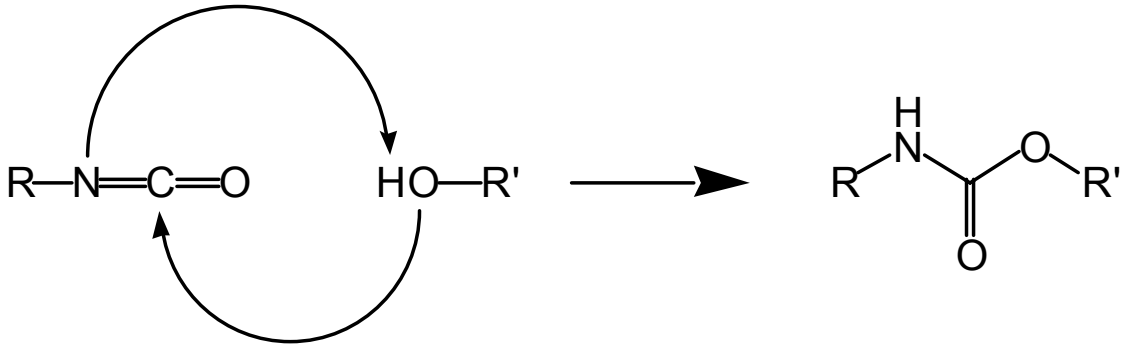

Figure 3.4 Nucleophilic addition of an alcohol with an isocyanate leads to the formation of an urethane.[38]

References

(1) Schaller, U.; Bakker, E.; Spichiger, U. E.; Pretsch, E. Ionic Additives for Ion-Selective Electrodes Based on Electrically Charged Carriers. *Anal. Chem.* **1994,** *66*, 391-398.

(2) Yajima, S.; Tohda, K.; Bühlmann, P.; Umezawa, Y. Donnan Exclusion Failure of Neutral Ionophore-Based Ion-Selective Electrodes Studied by Optical Second-Harmonic Generation. *Anal. Chem.* **1997,** *69*, 1919-1924.

(3) Bühlmann, P.; Pretsch, E.; Bakker, E. Carrier-Based Ion-Selective Electrodes and Bulk Optodes. 2. Ionophores for Potentiometric and Optical Sensors. *Chem. Rev.* **1998,** *98*, 1593-1687.

(4) Visser, H. C.; Reinhoudt, D. N.; de Jong, F. Carrier-Mediated Transport Through Liquid Membranes. *Chem. Soc. Rev.* **1994,** *23*, 75-81.

(5) Morf, W. E.; Badertscher, M.; Zwickl, T.; Reichmuth, P.; de Rooij, N. F.; Pretsch, E. Calculated Effects of Membrane Transport on the Long-Term Response Behavior of Polymeric Membrane Ion-Selective Electrodes. *J. Phys. Chem. B* **2000,** *104*, 8201-8209.

(6) Morf, W. E.; Badertscher, M.; Zwickl, T.; de Rooij, N. F.; Pretsch, E. Effects of Ion Transport on the Potential Response of Ionophore-Based Membrane Electrodes: A Theoretical Approach. *J. Phys. Chem. B* **1999**, 11346-11356.

(7) Bakker, E.; Nägele, M.; Schaller, U.; Pretsch, E. Applicability of the Phase Boundary Potential Model to the Mechanistic Understanding of Solvent Polymeric Membrane-Based Ion-Selective Electrodes. *Electroanalysis* **1995,** *7*, 817-822.

(8) Morf, W. E. *The Principles of Ion-Selective Electrodes and of Membrane Transport*; Elsevier Science: New York, 1981.

(9) Umezawa, Y. *Handbook of Ion-Selective Electrodes: Selectivity Coefficients*; CRC Press: Boca Raton, 1990.

(10) Nägele, M.; Bakker, E.; Pretsch, E. General Description of the Simultaneous Response of Potentiometric Ionophore-Based Sensors to Ions of Different Charge. *Anal. Chem.* **1999,** *71*, 1041-1048.

(11) Bakker, E.; Pretsch, E.; Bühlmann, P. Selectivity of Potentiometric Ion Sensors. *Anal. Chem.* **2000,** *72*, 1127 -1133.

(12) Bakker, E. Determination of Unbiased Selectivity Coefficients of Neutral Carrier-Based Cation-Selective Electrodes. *Anal. Chem.* **1997,** *69*, 1061-1069.

(13) Bakker, E.; Bühlmann, P.; Pretsch, E. Carrier-Based Ion-Selective Electrodes and Bulk Optodes. 1. General Characteristics. *Chem. Rev.* **1997,** *97*, 3083-3132.

(14) Ceresa, A.; Pretsch, E. Determination of Formal Complex Formation Constants of Various Pb2+ Ionophores in the Sensor Membrane Phase. *Anal. Chim. Acta* **1999,** *395*, 41-52.

(15) Guilbault, G. G.; Durst, R. A.; Frant, M. S.; Freiser, H.; Hansen, E. H.; Light, T. S.; E. Pungor; Rechnitz, G.; Rice, N. M.; Rohm, T. J.; Simon, W.; Thomas, J. D. R. Recommendations for Nomenclature of Ion-Selective Electrodes. *Pure Appl. Chem.* **1976,** *48*, 127-132.

(16) Sokalski, T.; Zwickl, T.; Bakker, E.; Pretsch, E. Lowering the Detection Limit of Solvent Polymeric Ion-Selective Electrodes. 1. Modeling the Influence of Steady-State Ion Fluxes. *Anal. Chem.* **1999,** *71*, 1204-1209.

(17) Sokalski, T.; Ceresa, A.; Zwickl, T.; Pretsch, E. Large Improvement of the Lower Detection Limit of Ion-Selective Polymer Membrane Electrodes. *J. Am. Chem. Soc.* **1997,** *119*, 11347-11348.

(18) Fiedler, U. Influence of the Dielectric Constant of the Medium on the Selectivities of Neutral Carrier Ligands in Electrode Membranes. *Anal. Chim. Acta* **1977,** *89*, 111-118.

(19) Bakker, E.; Bühlmann, P.; Pretsch, E. Polymer Membrane Ion-Selective Electrodes-What are the limits? *Electroanalysis* **1999,** *11*, 915-933.

(20) Cha, G. S.; Liu, D.; Meyerhoff, M. E.; Cantor, H. C.; Midgley, A. R.; Goldberg, H. D.; Brown, R. B. Electrochemical Performance, Biocompatibility and Adhesion of New Polymer Matrices for Solid-State Ion Sensors. *Anal. Chem.* **1991,** *63*, 1666-1672.

(21) Reinhoudt, D. N.; Engbersen, J. F. J.; Brzózka, Z.; van den Vlekkert, H. H.; Honig, G. W. N.; Holterman, H. A. J.; Verkerk, U. H. Development of Durable K^+-Selective Chemically Modified Field Effect Transistors with Functionalized Polysiloxane Membranes. *Anal. Chem.* **1994,** *66*, 3618-3623.

(22) Antonisse, M. M. G.; Lugtenberg, R. J. W.; Egberink, R. J. M.; Engbersen, J. F. J.; Reinhoudt, D. N. Durable Nitrate-Selective Chemically Modified Field Effect Transistors Based on New Polysiloxane Membranes. *Anal. Chim. Acta* **1996,** *332*, 123-129.

(23) Brunink, J. A. J.; Lugtenberg, R. J. W.; Brzozka, Z.; Engbersen, J. F. J.; Reinhoudt, D. N. The Design of Durable Na^+-Selective CHEMFETs Based on Polysiloxane Membranes. *J. Electroanal. Chem.* **1994,** *378*, 185-200.

(24) Högg, G.; Lutze, O.; Cammann, K. Novel Membrane Material for Ion-Selective Field-Effect Transistors with Extended Lifetime and Improved Selectivity. *Anal. Chim. Acta* **1996,** *335*, 103-109.

(25) Tsujimura, Y.; Sunagawa, T.; Yokoyama, M.; Kimura, K. Sodium Ion-Selective Electrodes Based on Silicone-Rubber Membranes Covalently Incorporating Neutral Carriers. *Analyst (Cambridge, U.K.)* **1996,** *121*, 1705-1709.

(26) van der Wal, P. D.; Skowronska Ptasinska, M.; van den Berg, A.; Bergveld, P.; Sudhölter, E. J. R.; Reinhoudt, D. N. New Membrane Materials for Potassium-Selective Ion-Sensitive Field-Effect Transistors. *Anal. Chim. Acta* **1990,** *231*, 41-52.

(27) Uhlig, A.; Lindner, E.; Teutloff, C.; Schnakenberg, U.; Hintsche, R. Miniaturized Ion-Selective Chip Electrode for Sensor Application. *Anal. Chem.* **1997,** *69*, 4032-4038.

(28) Meyerhoff, M. E.; Cha, G. S.; Ma, S. C.; Goldberg, H. D.; Brown, R. B.; Midgley, A. R.; Cantor, H. C. New Polymeric Membrane Materials for Fabricating Potentiometric Ion- and Bioselective Sensors. *Polym. Mater. Sci. Eng.* **1991,** *64*, 292-293.

(29) Ufer, S.; Cammann, K. Ion-Sensitive Field-Effect Transistor with Improved Membrane Adhesion. *Sens. Actuators, B* **1992,** *7*, 572-575.

(30) Bratov, A.; Abramova, N.; Munoz, J.; Dominguez, C.; Alegret, S.; Bartoli, J. Photocurable Polymer Matrices for Potassium-Sensitive Ion-Selective Electrode Membranes. *Anal. Chem.* **1995,** *67*, 3589-3595.

(31) Bratov, A.; Abramova, N.; Munoz, J.; Dominguez, C.; Alegret, S.; Batroli, J. Optimization of Photocurable Polyurethane Membrane Composition for Ammonium Ion Sensor. *J. Electrochem. Soc.* **1997,** *144*, 617-621.

(32) PuigLleixa, C.; Jimenez, C.; Fabregas, E.; Bartroli, J. Potentiometric pH Sensors Based on Urethane-Acrylate Photocurable Polymer Membranes. *Sens. Actuators, B* **1998,** *49*, 211-217.

(33) Yun, S. Y.; Hong, Y. K.; Oh, B. K.; Cha, G. S.; Nam, H.; Lee, S. B.; Jin, J. Potentiometric Properties of Ion-Selective Electrode Membranes Based on Segmented Polyether Urethane Matrices. *Anal. Chem.* **1997,** *69*, 868-873.

(34) Espadas-Torre, C.; Meyerhoff, M. E. Thrombogenic Properties of Untreated and Poly(ethylene oxide)-Modified Polymeric Matrices Useful for Preparing Intraarterial Ion-Selective Electrodes. *Anal. Chem.* **1995,** *67*, 3108-3114.

(35) Lindner, E.; Cosofret, V. V.; Richard, P. B.; Johnson, T. A.; Ash, R. B.; Neumann, M. R.; Kao, W. J.; Anderson, J. M. Electroanalytical and Biocompatibility Studies on Microfabricated Array Sensors. *Electroanalysis* **1995,** *7*, 864-870.

(36) Cosofret, V. V.; Erdosy, M.; Raleigh, J. S.; Johnson, T. A.; Neuman, M. R.; Buck, R. P. Aliphatic Polyurethane as a Matrix for pH Sensors: Effects of Native Sites and Added Proton Carrier on Electrical and Potentiometric Properties. *Talanta* **1996,** *43*, 143-151.

(37) Uhlig, K. *Discovering Polyurethanes*; Hanser-Gardner, 1999.

(38) Dieterich, D.; Grigat, E.; Hahn, W. In *Kunststoff-Handbuch Polyurethane*; Becker, G. W., Braun, D., Eds.; Hanser: München, 1983; Vol. 7.

(39) Schöning-Hammer, A., Personal Communication, Zurich, 1998.

4 "Self-Plasticizing" Ion-Selective Membrane Electrodes with Covalently Bound Carriers

4.1 Introduction

There is a huge interest in miniaturized and low-prize ion-selective sensors for biomedical, industrial, and environmental applications.[1] These requirements are better met with solid-state membrane sensors than with liquid-contacted ISEs. There are different kinds of microfabricated solid-state devices based on ionophores. Examples are solid-state membrane electrodes[2-7] and chemically sensitive field-effect transistors (CHEMFETs).[8, 9] Solid-state membrane sensors usually do not have a high potential stability in comparison with liquid-contacted ISEs. The solid-state devices suffer from a thermodynamically ill-defined phase boundary potential between membrane and solid contact. Carbon dioxide and organic acids can alter the internal pH at the membrane/insulator interface of CHEMFETs and therefore interfere with the measurement of the analyte ions.[10] This signal instability is a severe drawback for CHEMFETs.[11]

A novel method based on a pH-compensating double membrane is proposed in this doctoral dissertation to create a thermodynamically well-defined insulator/membrane interface for CHEMFETs. The polymer membrane of CHEMFETs was modified by a covalently bound ionophore.[12, 13] For the immobilization of the carriers, polyurethane with "self-plasticizing" properties was used.[14] The characterization of the novel covalently bound ionophores in ISEs is described in the first part of this chapter. The new method to improve the signal stability of CHEMFETs was tested by ISEs in the second part of this chapter and applied to CHEMFETs in Chapter 5.

4.2 Theory of Solid-State Membrane Sensors

4.2.1 CHEMFETs

Figure 4.1 shows a field-effect device based on a metal-insulator-semiconductor transistor, which is called MISFET.[8] The semiconductor is typically silicon and the insulator is normally silicon dioxide. The interesting property of MISFETs is that the

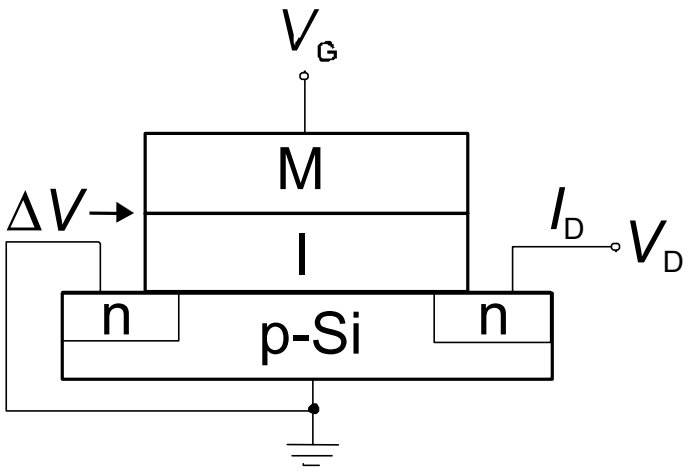

Figure 4.1 Schematic diagram of a metal-insulator-semiconductor transistor (MISFET).[8] The channel length is the distance between the two *n*-type semiconductor regions. I: insulator, I_D: drain current, M: metal, p-Si: p-type semiconductor, ΔV: voltage drop, V_D: drain voltage, V_G: gate voltage.

charge distribution at the insulator-semiconductor interface can be controlled by the potential on the metal.

For a p-type semiconductor, a negative potential on the metal accumulates (positive) holes at the semiconductor surface. When the potential on the metal surface becomes positive, holes are pushed away from the semiconductor surface, and a depleted region at the surface is left. If the positive charge is large enough, electrons start to accumulate at the semiconductor surface and they are forming a conducting channel. This process is called inversion.[15] For a MISFET, the current in the conducting channel I_D (drain current) depends on the gate-source voltage (V_{GS}). The threshold voltage (V_T) is defined as V_{GS}, at which current starts to flow along the semiconductor surface, which occurs when the inversion layer is formed.

In ion-selective field-effect transistors (ISFETs) the gate insulator consists of an ion-selective layer (like Si_3N_4, Al_2O_3, or Ta_2O_5) and the gate "metal" of an aqueous solution with a reference electrode.[8] V_T of ISFETs does not only depend on solid-state properties, it also depends on the potential difference of the added surfaces.

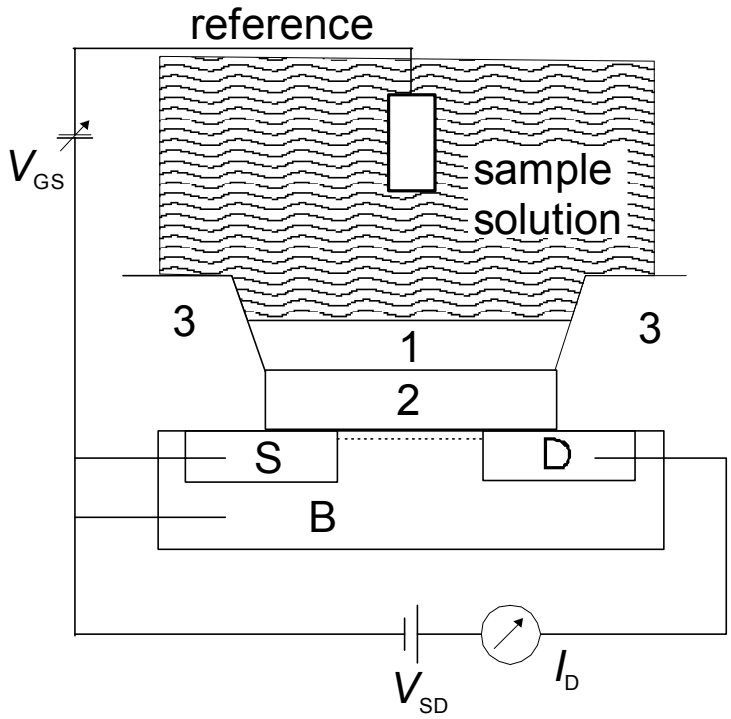

Figure 4.2 Schematic illustration of a CHEMFET.[16] 1: polymer membrane, 2: gate oxide, 3: isolating resin, B: bulk, D: drain, S: source, I_D: drain current, V_{GS}: gate-source voltage, V_{SD}: source-drain voltage.

A CHEMFET is an ISFET, in which the gate surface is covered with a sensing membrane,[17] as shown in Figure 4.2. The V_T of a CHEMFET can be described with the help of the following equation:[8]

$$V_T = E^0 + \frac{RT}{zF}\ln\sum_m K_m a'_m - \frac{RT}{zF}\ln\sum_m K_m a''_m \qquad (4.1)$$

This expression is analogous to equation 3.11 for ISEs described in Chapter 3. However, the formulation of term E^0 in CHEMFETs, as shown in equation 4.2, is different in comparison with ISEs.

$$E^0 = E_{reference} + \Psi_0 + V_{SS} \qquad (4.2)$$

where $E_{reference}$ is the potential of the reference electrode, which also includes the liquid junction potential. The potential difference between the insulator and the thin water film is Ψ_0. Potential contributions originating from the solid-state part of the system are included in V_{SS}.

The preferred mode of operation of a CHEMFET is the constant-current mode with constant drain-source voltage.[8] A feedback circuit compensates for induced changes in the drain-source current (I_{DS}) by adjusting the gate-source voltage (V_{GS}). This causes a parallel shift (ΔV) of the I_{DS} - V_{GS} curve, as illustrated in Figure 4.3.[8] Furthermore, the packaging[18] in the fabrication process and the adhesion of the membrane on the substrate during the use of the CHEMFET[19, 20] can be problematic.

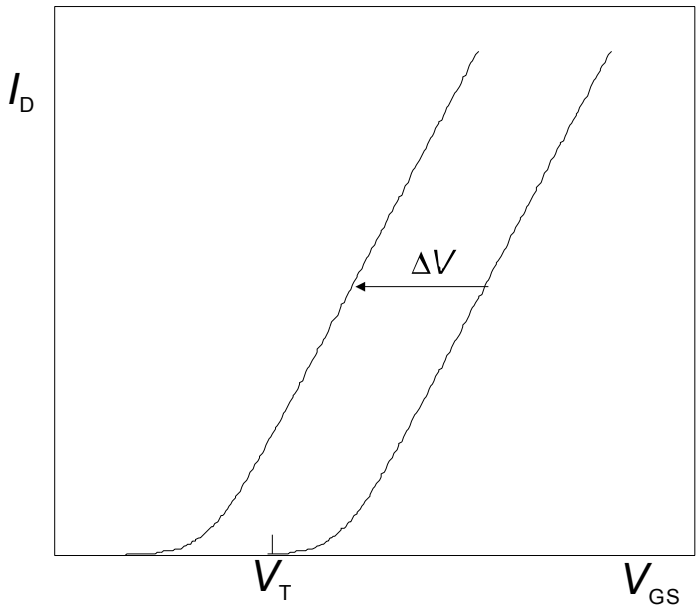

Figure 4.3 Electrical properties of an ISFET with a voltage drop (ΔV) along the voltage axis.[8] I_D: drain current, V_{GS}: gate-source voltage, V_T: threshold voltage.

In the ideal case, the response signal of a CHEMFET is determined by the activity of the analyte ion in the sample solution. However, CHEMFETs usually do not have a high potential stability in comparison with liquid-contacted ISEs. This restriction is mainly attributed to the lack of a thermodynamically defined interfacial potential

between the gate material and the membrane.[11, 21] The interface between the sensing membrane and the insulator includes a thin water layer, which can be regarded as an additional phase sensitive to the composition of the sample solution. Compounds like, for example, CO_2, which diffuse through the membrane into this aqueous layer, may disturb the interfacial potential between liquid and solid by locally altering the pH and may cause a drift of the potential.[10, 22] Similar results were reported by Harrison *et al.*[23] for a membrane/insulator/semiconductor electrode. The diffusion of a gas like CO_2 through a membrane can be described mathematically by the following expressions:[24, 25]

$$c''_{aq}(t \geq 0) = c'_{aq}(t < 0) + \Delta c'_{aq} f(t) \tag{4.3}$$

$$f(t) = 1 - \frac{4}{\pi} \sum_{n=0}^{\infty} \left(\frac{(-1)^n}{2n+1} \mathrm{e}^{\frac{-(2n+1)^2 \pi^2 D t}{4d^2}} \right) \tag{4.4}$$

where c''_{aq} is the concentration of CO_2 in the water film between membrane and gate and c'_{aq} ($t < 0$) is the initial concentration of CO_2 in the sample solution. $\Delta c'_{aq}$ is the change of the CO_2 concentration in the sample solution and t is the time. D is the diffusion coefficient of CO_2 within the polymer membrane whose thickness is d.

Several methods have been reported to improve the stability of the membrane-insulator interface of CHEMFETs. A simple solution was to place a thin layer of Ag-AgCl on top of the solid contact of a membrane/insulator/semiconductor electrode.[23] Sudhölter *et al.*[26] proposed to use an intermediate hydrogel containing both a pH buffer (pH ≅ 4) and the ion to be sensed by the membrane. CHEMFETs based on this buffer solution used poly(hydroxylethyl methacrylate) (pHEMA) as polymer.[16, 27-30] Other workers deposited an additional layer between the sensing membrane and the insulator using a hydrophobic negative photoresist.[31] The inner layer provided both good adhesion to the ISFET and a water-repellent barrier to the sample solution.

4.2.2 Solid-State Membrane Electrodes

The question of the thermodynamical stability of the membrane-insulator interface of CHEMFETs is similar to the situation found for conventional solid-state membrane electrodes.[8] Certain types of solid-state membrane electrodes are also called coated-wire electrodes (CWEs). In a CWE an electroactive species is incorporated in a thin polymeric film and coated directly onto a metallic conductor.[2] This results in the elimination of the internal filling solution in comparison with liquid-contacted ISEs.

It was found that most metallic conductors used in CWEs suffer from a potential dependence on oxygen partial pressure, as caused by the ill-defined membrane-metal potential.[32] Therefore, the response function of solid-state membrane electrodes can be considered to be due to the formation of an oxygen half-cell at the membrane-metal interface as a consequence of water and oxygen permeation.

Several methods have been reported to improve the redox-stability of the membrane-solid interface. A frequently used solution was the deposition of an additional layer between the sensing membrane and the solid contact using, for example, poly(vinyl ferrocene),[33] a lipophilic redox-active self-assembled monolayer,[34] or a hydrogel doped with the primary ions and chloride ions.[7, 35, 36] Other methods to enhance the thermodynamical stability of the interfacial potential include a conductive polymer like poly(3,4-ethylenedioxythiophene), [37] polyaniline,[38] or polypyrrole[32, 39] as ion-to-electron transducer. Additionally, the incorporation of a lipophilic silver-ligand complex[40] into the membrane, which was coated on an Ag/AgCl contact, is described. Moreover, a CWE with a double-membrane was reported.[41] This CWE was prepared with an internal conducting membrane based on tetrabutylammonium bromide in PVC and an external membrane containing an ionophore. Furthermore, double membranes were used to enhance the selectivity of ion-selective sensors[42-44] and biosensors,[45-47] or to carry an acid neutralizing solution between the inner and the outer membrane.[48]

4.2.3 Double Membranes with Mobile and Covalently Bound Ionophores

In this work, a double membrane is introduced as a novel approach to improve the stability of the interfacial potential of CHEMFETs. The main goal was to reduce or even eliminate the sensitivity to interfering CO_2 or to sample solutions with varying

pH. The part of the double membrane in contact with the sample contains a mobile ammonium-selective ionophore, as shown in Figures 4.4 and 4.5. The inner membrane on the solid contact embodies the same carrier and, in addition, an immobilized H^+-selective ionophore.

The covalent immobilization of ionophores has been reported for polymeric matrices like polysiloxane,[49-51] PVC-COOH,[52-54] poly(styrene-butadiene),[55] methacrylic-acrylic copolymers,[56] and polyurethane.[14, 57] Extensive simulations and experimental work with all possible combinations of free and covalently bound ionophores and borate anions was done by Reinhoudt *et al*.[49, 58] These authors observed that the covalent binding of the ionophore slightly decreased the slope of CHEMFETs and increased the response time owing to limited diffusion within the membrane phase. However, the lifetime of the sensor was enhanced due to a hindered

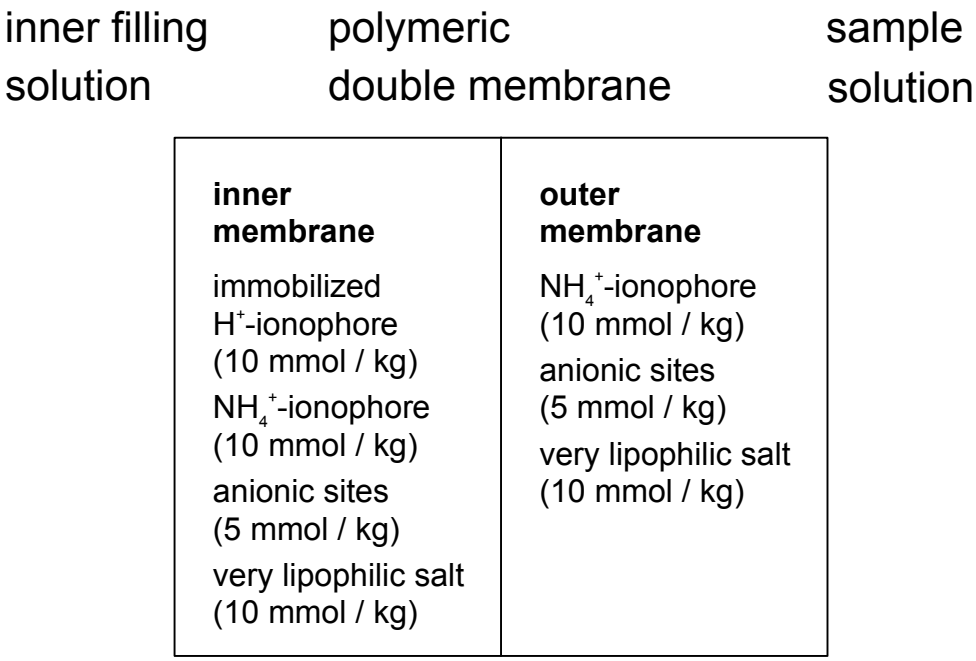

Figure 4.4 Schematic view of polyurethane based double membrane used for ion-selective sensors. Tetradodecylammonium tetrakis-(4-chlorophenyl)borate (ETH 500) was used as lipophilic salt.

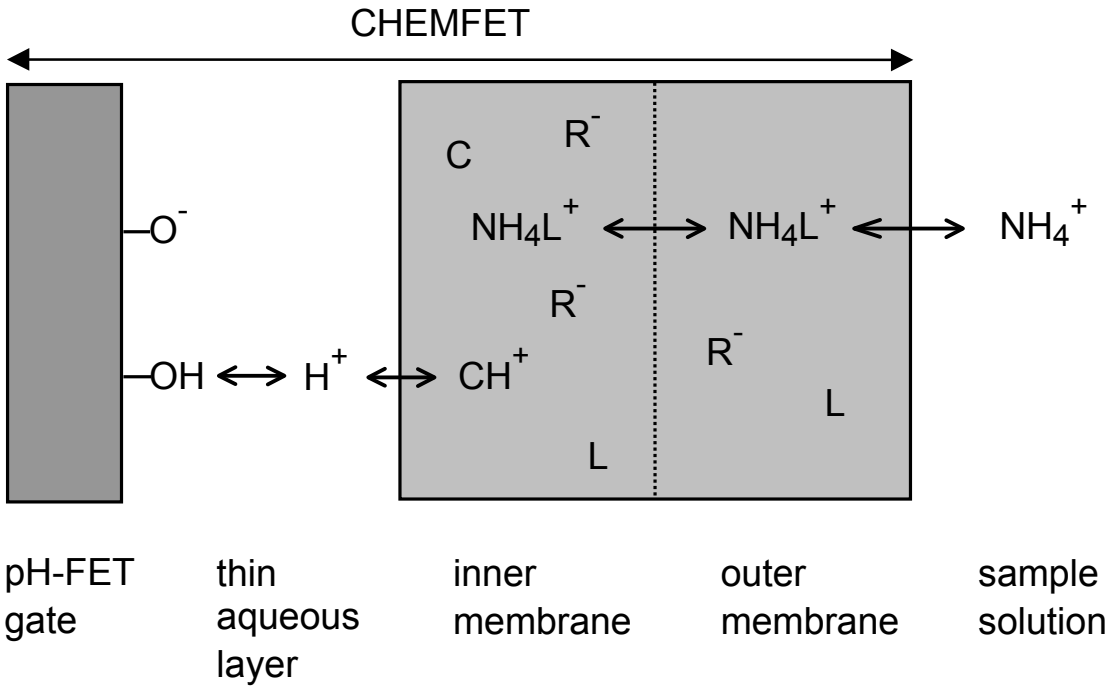

Figure 4.5 Simplified schematic view of a CHEMFET prepared with a double membrane: L and NH_4L^+, free and complexed nonactin; C and CH^+, unprotonated and protonated covalently bound hydrogen-ion-selective ionophore; R^-, lipophilic anionic site.

loss of ionophore into the sample. The covalent attachment of the carrier also resulted in improved lower detection limits.[54] Furthermore, carboxylated[59] and aminated[60] PVC-based ISEs were found to be pH sensitive and showed the same response characteristics as ISEs with immobilized H^+-selective ionophores.

In this work, novel H^+-selective carriers covalently bound to a polyurethane matrix are presented. The synthesis and the immobilization of these ionophores were done in our laboratory.[12, 13] The polymer matrix used for immobilization was based on poly[(*R*)-3-hydrobutyric acid] diol (PHB) and 2,2,4-trimethylhexamethylene diisocyanate (TMDI). A high degree of biocompatibility was found for materials prepared from PHB and TMDI,[61, 62] but polyurethanes made only from these two components contain relatively hard polymer segments and are inappropriate for ISE

applications because of their high electrical resistivity.[63] To introduce soft polymer segments, poly(tetrahydrofurane) diol (PTHF) was added to PHB and TMDI. The soft segments function like a built-in plasticizer. On the basis of the low glass transition temperature of these polyurethanes, which is below room temperature, there is no need to add a conventional plasticizer.

Polyurethane is a suitable matrix for most solid-state membrane devices, since the adhesion on metals is good.[64-66] A commercially available polyurethane, called Tecoflex, was also studied in this work as membrane matrix. Tecoflex is well suited for ISEs, as shown in a series of previous studies.[1, 67-70] A vast number of different polyurethanes with structures similar to Tecoflex were synthesized in the group of Nam.[71] The addition of plasticizers to these polyurethanes was reported to increase the free ionophore concentration in the membrane by dissolving ionophores dispersed in partially structured soft segments or semicrystalline hard segments. Furthermore, photocurable polyurethanes were used for the preparation of CHEMFETs.[72]

The first part of this chapter includes the characterization of ISEs with immobilized H^+-carriers. In the second part of this chapter, liquid-contacted ISEs with immobilized ionophores in double-membranes were used. The application of such double membranes to eliminate the pH interference in the thin water layer between membrane and insulator of CHEMFETs is described in Chapter 5.

4.3 Immobilized Bis-2,6-hydroxymethyl pyridine

The hydrogen ion-selective ionophore bis-2,6-hydroxymethyl pyridine (Figure 4.6) was immobilized in polyurethane (PHB/PTHF) using TMDI,[14] as shown in Figure 3.4. Due to the short alkyl chains of the immobilized ionophore, a relatively rigid anchoring of the compound within the polymer should result. Figure 4.7 depicts a calibration curve of ISEs based on this carrier. It was reported in previous studies that the dynamic pH range of hydrogen ion-selective ionophores depends on the acid dissociation constant of the ionophores.[73, 74] Accordingly, the lower detection limit of the immobilized bis-2,6-hydroxymethyl pyridine might be caused by the size of the acid dissociation constant (p*K*a).[75] Furthermore, the influence of the borate concentration in the membrane on the lower detection limit was tested. ISEs with only

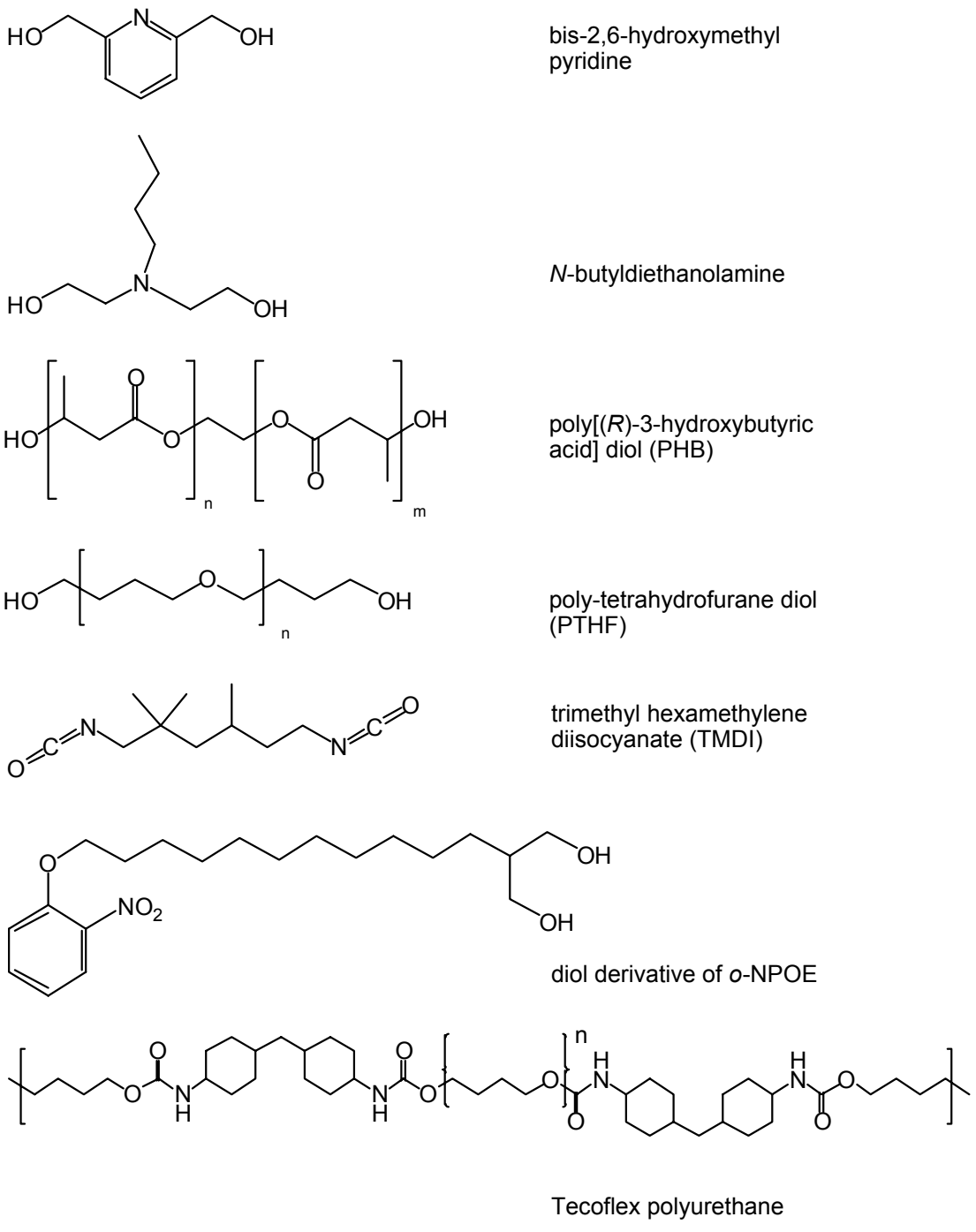

Figure 4.6 Structural formulas and abbreviations of immobilized ionophores, immobilized plasticizer, and polyurethane components.

0.5 mol %, 5 mol %, or 10 mol % of added borate relative to the ionophore all had the same detection limit (pH 5.7),[12] in contrast to the data of Xu.[76]

ISEs based on the soft polyurethane (PHB/PTHF 1:5) almost had the same slopes of response and the same lower detection limits as the ones made from the hard polyurethane (PHB/PTHF 1:1), as shown in Table 4.1. The selectivity coefficients of these ISEs were similar to the ones obtained for ISEs based on Tecoflex, 2-nitrophenyl octyl ether (*o*-NPOE), without any additioned ionophore or borate.[77] The measurements of the latter showed a preference towards hydrogen ions.[6, 78] Urethane carbonyl and poly(ether oxygen) from the polyurethane matrix can act as H^+ acceptor.[79] It appears that the response and selectivity behavior of all the ISEs studied in this section are partly determined by ion-binding properties of such acceptor or ion-exchange sites.

4.4 Immobilized *N*-Butyldiethanolamine

The response curve of ISEs based on the ionophore *N*-butyldiethanolamine, which was anchored with its diol substituents to polyurethane, is shown in Figure 4.8. These membranes contained the covalently bound ionophore, which was added like a classical mobile ionophore to a solution of PVC and bis(2-ethylhexyl) sebacate (DOS). The lower detection limit of ISEs with 50 mol % borate relative to the ionophore was at pH 5. The corresponding selectivity coefficients were found to be comparable with the ones obtained for ISEs with the ionophore bis-2,6-hydroxymethyl pyridine. When a polyurethane (PHB/PTHF) matrix was used instead of PVC/DOS, the selectivities were deteriorated by one order of magnitude. This change for the worse was due to the increased extraction of interfering ions from the sample into the polyurethane membrane.

As seen in Figure 4.8, a reduction of the amount of borate resulted in a large decrease of the lower detection limit. These ISEs were based on PVC/DOS membranes with 0, 1 or 5 mol % borate. For ISEs with a polyurethane matrix (PHB/PTHF) instead of PVC/DOS, the lower detection limit was also found to be improved, as shown in Figure 4.9. The corresponding polyurethane membranes of type 4E (H^+) - 4G (H^+) contained 1, 4, or 10 mol % anionic sites. The enhanced

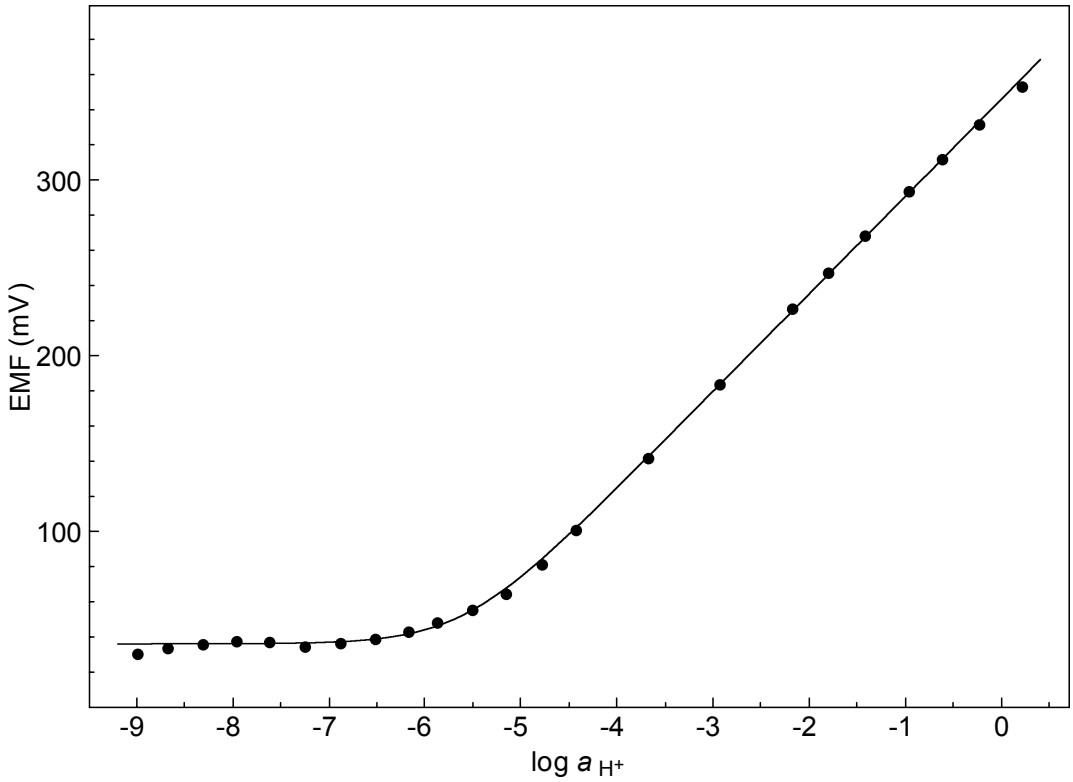

Figure 4.7 pH response curve of a PHB/PTHF 1:1 membrane containing the immobilized H^+ carrier bis-2,6-hydroxymethyl pyridine and the lipophilic anionic additive NaTFPB (membrane type 4A (H^+)). The samples contained a constant background of 10^{-4} M Mg^{2+}.

Table 4.1 Linear measuring ranges, lower detection limits, selectivity coefficients and slopes (mV dec^{-1}) obtained for polyurethane membranes based on immobilized pH ionophores and the ion exchanger NaTFPB. The selectivity coefficients were determined using FIM. At least three identical electrodes were used to calculate the mean value and the standard deviation.

immobilized ionophore	bis-2,6-hydroxymethyl pyridine	bis-2,6-hydroxymethyl pyridine	*N*-butyl-diethanolamine	*N*-butyl-diethanolamine
membrane matrix	PHB/PTHF 1:5	PHB/PTHF 1:1	PHB/PTHF 1:5	Tecoflex and *o*-NPOE
membrane type	4B (H^+)	4A (H^+)	4C (H^+)	4D (H^+)
linear range (M)	$10^{-0.5} - 10^{-4.0}$	$10^{0.2} - 10^{-5.5}$	$10^{-4.5} - 10^{-10.0}$	$10^{-4.0} - 10^{-7.5}$
lower detection limit (M)	$10^{-5.7}$	$10^{-5.7}$	$< 10^{-10}$	$10^{-10.2}$
slope for H^+ (without any interfering ion)	55.3 ± 1.0	55.5 ± 0.5		
log $K^{pot}_{H, NH4}$ (slope)	–	-1.8 ± 0.1 (56.4 ± 0.4)	< -9.0 ± 0.2 (44.8 ± 0.3)	< -9.0 ± 0.4 (47.9 ± 0.5)
log $K^{pot}_{H, Li}$ (slope)	–	-2.0 ± 0.1 (52.6 ± 0.4)	-5.0 ± 0.4 (40.2 ± 3.5.)	-5.0 ± 0.1 (46.6 ± 0.8)
log $K^{pot}_{H, K}$ (slope)	–	-2.3 ± 0.3 (54.4 ± 0.9)	-5.3 ± 0.1 (46.0 ± 1.2)	-5.8 ± 0.3 (50.8 ± 0.3)
log $K^{pot}_{H, Na}$ (slope)	–	-2.5 ± 0.2 (54.4 ± 1.5)	-5.7 ± 0.3 (47.9 ± 0.5)	-6.2 ± 0.2 (49.5 ± 0.9)
log $K^{pot}_{H, Ca}$ (slope)	–	-3.6 ± 0.0 (56.4 ± 0.4)	-5.7 ± 0.3 (44.8 ± 0.6)	-6.9 ± 0.3 (49.2 ± 1.4)
log $K^{pot}_{H, Mg}$ (slope)	–	-3.7 ± 0.1 (55.5 ± 0.5)	-5.8 ± 0.2 (42.6 ± 1.8)	-7.0 ± 0.1 (47.8 ± 0.6)

detection limits can be explained by a low concentration of the available free carrier in the membrane. The concentration of the ionophore may be much lower than expected due to incomplete immobilization. Hence, the ISEs with 50 mol % borate predominately behaves as cation-exchanger membranes. Such electrodes were shown to be suitable for measurements in the pH range 0 – 4 even in the presence of hydrofluoric acid,[80] which dissolves the conventional pH glass electrodes. For the following experiments with the studied ionophore, membranes with a reduced amount of borate were used.

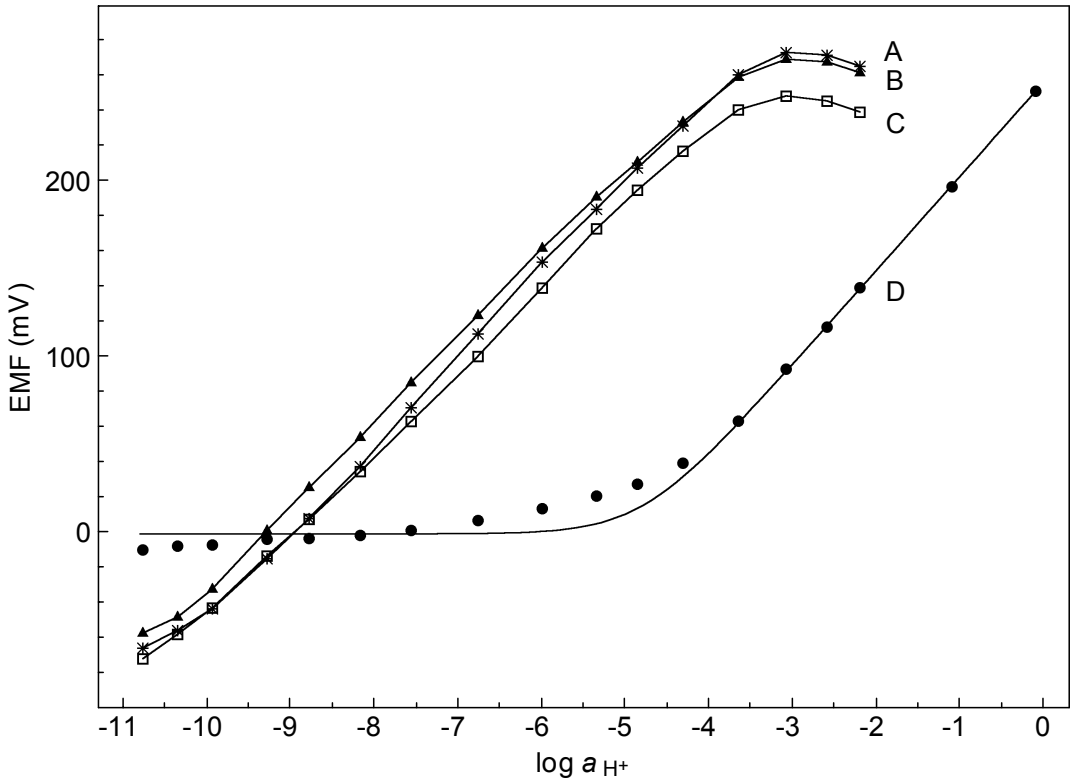

Figure 4.8 Measuring range of ISEs based on PVC/DOS, immobilized *N*-butyldiethanolamine and different concentrations of the anionic additive KTFPB (membrane types 4H (H^+) – 4K (H^+)): A, 5 mol % KTFPB relative to the ionophore, 49.8 ± 0.2 mV dec^{-1}; B, 1 mol % KTFPB, 50.3 ± 0.2 mV dec^{-1}; C, no KTFPB, 46.8 mV dec^{-1}; D, 50 mol % KTFPB, 51.9 ±1.7 mV dec^{-1}. The samples contained a constant 5 x 10^{-4} M sodium and 5 x 10^{-4} M tris(hydroxymethyl)aminomethane (Tris) background.

The results in Table 4.1 illustrate that the selectivity coefficients depend on the membrane matrix. In order to prevent leaching of the plasticizer, the influence of the covalent attachment of *o*-NPOE on the response behavior was investigated.[12] ISEs based on Tecoflex and immobilized *o*-NPOE had better selectivities than the ones made from polyurethane (PHB/PTHF) without plasticizer. Referring to the data of Heng,[56] the use of methacrylic-acrylic copolymer with an immobilized ionophore resulted in a Nernstian response.

The results of comprehensive studies on the influence of the polymer matrix on the response behavior are summarized in Table 4.2. In general, ISEs based on PHB/PTHF had slightly better slopes than ISEs prepared with a Tecoflex matrix, which may be due to the higher membrane resistance of the latter. The lowest slope of 41.8 mV dec^{-1} was obtained with ISEs based on Tecoflex without plasticizer. This result is in good accordance with data obtained by Lee *et al.*[81] They showed that Tecoflex electrodes without plasticizer, ionophore or borate had a pH sensitivity of 42 mV dec^{-1}. Furthermore, it was reported that the slope and the selectivity of potassium-selective ISEs prepared with Tecoflex and without plasticizer were inferior to those of standard PVC/DOS ISEs: For the Tecoflex electrodes, the slope was 53.6 mV dec^{-1} from 10^{-5} to 10^{-1} M K^+, whereas the PVC electrodes gave a slope of 57.1 mV dec^{-1}.[64]

The addition of *o*-NPOE or immobilized *o*-NPOE resulted in increased slopes of the ISEs, as shown in Table 4.2. The presence of the plasticizer lowered the membrane resistance and reduced the cation interference. The improvement of the slope was larger when *o*-NPOE was not immobilized. This might be a consequence of the higher diffusion rate for mobile *o*-NPOE, or of the slightly different membrane matrix with an increased percentage of Tecoflex. Using protonated Tris instead of Na^+ as interfering ion led to a further improvement of the slope and the lower detection limit, as shown in Table 4.3. The same favorable effect of a Tris buffer solution was observed by PuigLleixa *et al.*[82] As seen in Table 4.4, continuously adding a base to an acidic solution, instead of adding an acid to a basic solution, resulted in higher slopes. These results can be explained by an efficient cation interference in the basic pH range. Furthermore, these experiments strongly indicate that extracted alkali metal ions are not bound by the H^+ ionophore, but are stabilized by the membrane matrix and/or the incorporated anionic sites. It is well known that metal ions preferably complex with the ether groups of polyurethane.[83] An even stronger influence of the membrane matrix is observed for ISEs based on carboxylated PVC,[59] which is found

to be quite selective for large monovalent cations. Therefore, buffer solutions that contain monovalent metal cations cannot be used to demonstrate the pH response of PVC-COOH membranes. For example, a pH calibration curve for ISEs based on PVC-COOH in a background of 0.14 M Na^+ showed a slope of only 6 mV dec^{-1}.[59] Furthermore, the immobilized pH ionophore was able to deprotonate functional groups within the polyurethane matrix. The deprotonated functional groups could act as negative sites[74] or complex cations occurring in the membrane.

Table 4.2 Electrochemical characteristics of different membrane matrices containing immobilized *N*-butyldiethanolamine and a lipophilic anionic additive (*n*: number of electrodes). The selectivity coefficients were determined by continuously adding a base (NaOH) to an acidic solution (HCl). There were a constant background concentration of 0.01 M sodium (FIM) and a Tris buffer in the sample.

polymer	plasticizer (weight %)	slope (mV dec^{-1})	selectivity coefficient log $K^{pot}_{H,\,Na}$	membrane type
PHB/PTHF	*o*-NPOE (10)	53.2	-6.2 (n = 1)	4F (H^+)
PHB/PTHF	(0)	45.8 ± 1.0	-5.7 ± 0.1 (n = 7)	4C (H^+)
Tecoflex	*o*-NPOE (10)	50.4 ± 1.7	-6.0 ± 0.0 (n = 3)	4L (H^+)
Tecoflex	immob. *o*-NPOE (5)	46.6 ± 2.8	-6.2 ± 0.3 (n = 4)	4M (H^+)
Tecoflex	immob. *o*-NPOE (12)	45.1 ± 1.0	-6.2 ± 0.0 (n = 5)	4D (H^+)
Tecoflex	(0)	41.8 ± 1.7	-5.8 ± 0.2 (n = 5)	4N (H^+)
PVC	DOS (64)	51.9 ± 1.7[a)]	-8.5 ± 0.1 (n = 4)	4J (H^+)

[a)] Continuously adding an acid (HCl) to a basic solution (NaOH).

All measurements with the immobilized *N*-butyldiethanolamine gave stable response signal within a few minutes after the change of the sample. A prolongation of the measuring time to several hours after changing the concentration did not improve the slope nor the selectivity of the ISEs. The results summarized in Tables 4.2 – 4.4 were obtained with ISEs which contained a citric acid buffer as the inner solution. Replacing this solution by a HCl solution, a phosphate buffer, or an acetic acid buffer did not change the response curve. An influence of a transmembrane transport of acetic acid[84] on the local pH value near the outer phase boundary was not observed. Finally, membranes based on PHB/PTHF showed a stronger adhesion on solid contacts than the ones made from the commercial Tecoflex.

Table 4.3 Slopes and selectivity coefficients of ISEs containing immobilized *N*-butyldiethanolamine and a lipophilic anionic additive (*n*: number of electrodes). The pH titrations were proceeded by continuously adding a base (NaOH) to an acidic solution (HCl) or by adding an acid (HCl) to a basic solution (Tris). There was a constant 0.01 M background concentration of the interfering ion in the sample (FIM).

polymer	plasticizer (weight %)	addition of a base (NaOH) to an acidic solution (HCl)	addition of an acid (HCl) to a basic solution (Tris)	membrane type
PHB/PTHF	(0)	45.8 ± 1.0 mV dec^{-1} log $K^{pot}_{H, Na}$ -5.7 ± 0.1 (n = 7)	47.9 ± 0.5 mV dec^{-1} log $K^{pot}_{H, Tris}$ -8.4 ± 0.1 (n = 4)	4C (H^+)
Tecoflex	*o*-NPOE (10)	50.4 ± 1.7 mV dec^{-1} log $K^{pot}_{H, Na}$ -6.0 ± 0.0 (n = 3)	51.3 ± 1.6 mV dec^{-1} log $K^{pot}_{H, Tris}$ -8.5 ± 0.2 (n = 6)	4L (H^+)
Tecoflex	(0)	41.8 ± 1.7 mV dec^{-1} log $K^{pot}_{H, Na}$ -5.8 ± 0.2 (n = 5)	50.0 ± 2.1 mV dec^{-1} log $K^{pot}_{H, Tris}$ -8.6 ± 0.3 (n = 3)	4N (H^+)

Table 4.4 Slopes and selectivity coefficients of ISEs containing immobilized *N*-butyldiethanolamine and a lipophilic anionic additive (*n*: number of electrodes). The pH titrations were proceeded by continuously adding a base to an acidic solution or vice versa. There were a constant background concentration of 0.01 M sodium (FIM) and a Tris buffer in the sample.

polymer	plasticizer (weight %)	addition of a base (NaOH) to an acidic solution (HCl)	addition of an acid (HCl) to a basic solution (NaOH)	membrane type
PHB/PTHF	*o*-NPOE (10)	53.2 mV dec^{-1} log $K^{pot}_{H, Na}$ -6.2 (n = 1)	45.3 ± 0.7 mV dec^{-1} log $K^{pot}_{H, Na}$ -6.4 ± 0.2 (n = 3)	4F (H^+) and 4G (H^+)
Tecoflex	*o*-NPOE (10)	50.4 ± 1.7 mV dec^{-1} log $K^{pot}_{H, Na}$ -6.0 ± 0.0 (n = 3)	43.2 ± 0.6 mV dec^{-1} log $K^{pot}_{H, Na}$ -7.2 ± 0.2 (n = 6)	4L (H^+)

4.5 Nonactin

The ammonium ion was chosen as analyte ion since it plays a significant role in medicine, for example, as a component of blood.[85] Additionally, the ammonium content is important in environmental systems like rain water or river water.[86, 87]

ISEs based on the ammonium ionophore nonactin in the soft (PHB/PTHF 1:5) or the hard (PHB/PTHF 1:1) polyurethane matrix gave almost as good slopes and selectivities as the ones obtained with the corresponding PVC/DOS membranes, as shown in Table 4.5. The hydrogen ion selectivity of the polyurethane (PHB/PTHF) electrodes was one order of magnitude worse in comparison with the convential PVC/plasticizer electrodes.[88] This is a consequence of the pH sensitivity of the polyurethane matrix, as explained in Chapter 4.4.

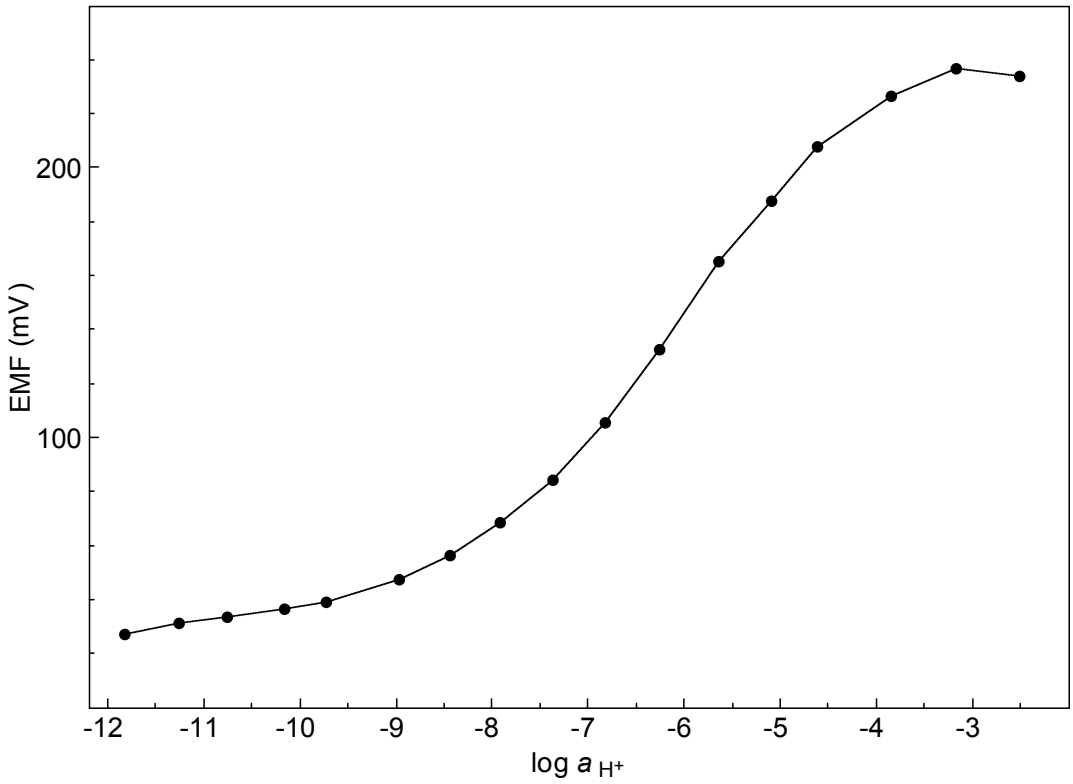

Figure 4.9 Response to H^+ of a membrane based on PHB/PTHF, *o*-NPOE, immobilized *N*-butyldiethanolamine, and NaTFPB (membrane type 4F (H^+)). The sample contained 0.01 M NaCl, HCl and 3 x 10^{-3} M Tris. The titration solution was 0.01 M NaOH and 3 x 10^{-3} M Tris.

4.6 Membranes with Two Ionophores

Membranes containing two ionophores were used for experiments with double membranes, as described in the following paragraphs. The composition of the inner filling solution was optimized in order that the phase boundary potential between the membrane with two ionophores and the inner solution was dominated by the pH of the inner solution. The pH response behavior of such an ISE which contained nonactin and immobilized bis-2,6-hydroxymethyl pyridine is shown in Figure 4.10. Electrodes of this type were only sensitive to hydrogen ions in the acidic pH range.[89, 90] In fact, the complex formation constant of bis-2,6-hydroxymethyl pyridine with H^+ is larger than the one of nonactin with NH_4^+.[91] The selectivity coefficient determined from these measurements (log $K^{pot}_{H, NH4}$ -1.4) was almost the same as the one for a membrane which contained only the pH ionophore (log $K^{pot}_{H, NH4}$ -1.8).

Table 4.5 Lower detection limits, selectivity coefficients, and slopes obtained for ISEs based on the ammonium ionophore nonactin and a lipophilic anionic additive. The mean values and standard deviations were calculated from data for three identical electrodes.

polymer matrix	PHB/PTHF 1:5	PHB/PTHF 1:5	PHB/PTHF 1:1	PVC/DOS
membrane type	4O (NH_4^+)	4O (NH_4^+)	4P (NH_4^+)	4Q (NH_4^+)
slope (mV dec^{-1})	52.7 ± 1.1	52.7 ± 1.1	57.1 ± 0.8	55.9 ± 0.1
lower detection limit (M)	$10^{-5.8}$	$10^{-5.8}$	$10^{-7.3}$	$10^{-6.7}$
method to determinate the selectivity coefficients	SSM	FIM	SSM	–
log $K^{pot}_{NH4,\ K}$	-0.4	–	-0.5 ± 0.2	–
slope (mV dec^{-1})	(53.1)		(51.9 ± 1.2)	
log $K^{pot}_{NH4,\ H}$	-1.8 ± 0.2	-1.3 ± 0.1	-1.8 ± 0.1	–
slope (mV dec^{-1})	(53.7 ± 1.4)	(60.6 ± 1.3)	(52.2 ± 0.9)	
log $K^{pot}_{NH4,\ Na}$	-2.6	–	-2.6 ± 0.2	–
slope (mV dec^{-1})	(50.9)		(55.9 ± 1.0)	
log $K^{pot}_{NH4,\ Li}$	–	–	-3.5 ± 0.3	–
slope (mV dec^{-1})			(57.6 ± 3.1)	
log $K^{pot}_{NH4,\ Ca}$	-4.6	–	-4.4 ± 0.1	–
slope (mV dec^{-1})	(24.3)		(32.4 ± 0.5)	
log $K^{pot}_{NH4,\ Mg}$	–	–	-3.6 ± 0.1	–
slope (mV dec^{-1})			(29.2 ± 0.7)	

Figure 4.11 shows the response curves of ISEs with a membrane based on nonactin and immobilized *N*-butyldiethanolamine. Keeping the pH constant during a successive dilution of a 0.1 M K^+ solution resulted in a pronounced potential change after the first dilution step only (curve C in Figure 4.11). In contrast, during pH calibration measurements in samples with a constant Tris background, a continuous potential change over a wide pH range was observed (curve B in Figure 4.11). Accordingly, the studied ISEs turn out to be much more sensitive to H^+ than to K^+. It is reported that nonactin forms complexes with protonated Tris, which conforms to the observed selectivity coefficients (log $K^{pot}_{NH4,\ Tris}$ -3.2).[92-94] Hence, the increased

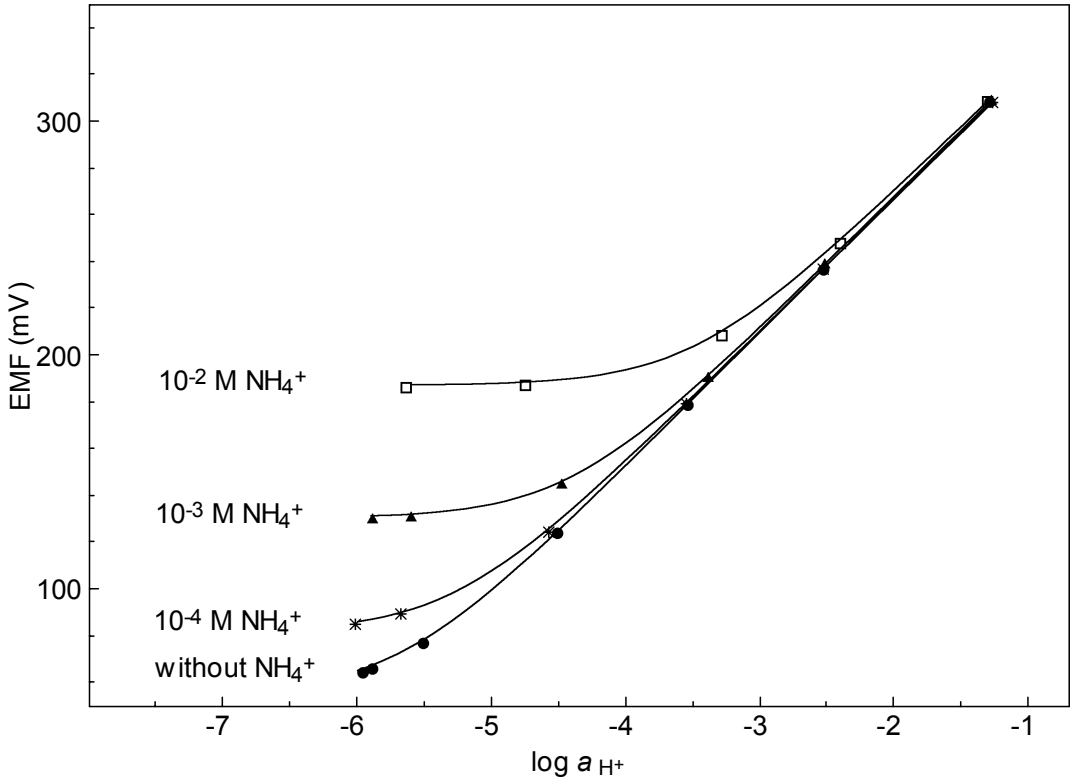

Figure 4.10 pH response curves of PHB/PTHF membranes containing the immobilized H^+ carrier bis-2,6-hydroxymethyl pyridine, nonactin/monactin as ammonium ionophore, and the lipophilic anionic additive NaTFPB (membrane type 4R (H^+)). The measurements were performed in HCl solutions with different NH_4^+ backgrounds.

slope between pH 8.5 - 10 may be due to the deprotonation of Tris, which has a pH dissociation constant of 8.1 in water. A pH calibration in samples with a constant 0.01 M K^+ background yielded a lower detection limit around pH 8 caused by cation interference, as depicted in curve A of Figure 4.11. It should be noted that nonactin may also complex protonated *N*-butyldiethanolamine, but the respective complex formation constant is presumably much smaller than the one of nonactin with ammonium ion.

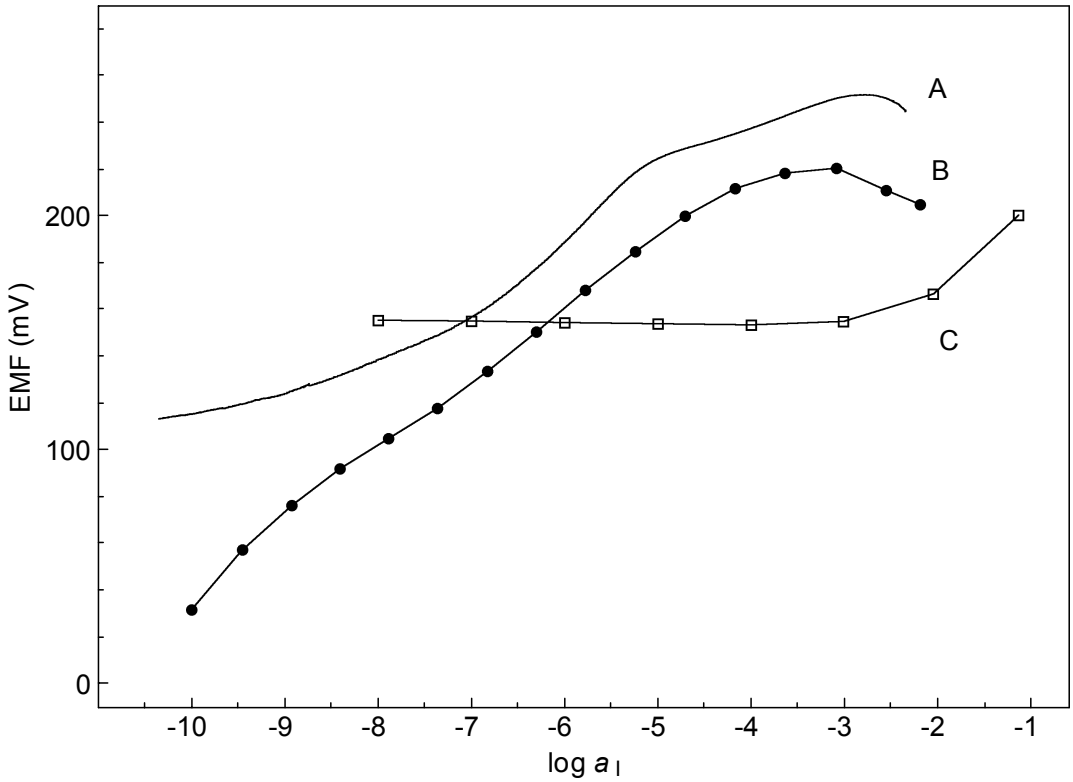

Figure 4.11 Response curves of PHB/PTHF membranes containing the immobilized H^+ carrier *N*-butyldiethanolamine, the lipophilic anionic additive NaTFPB, and in addition nonactin/monactin as ammonium ionophore (membrane type 4S (H^+)). The calibrations were performed in Tris solutions using the following titration procedures: A: addition of KOH to an acidic solution; B: addition of HCl to a basic solution; C: potassium calibration at a constant pH of 6.7.

In order to improve the electrode performance, the salt tetradodecylammonium tetrakis-(4-chlorophenyl)borate (ETH 500) with a lipophilic anion and a lipophilic cation was added to the membrane. ETH 500 is know to significantly reduces the resistivity of Tecoflex based membranes without plasticizer.[95, 96] ISEs made of membranes containing either two ionophores (with and without ETH 500) or only one carrier (*N*-butyldiethanolamine) were all found to be rather unselective for potassium,

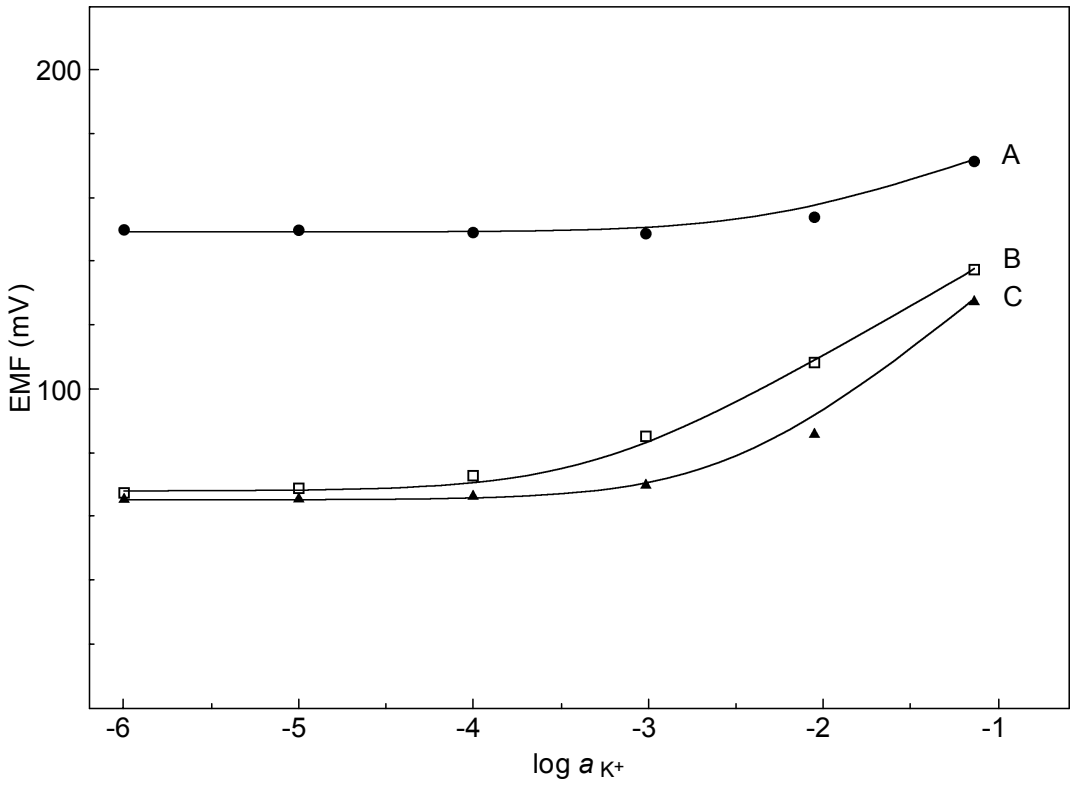

Figure 4.12 Potassium calibrations of PHB/PTHF membranes containing the lipophilic anionic additive NaTFPB and different ionophores: A: *N*-butyldiethanolamine and nonactin (membrane type 4T (H^+)); B: *N*-butyldiethanolamine, nonactin, and in addition the lipophilic salt ETH 500 (membrane type 4U (H^+)); C: *N*-butyldiethanolamine (membrane type 4V (H^+)). A Tris buffer was used to keep the pH at a constant value of 8.1.

as shown in Figure 4.12. The pH response curves of these ISEs are illustrated in Figure 4.13. The electrodes with two ionophores and ETH 500 (Figure 4.13, curve B) showed a large linear measuring range in comparison with the ones without ETH 500 (Figure 4.13, curve A). This improvement was due to ETH 500, which increases the ionic strength and the charge transfer within the membrane.

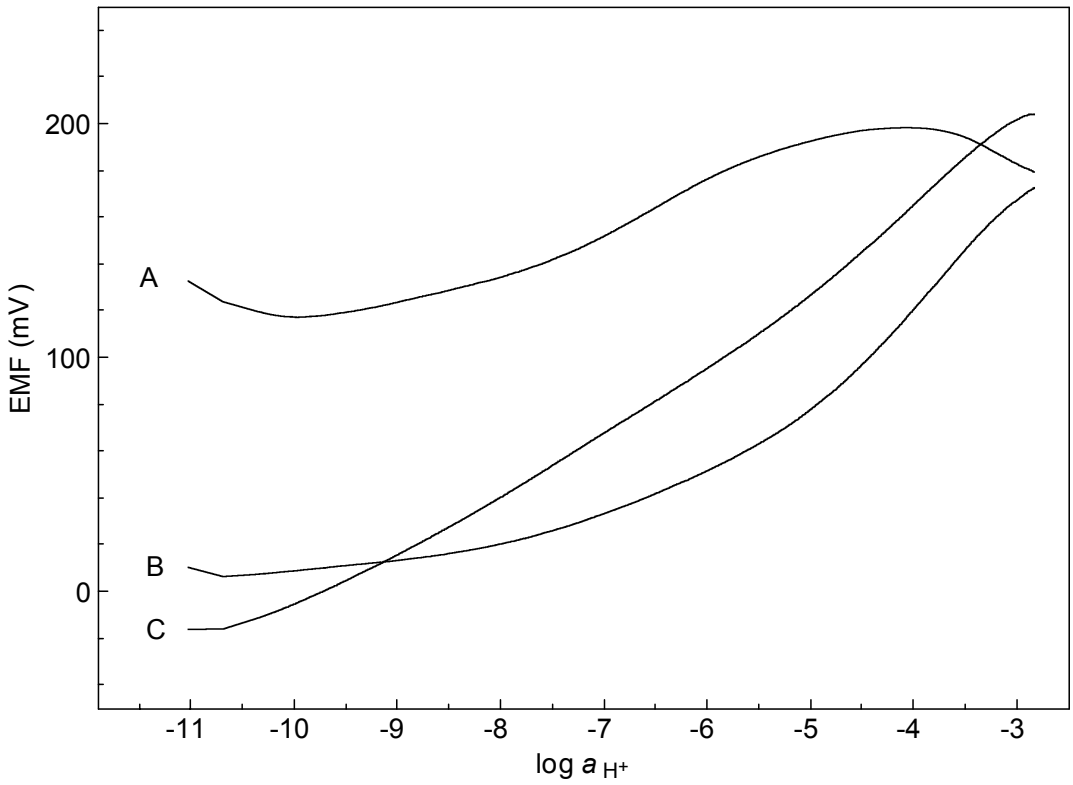

Figure 4.13 pH response curves of PHB/PTHF membranes containing the lipophilic anionic additive NaTFPB and different ionophores: A: *N*-butyldiethanolamine and nonactin (membrane type 4T (H^+)); B: *N*-butyldiethanolamine, nonactin, and in addition the lipophilic salt ETH 500 (membrane type 4U (H^+)); C: *N*-butyldiethanolamine (membrane type 4V (H^+)). The sample solutions consisted of phosphate buffers with a constant concentration of 0.002 M potassium.

4.7 Double Membranes in Measuring Cells

In this work, a double membrane is utilized as novel method to improve the stability of the interfacial potential between liquid membrane and solid inner device of CHEMFETs. At present, instabilities are usually observed that are mainly caused by interfering CO_2 or by samples with different pH. The following equations describe the potential response of such a double membrane electrode. The outer membrane of this double membrane in contact with the sample contains the ion-carrier L. The inner membrane of this double membrane contacting the inner solution carries in addition to L a covalently bound hydrogen ion-selective ionophore C. If the complex formation constant of C with H^+ is much larger than the one of L with I^+ or J^+,[91] the phase boundary potential between membrane and inner solution is predominately determined by the pH of the inner solution. Consequently, the potential of a reference electrode placed in the inner solution of the double membrane electrode and measured versus an external reference electrode, can be described as follows:

$$E = E_1^0 + E_{J(sample)} - E_{J(inner-solution)} + \frac{RT}{z_i F}\ln\left(a'_i + \sum_{j\neq i} K_{ij}^{pot} a'^{z_i/z_j}_j\right) - \frac{RT}{F}\ln\left(a''_H + \sum_{j\neq H} K_{Hj}^{pot} a''^{1/z_j}_j\right) \tag{4.5}$$

where $E_{J(sample)}$ is the liquid-junction potential for the reference electrode in the sample, $E_{J(inner\text{-}solution)}$ is the liquid-junction potential for the reference electrode in the inner solution, E_1^0 is the sum of all constant potential contributions of the ISE cell, a''_H is the hydrogen ion activity in the inner solution. K_{ij}^{pot} and K_{Hj}^{pot} are the selectivity coefficients of the outer and the inner membrane, respectively. The potential of a pH electrode introduced in the inner solution and measured versus the external reference electrode can be described by equation 4.6:

$$E = E_1^0 + E_{J(sample)} + \frac{RT}{z_i F}\ln\left(a'_i + \sum_{j\neq i} K_{ij}^{pot} a'^{z_i/z_j}_j\right) - \frac{RT}{F}\ln\left(a''_H + \sum_{j\neq H} K_{Hj}^{pot} a''^{1/z_j}_j\right) + \frac{RT}{F}\ln\left(a''_H + \sum_{j\neq H} \overline{K}_{Hj}^{pot} a''^{1/z_j}_j\right) \tag{4.6}$$

where $\overline{K}_{Hj}^{pot}$ is the selectivity coefficient of the pH electrode. If the activity a''_H predominates in the last two logarithmic terms, equation 4.6 further reduces to:

$$E = E_1^0 + E_{J(sample)} + \frac{RT}{z_i F} \ln\left(a_i' + \sum_{j \neq i} K_{ij}^{pot} a_j'^{z_i/z_j} \right) \qquad (4.7)$$

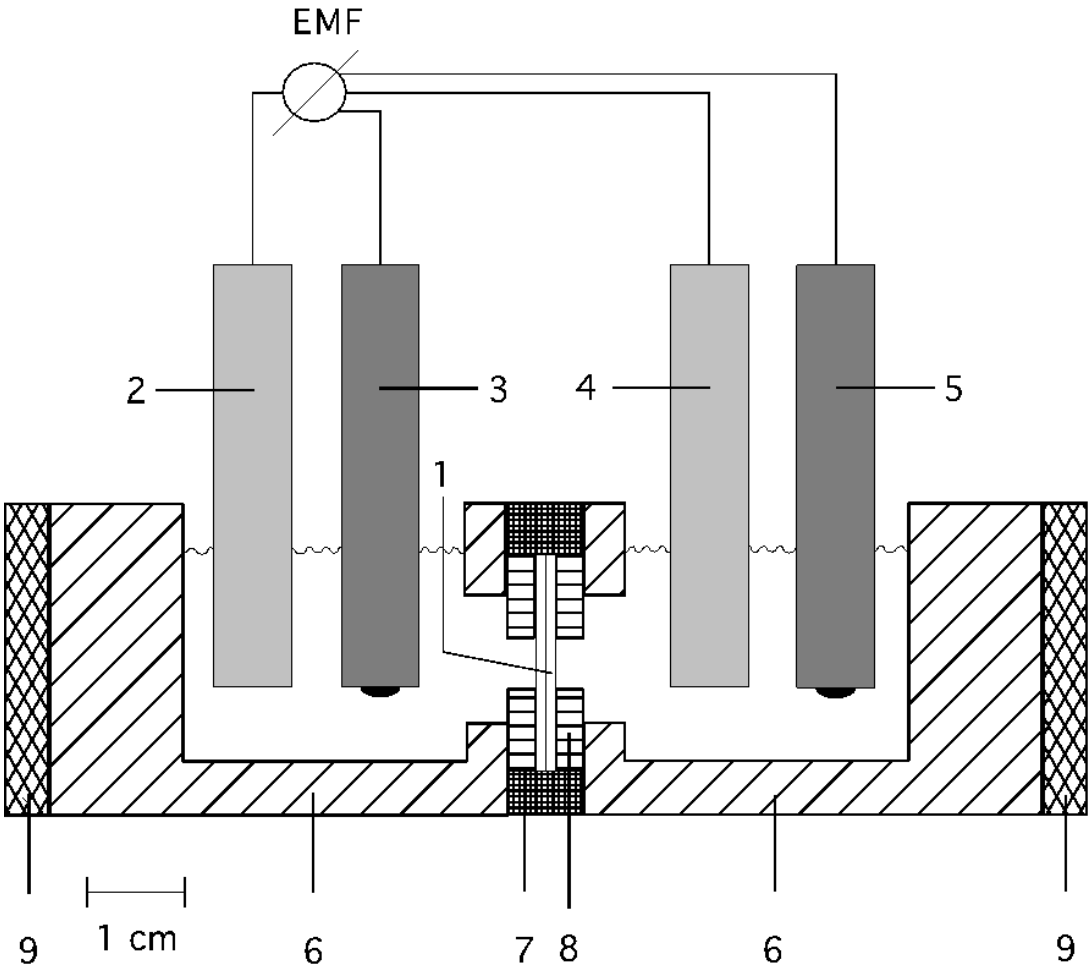

Figure 4.14 Schematic diagram of the measuring cell: 1: double membrane (asymmetric membrane); 2: reference electrode in the sample; 3: pH glass electrode in the sample; 4: reference electrode in the inner solution; 5: pH glass electrode in the inner solution; 6: cell body made from Teflon; 7: outer membrane holder; 8: inner membrane holder made from PVC; 9: cell holder.

This propagated response mechanism of the double membrane was verified in the following experiments using the measuring cell shown in Figure 4.14.[69, 97] The outer membrane of the double membrane in contact with the sample contained nonactin, whereas the inner membrane contacting the inner solution contained nonactin and covalently bound bis-2,6-hydroxymethyl pyridine. To control the inner electrolyte solution with a pH glass electrode and a reference electrode, the double membrane was built into a symmetric measuring cell. The potential at the interface between membrane and inner solution should be dtermined by the pH of the inner solution according to the results in Figure 4.10.

Figure 4.15 shows the electromotoric force responses to varying pH values of the inner solution for ISEs that are based on double membranes with bis-2,6-hydroxymethyl pyridine as pH ionophore in the inner membrane. The potential of the pH glass electrode in the inner solution versus the external reference electrode was nearly constant in the pH range 1 - 3.8. In contrast, the inner reference electrode versus the outer reference electrode gave a distinct response with a negative, nearly Nernstian, slope in the same pH range. These results are in good accordance with the proposed theoretical model (equations 4.5 – 4.7).

The perfectly parallel curves A and B in Figure 4.16 illustrate that the pH of the inner solution was constant during an ammonium ion calibration in the sample. This behavior agrees with the findings according to equations 4.5 and 4.7. The same experimental results were obtained with double membranes, whose inner membrane contained *N*-butyldiethanolamine, nonactin, and ETH 500 (membrane type 4W (double)). In the latter measurements, the slope of the pH glass electrode in the inner solution was found to be 60.3 mV dec^{-1}, and the inner reference electrode showed a slope of 61.1 mV dec^{-1}.

The selectivity coefficients of ISEs based on double membranes (Table 4.6) were comparable with those of normal ISEs containing only nonactin (Table 4.5). An exception was the poor selectivity of the double membrane with respect to hydrogen ions. Repeated measurements with the same membrane over a period of two months always resulted in nearly the same selectivity coefficient for H^+. Accordingly, there was no detectable diffusion of the hydrogen ion-selective ionophore from the inner membrane into the outer membrane during this period. This is a convincing proof for the durable immobilization of the ionophore by covalent attachment to the

polyurethane matrix. The selectivity coefficients obtained by the SSM were the same as the ones using the FIM.

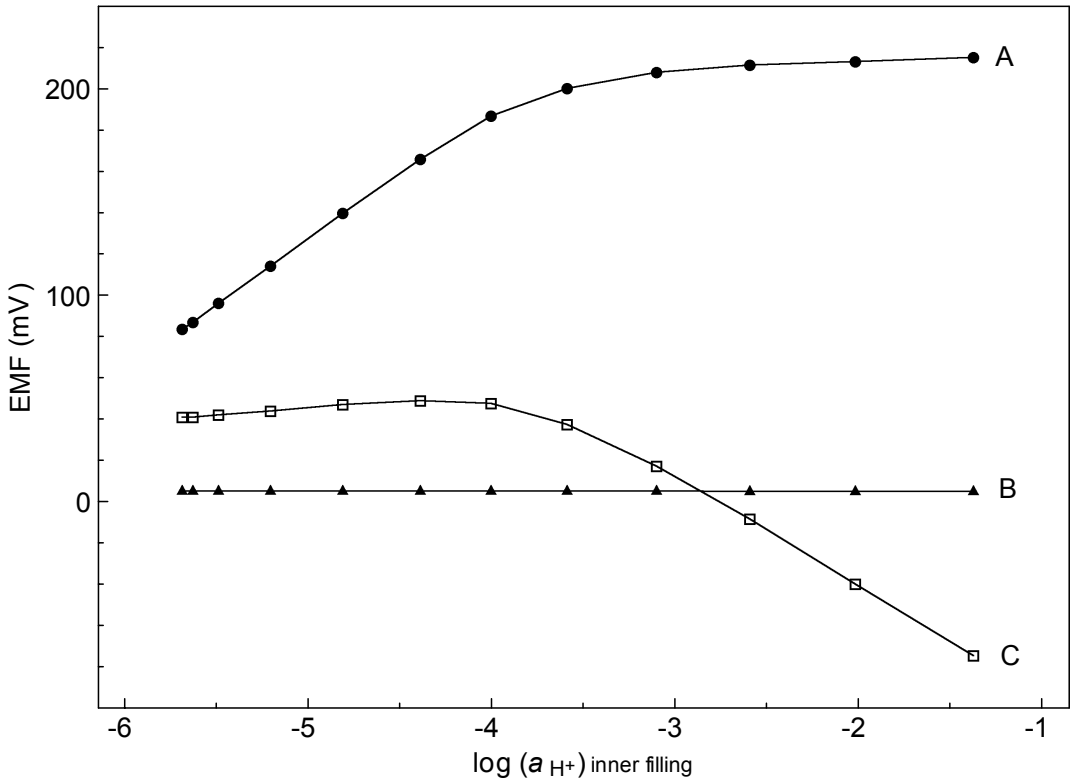

Figure 4.15 Response curves measured for a cell with a PHB/PTHF double membrane (Figure 4.14) as a function of the pH value of the inner solution. The outer membrane in contact with the sample solution contained nonactin and NaTFPB, and the inner membrane contained nonactin, NaTFPB, and covalently bound bis-2,6-hydroxymethyl pyridine (membrane type 4X (double)). A: pH glass electrode in the inner solution versus reference electrode in the sample, 4.0 mV dec^{-1} (pH 1.3 – 3.2); B: pH glass electrode versus reference electrode in the sample, which measured pH 7.1; C: reference electrode in the inner solution versus reference electrode in the sample, -53.2 mV dec^{-1} (pH 1.3 – 3.2).

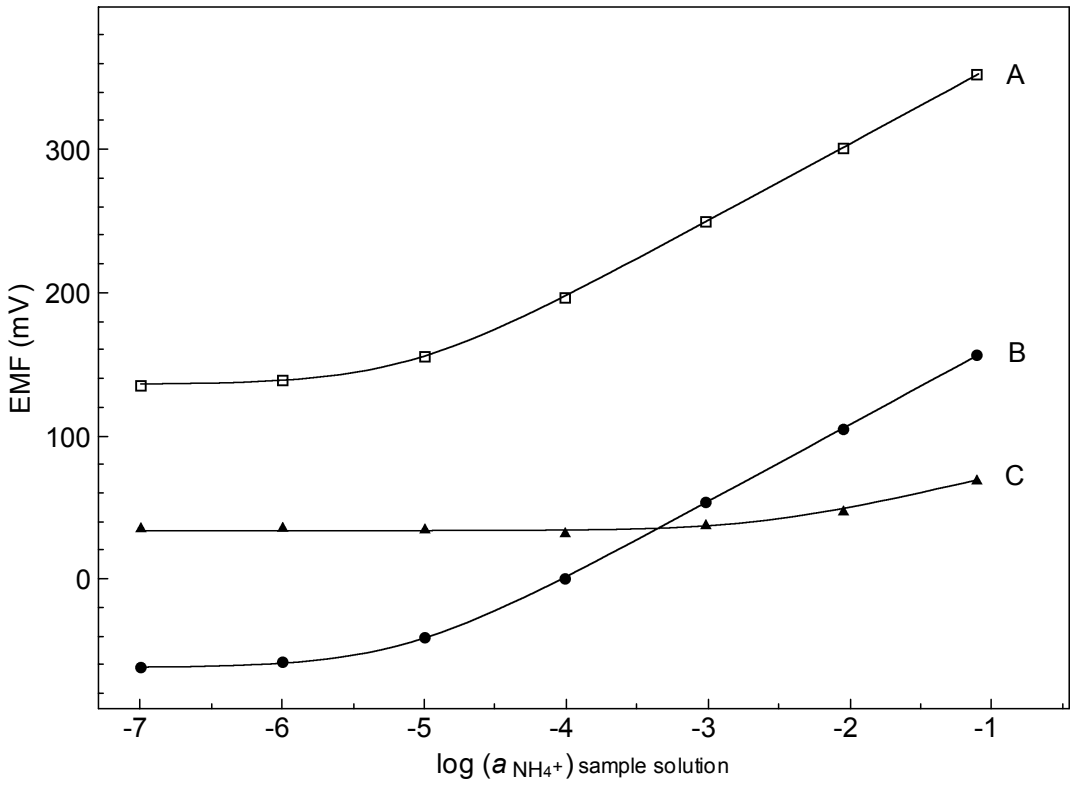

Figure 4.16 Response curves measured for a cell with a PHB/PTHF double membrane (Figure 4.14) as a function of the logarithm of the ammonium ion activity in the sample solution. The outer membrane in contact with the sample solution contained nonactin and NaTFPB, and the inner membrane contained nonactin, NaTFPB, and covalently bound bis-2,6-hydroxymethyl pyridine (membrane type 4X (double)). A: pH glass electrode in the inner solution versus reference electrode in the sample, 54.9 mV dec^{-1}; B: reference electrode in the inner solution versus external reference electrode, 55.4 mV dec^{-1}; C: pH glass electrode versus reference electrode in the sample, for which a pH range of 5.8 – 6.6 was measured.

Table 4.6 Selectivity coefficients of a PHB/PTHF double membrane (measuring cell according to Figure 4.14), as obtained from measurements with different sample solutions. The outer membrane in contact with the sample contained nonactin and NaTFPB, and the inner membrane in contact with the inner solution contained nonactin, NaTFPB, and immobilized bis-2,6-hydroxymethyl pyridine (membrane type 4X (double)). Mean values and standard deviations were calculated from measurements on three identical membranes.

interfering ion	K^+	H^+	Na^+	Ca^{2+}
log $K^{pot}_{NH4,\ J}$	-0.5 ± 0.1	-1.0 ± 0.2	-2.2 ± 0.1	-3.8 ± 0.3
slope (mV dec^{-1})	49.2 ± 3.6	54.0 ± 2.8	47.3 ± 2.9	21.4 ± 3.1
method to determinate the selectivity coefficients	SSM	FIM	SSM	SSM

4.8 Conclusions

In summary, the selectivities of ISEs based on polyurethane (PHB/PTHF) were shown to be comparable to the ones obtained for ISEs made from plasticized PVC matrices. However, polyurethane membranes generally exhibited a poorer selectivity with respect to hydrogen ions.

Immobilized H^+-selective ionophores were tested in ISEs with different polymer matrices. The durable immobilization of the ionophores by covalent attachment to the polyurethane matrix was confirmed by long-term diffusion experiments. Polyurethane-based electrodes showed sub-Nernstian slopes because of a high membrane resistance. The addition of plasticizer or ETH 500 resulted in greatly improved slopes, as in the case of conventional PVC/DOS electrodes. ISEs made from these optimized membranes may be highly useful for various biomedical applications. Firstly, in vitro and in vivo evaluations showed a high biocompatibility of these polyurethanes.[61, 62] Secondly, there is no problem of intoxication of the sample solution by plasticizer leaching from the membrane since the present polymers

have "self-plasticizing" properties. Finally, the covalent binding of the ionophore should result in a prolonged lifetime of the ISEs.

The propagated novel response mechanism of a double membrane was verified by experiments performed on liquid-contacted ISEs. Particularly exciting is the compensation for the effect of pH changes in the inner solution by the inner phase boundary potential of the new membrane electrodes. In Chapter 5, the application of the double membrane for the realization of CHEMFETs with improved response stability is described.

References

(1) Lindner, E.; Buck, R. P. Microfabricated Potentiometric Electrodes and Their In Vivo Applications. *Anal. Chem.* **2000**, 336 A-345 A.

(2) Madou, M. J.; Morison, S. R. *Chemical Sensing with Solid State Devices*; Academic Press: Boston, 1989.

(3) Lindner, E.; Cosofret, V. C.; Nahir, T. M.; Buck, R. P. Characterization of Stability of Modified Poly(vinyl chloride) Membranes for Microfabricated Ion-Selective Electrode Arrays in Biomedical Applications. *Diagnostic Biosensor Polymers, ACS Symposium Series* **1993,** *556*, 149-157.

(4) Cosofret, V. V.; Erdosy, M.; Johnson, T. A.; Buck, R. P.; Ash, R. B.; Neuman, M. R. Microfabricated Sensor Arrays Sensitive to pH and K^+ for Ionic Distribution Measurements in the Beating Heart. *Anal. Chem.* **1995,** *67*, 1647-1653.

(5) Lindner, E.; Cosofret, V. V.; Richard, P. B.; Johnson, T. A.; Ash, R. B.; Neumann, M. R.; Kao, W. J.; Anderson, J. M. Electroanalytical and Biocompatibility Studies on Microfabricated Array Sensors. *Electroanalysis* **1995,** *7*, 864-870.

(6) Cosofret, V. V.; Olson, W. W.; Marzouk, S. A. M.; Erdosy, M.; Johnson, T. A.; Buck, R. P. Calcium Selective Polymeric Membranes for Microfabricated Sensor Arrays. *Anal. Lett.* **1996,** *29*, 725-743.

(7) Uhlig, A.; Lindner, E.; Teutloff, C.; Schnakenberg, U.; Hintsche, R. Miniaturized Ion-Selective Chip Electrode for Sensor Application. *Anal. Chem.* **1997,** *69*, 4032-4038.

(8) Lundström, I.; van den Berg, A.; van der Schoot, B. H.; van den Vlekkert, H. H.; Armgarth, M.; Nylander, C. J. In *Chemical and Biochemical Sensors: Part I*; Göpel, W., Jones, T. A., Kleitz, M., Lundström, J., Seiyama, T., Eds.; VCH: Weinheim, 1991; Vol. 2, pp 467-528.

(9) Bergveld, P.; Sibbald, A. *Analytical and Biomedical Applications of Ion-Selective Field-Effect Transistors*; Elsevier: Amsterdam, 1988.

(10) Fogt, E. J.; Untereker, D. F.; Norenberg, M. S.; Meyerhoff, M. E. Response of Ion-Selective Field Effect Transistors to Carbon Dioxide and Organic Acids. *Anal. Chem.* **1985,** *57*, 1995-1998.

(11) Janata, J. Twenty Years of Ion-Selective Field-Effect Transistors. *Analyst (Cambridge, U.K.)* **1994,** *119*, 2275-2278.

(12) Schöning-Hammer, A., Personal Communication, Zurich, 1998.

(13) Püntener, M., Doctoral Dissertation in Preparation, ETH, Zurich.

(14) Hammer, A.; Gloor-Értékes, D.; Reichmuth, P.; Pretsch, E.; Morf, W. E.; de Rooij, N. F. *Chemical Sensors Based on Novel Polyurethane Membranes with Covalently Bound Ion-Selective Components*: Proceedings of the 9th International Conference on Modern Materials and Technologies; Florence, Italy, 1999.

(15) Sze, S. M. *Physics of Semiconductor Devices*, 2nd ed.; Wiley: New York, 1981.

(16) Reinhoudt, D. N. Durable Chemical Sensors Based on Field-Effect Transistors. *Sens. Actuators, B* **1995,** *24-25*, 197-200.

(17) Reinhoudt, D. N.; Cobben, P. L. H. M. In *Dechema-Monographien Band*; VCH Verlagsgesellschaft, 1992; Vol. Band 126, pp 219-236.

(18) de Rooij, N. F.; van den Vlekkert, H. H. In *Chemical Sensor Technology*; Yamazoe, N., Ed.; Kodansha and Elsevier: Tokyo, 1991; Vol. 3, pp 213-231.

(19) van der Wal, P.; de Rooij, N. F.; Koudelka-Hep, M. *Covalently Bound Plasticized PVC Membranes for Solid State Ion-Selective Devices*: Proceedings of the 196th Meeting of The Electrochemical Society, Inc. - Chemical Sensors IV; Honolulu, Hawaii, 1999.

(20) Högg, G.; Lutze, O.; Cammann, K. Novel Membrane Material for Ion-Selective Field-Effect Transistors with Extended Lifetime and Improved Selectivity. *Anal. Chim. Acta* **1996,** *335*, 103-109.

(21) Sandifer, J. R. Theory of Interfacial Potential Differences: Effects of Adsorption onto Hydrated (Gel) and Nonhydrated Surfaces. *Anal. Chem.* **1988,** *60*, 1553-1562.

(22) van den Berg, A. Ion Sensors Based on ISFET's with Synthetic Ionophores, Doctoral Dissertation, University of Twente, 1988.

(23) Li, X.; Verpoorte, E. M. J.; Harrison, D. J. Elimination of Neutral Species Interferences at the Ion-Sensitive Membrane/Semiconductor Device Interface. *Anal. Chem.* **1988,** *60*, 493-498.

(24) Mostert, I. A. Theoretische und experimentelle Untersuchungen an potentiometrischen Sensoren für Gase und Bicarbonat, Doctoral Dissertation No. 7776, ETH, Zurich, 1985.

(25) Crank, J. *The Mathematics of Diffusion*, 2nd ed.; Oxford University Press: New York, 1993.

(26) Sudhölter, E. J. R.; van der Wal, P. D.; Skowronska Ptasinska, M.; van den Berg, A.; Bergveld, P.; Reinhoudt, D. N. Modification of ISFETs by Covalent Anchoring of Poly(hydroxyethylmethacrylate) Hydrogel: Introduction of a Thermodynamically Defined Semiconductor-Sensing Membrane Interface. *Anal. Chim. Acta* **1990,** *230*, 59-65.

(27) van der Wal, P. D.; Skowronska Ptasinska, M.; van den Berg, A.; Bergveld, P.; Sudhölter, E. J. R.; Reinhoudt, D. N. New Membrane Materials for Potassium-

Selective Ion-Sensitive Field-Effect Transistors. *Anal. Chim. Acta* **1990,** *231*, 41-52.

(28) Reinhoudt, D. N.; Engbersen, J. F. J.; Brzózka, Z.; van den Vlekkert, H. H.; Honig, G. W. N.; Holterman, H. A. J.; Verkerk, U. H. Development of Durable K^+-Selective Chemically Modified Field Effect Transistors with Functionalized Polysiloxane Membranes. *Anal. Chem.* **1994,** *66*, 3618-3623.

(29) Stauthamer, W. P. R. V.; Engbersen, J. F. J.; Verboom, W.; Reinhoudt, D. N. Influence of Plasticizer on the Selectivity of Nitrate-Sensitive CHEMFETs. *Sens. Actuators, B* **1994,** *17*, 197-201.

(30) Brzozka, Z.; Dawgul, M.; Pijanowska, D.; Torbicz, W. Durable NH_4^+-Sensitive CHEMFET. *Sens. Actuators, B* **1997,** *44*, 527-531.

(31) Park, L. S.; Hur, Y. J.; Sohn, B. K. Effect of Membrane Structure on the Performance of Field-Effect Transistor Potassium-Sensitive Sensor. *Sens. Actuators, A* **1996,** *57*, 239-243.

(32) Cadogan, A.; Gao, Z.; Lewenstam, A.; Ivaska, A.; Diamond, D. All-Solid-State Sodium-Selective Electrode Based on a Calixarene Ionophore in a Poly(vinyl chloride) Membrane with a Polypyrrole Solid Contact. *Anal. Chem.* **1992,** *64*, 2496-2501.

(33) Hauser, P. C.; Chiang, D. W. L.; Wright, G. A. A Potassium-Ion Selective Electrode with Valinomycin Based Poly(vinyl Chloride) Membrane and a Poly(vinyl Ferrocene) Solid Contact. *Anal. Chim. Acta.* **1995,** *302*, 241-248.

(34) Fibbioli, M.; Bandyopadhyay, K.; Liu, S. G.; Echegoyen, L.; Enger, O.; Diederich, F.; Bühlmann, P.; Pretsch, E. Redox-Active Self-Assembled Monolayers as Novel Solid Contacts for Ion-Selective Electrodes. *Chem. Commun.* **2000**, 339-340.

(35) Miyahara, Y.; Yamashita, K.; Ozawa, S.; Watanabe, Y. Shift and Drift of Electromotive Forces of Solid-State Electrodes with Ion-Selective Liquid Membranes. *Anal. Chem. Acta* **1996,** *331*, 85-95.

(36) Walsh, S.; Diamond, D.; McLaughlin, J.; McAdams, E.; Woolfson, D.; Jones, D.; Bonner, M. Solid-State Sodium-Selective Sensors Based on Screen-Printed Ag/AgCl Reference Electrodes. *Electroanalysis* **1997,** *9*, 1318-1324.

(37) Bobacka, J. Potential Stability of All-Solid-State Ion-Selective Electrodes Using Conductive Polymers as Ion-to-Electron Transfer. *Anal. Chem.* **1999,** *71*, 4932-4937.

(38) Bobacka, J.; Lindfors, T.; McCarrick, M.; Ivaska, A.; Lewenstam, A. Single-Piece All-Solid-State Ion-Selective Electrode. *Anal. Chem.* **1995,** *67*, 3819-3823.

(39) Momma, T.; Komaba, S.; Yamamoto, M.; Osaka, T.; Yamauchi, S. All-Solid-State Potassium-Selective Electrode Using Double-Layer Film of Polypyrrole/Polyanion Composite and Plasticized Poly(vinyl chloride) Containing Valinomycin. *Sensors and Actuators B* **1995,** *24-25*, 724-728.

(40) Liu, D.; Meruva, R. K.; Brown, R. B.; Meyerhoff, M. E. Enhancing EMF Stability of Solid-State Ion-Selective Sensors by Incorporating Lipophilic Silver-Ligand Complexes within Polymeric Films. *Anal. Chim. Acta* **1996,** *321*, 173-183.

(41) Diaz, C.; Vidal, J. C.; Galban, J.; Urarte, M. L.; Lanaja, J. A Double-Membrane Ion-Selective Electrode for the Potentiometric Determination of Potassium. *Microchem. J.* **1989,** *39*, 289-297.

(42) Espadas-Torre, C.; Oklejas, V.; Mowery, K.; Meyerhoff, M. E. Thromboresistant Chemical Sensors Using Combined Nitric Oxide Release/Ion Sensing Polymeric Films. *J. Am. Chem. Soc.* **1997,** *119*, 2321-2322.

(43) Liu, D.; Meyerhoff, M. E.; Goldberg, H. D.; Brown, R. B. Potentiometric Ion-Selective and Bioselective Electrodes Based on Asymmetric Polyurethane Membranes. *Anal. Chim. Acta* **1993,** *274*, 37-46.

(44) Sakong, D. S.; Cha, M. J.; Shin, J. H.; Cha, G. S.; Ryu, M. S.; Hower, R. W.; Brown, R. B. Asymmetric Membrane-Based Potentiometric Solid-State Ion Sensors. *Sens. Actuators, B* **1996,** *32*, 161-166.

(45) Shin, J. H.; Yoon, S. Y.; Yoon, I. J.; Choi, S. H.; Lee, S. D.; Nam, H.; Cha, G. S. Potentiometric Biosensors Using Immobilized Enzyme Layers Mixed with Hydrophilic Polyurethane. *Sens. Actuators, B* **1998,** *50*, 19-26.

(46) Jung, S.-K. W., George S. Polymeric Mercaptosilane-Modified Platinum Electrodes for Elimination of Interferants in Glucose Biosensors. *Anal. Chem.* **1996,** *68(4)*, 591-596.

(47) Kyrolainen, M.; Reddy, S. M.; Vadgama, P. M. Blood Compatibility and Extended Linearity of Lactate Enzyme Electrode Using Poly(vinyl Chloride) Outer Membranes. *Anal. Chim. Acta* **1997,** *353*, 281-289.

(48) Sekiguchi, T.; Nagai, Y.; Makino, T.; Ohno, K.; Nakamura, M.; Hosaka, H.; Sakio, H. S. B.; Ohtsu, S.; Takahashi, H. Gastric P-CO_2 Monitoring System Based on a Double Membrane Type P-CO_2 Sensor. *Sens. Actuators, B* **1998,** *49*, 171-178.

(49) Brunink, J. A. J.; Lugtenberg, R. J. W.; Brzozka, Z.; Engbersen, J. F. J.; Reinhoudt, D. N. The Design of Durable Na^+-Selective CHEMFETs Based on Polysiloxane Membranes. *J. Electroanal. Chem.* **1994,** *378*, 185-200.

(50) Antonisse, M. M. G.; Lugtenberg, R. J. W.; Egberink, R. J. M.; Engbersen, J. F. J.; Reinhoudt, D. N. Durable Nitrate-Selective Chemically Modified Field Effect Transistors Based on New Polysiloxane Membranes. *Anal. Chim. Acta* **1996,** *332*, 123-129.

(51) Tsujimura, Y.; Sunagawa, T.; Yokoyama, M.; Kimura, K. Sodium Ion-Selective Electrodes Based on Silicone-Rubber Membranes Covalently Incorporating Neutral Carriers. *Analyst (Cambridge, U.K.)* **1996,** *121*, 1705-1709.

(52) Lindner, E.; Cosofret, V. V.; Kusy, R. P.; Buck, R. P.; Rosatzin, T.; Schaller, U.; Simon, W.; Jeney, J.; Toth, K.; Pungor, E. Responses of Proton Selective Solvent Polymeric Membrane Electrodes Fabricated from Modified PVC Membranes. *Talanta* **1993,** *40*, 957-967.

(53) Rosatzin, T.; Holy, P.; Seiler, K.; Rusterholz, B.; Simon, W. Immobilization of Components in Polymer Membrane-Based Calcium-Selective Bulk Optodes. *Anal. Chem.* **1992,** *64*, 2029-2035.

(54) Daunert, S.; Bachas, L. G. Ion-Selective Electrodes Using an Ionophore Covalently Attached to Carboxylated Poly(vinyl Chloride). *Anal. Chem.* **1990,** *62*, 1428-1431.

(55) Ebdon, L.; Ellis, A. T.; Corfield, G. C. Ion-Selective Polymeric-Membrane Electrodes with Immobilized Ion-Exchanger Sites. *Analyst (Cambridge, U.K.)* **1982,** *107*, 288-294.

(56) Heng, L. Y.; Hall, E. A. H. Producing "Self-Plasticizing" Ion-Selective Membranes. *Anal. Chem.* **2000,** *72*, 42-51.

(57) Galiatsatos, C. H., Kiamars; Mark, James E.; Heineman, William R. A New Method for Enzyme Membrane Preparation Based on Polyurethane Technology. Electrode Modification for Sensor Development. *Biosensors* **1989,** *4(6)*, 393-402.

(58) Lugtenberg, R. J. W.; Egberink, R. J. M.; van den Berg, A.; Engbersen, J. F. J.; Reinhoudt, D. N. The Effects of Covalent Binding of the Electroactive Components in Durable CHEMFET Membranes - Impedance Spectroscopy and Ion Sensitivity Studies. *J. Electroanal. Chem.* **1998,** *452*, 69-86.

(59) Cosofret, V. V.; Buck, R. P.; Erdosy, M. Carboxylated Poly(vinyl Chloride) as a Substrate for Ion Sensors: Effects of Native Ion Exchange on Responses. *Anal. Chem.* **1994,** *66*, 3592-3599.

(60) Cosofret, V. V.; Lindner, E.; Buck, R. P.; Kusy, R. P.; Whitley, J. Q. Electrochemical Characterization of Aminated PVC-Based Ion-Selective Membranes. *Electroanalysis* **1993,** *5*, 725-730.

(61) Saad, B.; Hirt, T. D.; Welti, M.; Uhlschmid, G. K.; Neuenschwander, P.; Suter, U. W. Development of Degradable Polyesterurethanes for Medical Applications: In Vitro and in Vivo Evaluations. *J. Biomed. Mater. Res.* **1997,** *36*, 65-74.

(62) Saad, B.; Ciardelli, G.; Matter, S.; Welti, M.; Uhlschmid, G. K.; Neuenschwander, P.; Suter, U. W. Cell Response of Cultured Macrophages, Fibroblasts, and Co-Cultures of Kupffer Cells and Hepatocytes to Particles of Short-Chain Poly[(R)-3-hydroxybutyric acid]. *J. Mater. Sci.: Mater. Med.* **1996,** *7*, 56-61.

(63) Hirt, T. Synthese und Charakterisierung neuer biokompatibler, abbaubarer und zäher Blockcopolymere auf der Basis von Polyesterurethanen, Doctoral Dissertation No. 11088, ETH, Zurich, 1995.

(64) Cha, G. S.; Liu, D.; Meyerhoff, M. E.; Cantor, H. C.; Midgley, A. R.; Goldberg, H. D.; Brown, R. B. Electrochemical Performance, Biocompatibility and Adhesion of New Polymer Matrices for Solid-State Ion Sensors. *Anal. Chem.* **1991,** *63*, 1666-1672.

(65) Hower, R. W.; Shin, J. H.; Cha, G. S.; Meruva, R. K.; Meyerhoff, M. E.; Brown, R. B. New Solvent System for the Improved Electrochemical Performance of Screen-Printed Polyurethane Membrane-Based Solid-State Sensors. *Sens. Actuators, B* **1996,** *33*, 168-172.

(66) Lindner, E.; Cosofret, V. V.; Ufer, S.; Buck, R. P.; Kao, W. J.; Neuman, M. R.; Anderson, J. M. Ion-Selective Membranes with Low Plasticizer Content: Electroanalytical Characterization and Biocompatibility Studies. *J. Biomed. Mater. Res.* **1994,** *28*, 591-601.

(67) Espadas-Torre, C.; Meyerhoff, M. E. Thrombogenic Properties of Untreated and Poly(ethylene oxide)-Modified Polymeric Matrices Useful for Preparing Intraarterial Ion-Selective Electrodes. *Anal. Chem.* **1995,** *67*, 3108-3114.

(68) Coury, A. J.; Slaikeu, P. C.; Cahalan, P. T.; Stokes, K. B.; Hobot, C. M. Factors and Interactions Affecting the Performance of Polyurethane Elastomers in Medical Devices. *J. Biomaterials Applications* **1988,** *3*, 130-179.

(69) Haase, E. A. Untersuchung der Wechselwirkungen zwischen ionenselektiven Flüssigmembranen und Messgut im Hinblick auf die kontinuierliche Erfassung von Kationen im Vollblut, Doctoral Dissertation No. 10453, ETH, Zurich, 1993.

(70) Jeon, J. S.; Sperline, R. P.; Raghavan, S. Quantitative Analysis of Adsorbed Serum Albumin on Segmented Polyurethane Using FT-IR/ATR Spectroscopy. *Appl. Spectrosc.* **1992,** *46*, 1644-1648.

(71) Yun, S. Y.; Hong, Y. K.; Oh, B. K.; Cha, G. S.; Nam, H.; Lee, S. B.; Jin, J. Potentiometric Properties of Ion-Selective Electrode Membranes Based on Segmented Polyether Urethane Matrices. *Anal. Chem.* **1997,** *69*, 868-873.

(72) Munoz, J.; Jimenez, C.; Bratov, A.; Bartroli, J.; Alegret, S.; Dominguez, C. Photosensitive Polyurethanes Applied to the Development of CHEMFET and ENFET Devices for Biomedical Sensing. *Biosens. Bioelectron.* **1997,** *12*, 577-585.

(73) Oesch, U.; Ammann, D.; Brzozka, Z.; Pham, H. V.; Pretsch, E.; Rusterholz, B.; Simon, W.; Suter, G.; Welti, D. H.; Xu, A. P. Design of Neutral Hydrogen-Ion Carriers for Solvent Polymeric Membrane Electrodes of Selected pH Range. *Anal. Chem.* **1986,** *58*, 2285-2289.

(74) Bakker, E.; Xu, A.; Pretsch, E. Optimum Composition of Neutral Carrier Based pH Electrodes. *Anal. Chim. Acta* **1994,** *295*, 253-262.

(75) Perrin, D. D.; Dempsey, B.; Serjeant, E. P. *pKa Prediction for Organic Acids and Bases*; Chapmann and Hall: London, 1981.

(76) Xu, A. Beitrag zur Entwicklung einer potentiometrischen pH-Magensonde auf der Basis von ionenselektiven Flüssigmembranelektroden, Doctoral Dissertation No. 9516, ETH, Zurich, 1991.

(77) Cosofret, V. V.; Erdosy, M.; Raleigh, J. S.; Johnson, T. A.; Neuman, M. R.; Buck, R. P. Aliphatic Polyurethane as a Matrix for pH Sensors: Effects of Native Sites and Added Proton Carrier on Electrical and Potentiometric Properties. *Talanta* **1996,** *43*, 143-151.

(78) Nägele, M.; Pretsch, E. New Method for Determining the Concentration of Ionic Impurities in Solvent Polymeric Membranes. *Mikrochim. Acta* **1995,** *121*, 269-279.

(79) Teo, L. S.; Kuo, J. F.; Chen, C. Y. Permeation and Sorption of CO_2 through Amine-Containing Polyurethane and Poly(urea-urethane) Membranes. *J. Appl. Polym. Sci.* **1996,** *59(10)*, 1627-38.

(80) Erne, D.; Schenker, K. V.; Ammann, D.; Pretsch, E.; Simon, W. Applicability of a Carrier Based Liquid Membrane pH Electrode to Measurements in Acidic Solutions. *Chimia* **1981,** *35*, 178-179.

(81) Lee, H. J.; Hong, U. S.; Lee, D. K.; Shin, J. H.; Nam, H.; Cha, G. S. Solvent-Processible Polymer Membrane-Based Liquid Junction-Free Reference Electrode. *Anal. Chem.* **1998,** *70*, 3377-3383.

(82) PuigLleixa, C.; Jimenez, C.; Fabregas, E.; Bartroli, J. Potentiometric pH Sensors Based on Urethane-Acrylate Photocurable Polymer Membranes. *Sens. Actuators, B* **1998,** *49*, 211-217.

(83) Thoma, R. J.; Tan, F. R.; Phillips, R. E. Ionic Interactions of Polyurethanes. *J. Biomaterial Applications* **1988,** *3*, 180-206.

(84) Jadhav, S.; Bakker, E. Acetic Acid Release from Polymeric Membrane pH Electrodes for Generating Local pH Gradients at Ion-Selective Membranes. *Electrochem. and Solid-State Letters* **1998,** *1*, 194-196.

(85) Meyerhoff, M. E.; Robins, R. H. Disposable Potentiometric Ammonia Gas Sensor for Estimation of Ammonia in Blood. *Anal. Chem.* **1980,** *52*, 2383-2387.

(86) Liu, R. M.; Sun, B. T. Determination of Ammonium by Using a Flow System with a Diffusion Cell Coupled to an Ammonium Ion-Selective Sensor. *Anal. Lett.* **1997,** *30*, 1255-1265.

(87) Senillou, A.; Jaffrezic-Renault, N.; Martelet, C.; Griffe, F. A Miniaturized Ammonium Sensor Based on the Integration of Both Ammonium and Reference FETs in a Single Chip. *Mater. Sci. Eng., C* **1998**, 59-63.

(88) Umezawa, Y. *Handbook of Ion-Selective Electrodes: Selectivity Coefficients*; CRC Press: Boca Raton, 1990.

(89) Moschou, E. A.; Chaniotakis, N. A. Ion-Partitioning Membrane-Based Electrochemical Sensors. *Anal. Chem.* **2000,** *72*, 1835-1842.

(90) Chaniotakis, N. A.; Moschou, E. A.; Constantinidis, G. Highly Selective Two-Ion-Carrier Chemically Modified FETs. *Microelectron. Eng.* **1998,** *41/42*, 481-484.

(91) Bakker, E.; Pretsch, E. Ion-Selective Electrodes Based on Two Competitive Ionophores for Determining Effective Stability Constants of Ion-Carrier Complexes in Solvent Polymer Membranes. *Anal. Chem.* **1998,** *70*, 295-302.

(92) Jimenez, C.; Bartroli, J. Development of an Ion-Sensitive Field Effect Transistor (ISFET) Based on PVC Membrane Technology with Improved Long-Term Stability. *Electroanalysis* **1997,** *9(4)*, 316-319.

(93) Jimenez, C.; Marques, I.; Bartroli, J. Continuous-Flow System for Online Water Monitoring Using Back-Side Contact ISFET-Based Sensors. *Anal. Chem* **1996,** *68*, 3801-3807.

(94) Bratov, A.; Abramova, N.; Munoz, J.; Dominguez, C.; Alegret, S.; Batroli, J. Optimization of Photocurable Polyurethane Membrane Composition for Ammonium Ion Sensor. *J. Electrochem. Soc.* **1997,** *144*, 617-621.

(95) Mathis, U. Trinkwassermessungen mit Pb^{2+}-selektiven Elektroden in nano- bis mikromolaren Konzentrationsbereich, Diploma Thesis, ETH, Zurich, 1999.

(96) Nägele, M. Bestimmung und Optimierung von Membranparametern ionenselektiver Flüssigmembranelektroden, Doctoral Dissertation No. 12695, ETH, Zurich, 1998.

(97) Dürselen, L. F. J. Beitrag zur Untersuchung asymmetrischer Eigenschaften von PVC-Flüssigmembranen, Doctoral Dissertation No. 8927, ETH, Zurich, 1989.

5 Ion-Selective Field-Effect-Transistors Based on Double Membranes with Mobile and Covalently Bound Ionophores

5.1 Introduction

Ionophore-based solid-state ion-selective sensors in general suffer from a thermodynamically ill-defined interface, as explained in Chapter 4.2. In the CHEMFET case, it is widely accepted that there is a hydration layer in the region between the polymer membrane and the gate oxide. This aqueous film is formed by penetration of water across the membrane.[1-4] Interferents dissolved in the sample solution, like for example carbon dioxide, can diffuse through the membrane and alter the pH in the thin water film. The gate oxide is pH-sensitive and thus the potential will vary. Therefore, the response signal of the CHEMFET will be changed, as explained in Chapter 4.2.1. The response of CHEMFETs in the presence of carbon dioxide will vary considerably depending on the extent of the thickness of the water layer.[5]

In biomedical applications, the variation of the partial pressure of carbon dioxide in blood samples poses a stability problem for CHEMFETs. The uptake and diffusion of carbon dioxide by ion-selective membranes has even been exploited to potentiometrically determine PCO_2 in whole blood.[6] Furthermore, the diffusion of carbon dioxide through polymeric membranes is used in Severinghaus-type CO_2 sensors.[7, 8]

The principal aim of this work was to improve the potential stability of CHEMFETs. The influence of acidic interferents to the different phase-boundary potentials of ISFETs covered with only one membrane was investigated in detail. Finally, the double membrane with a covalently bound ionophore, as presented in Chapter 4, was tested for the purpose of a reduction of the signal instability of CHEMFETs.

The adhesion of the hydrophobic ion-selective membrane to the hydrophilic gate oxide is often the limiting factor determining the lifetime of CHEMFETs.[9, 10] A lot of modified polymers[11-17] and mechanical or chemical fixations[8, 18] were proposed to improve the adherence of the membrane. In the first part of this chapter, the

membrane adhesion was optimized for the CHEMFETs used in the subsequent studies.

5.2 Characterization of CHEMFETs with a Single Membrane Based on One Ionophore

5.2.1 Ammonium- and Potassium-Selective CHEMFETs

In order to obtain a good adhesion of the membrane to the ISFET, several polymers were tested in preliminary experiments. The dissolved polymers were cast onto a glass substrate and the dried samples were set into water for four weeks. The hydrophilic glass was a substitute for the gate oxide of ISFETs. The hard polyurethane (PHB/PTHF 1:1), which is slightly hydrophilic, showed a poor adhesion on the glass surface, as shown in Table 5.1. After conditioning the samples in water, the polymers based on PHB and PTHF were opaquely and milky,[19] while the Tecoflex and PVC membranes remained transparent. It was reported that the large water-uptake of polyurethane based on PHB causes a structural transformation of the polymer.[20]

The dissolved polymers were cast onto the gate oxide of ISFETs and, after evaporation of the solvent, the CHEMFETs were stored in water for four weeks. The polyurethane membranes showed an even worse adhesion on ISFETs than on glass, as shown in Table 5.1. When the PVC or the polyurethane (PHB/PTHF 1:5) membranes were removed from the respective CHEMFETs, which was possible with a pair of tweezers, the membranes were completely destroyed. In contrast, the adhesion of the Tecoflex-based membrane was not very strong and it was possible to remove the whole membrane with tweezers without destroying it.[9] It is interesting to note that the size of the gate surface of an ISFET was about 1 mm^2. The area of the deposited membrane amounted to 25 mm^2. Hence, the interaction between the polymeric membrane and the encapsulation material, which surrounds the gate, was the determining factor for the adhesion of the membrane in our work.

Table 5.2 shows the response behavior of NH_4^+-selective CHEMFETs. It can be seen that the slope of the sensors based on PHB/PTHF was clearly sub-Nernstian. This is probably a consequence of the poor adhesion of PHB/PTHF on the encapsulation material consisting of epoxy resin. Figure 5.1 and Table 5.2 illustrate

that the slope of the CHEMFETs made from plasticized Tecoflex or PVC was Nernstian, as described in the literature.[14, 15, 21-27] For all of the following experiments, CHEMFETs based on Tecoflex or PVC were used, since the sealing of the membrane to the encapsulation substrate was good. CHEMFETs incorporating the potassium-selective ionophore valinomycin had the same slopes and detection limits as the NH_4^+-selective sensors.

Table 5.1 Adhesion of polymers on different substrates (*a*).

polymer	adhesion on glass	adhesion on ISFET
polyurethane (PHB/PTHF 1:1) [b]	poor	no adhesion
polyurethane (PHB/PTHF 1:5) [c]	excellent	good
Tecoflex/DOS [d]	very good	moderate
PVC/DOS [e]	good	good

[a] The polymer solutions were cast onto the substrate and, after evaporation of the solvent, the samples were stored in water for four weeks. Each series included ten samples. [b] membrane type 4P (NH_4^+); see Experimental. [c] membrane type 4O (NH_4^+). [d] membrane type 5A (NH_4^+). [e] membrane type 4Q (NH_4^+).

The thickness of the membrane was optimized. In order to obtain a Nernstian slope and a lifetime of several weeks, the deposition of at least 25 µL of the membrane dissolved in tetrahydrofuran onto the gate oxide was necessary. For all of the ISFETs used in the subsequent studies, which were covered with a single membrane, 25 µL of the membrane solution were cast onto the gate oxide. The thickness of the resulting membranes amounted to 50 µm.

Ammonium-selective membranes based on PVC/DOS or Tecoflex/DOS showed a growth of small crystals, in contrast to polymer membranes containing only NaTFPB. Probably, the membrane compound from which the crystals were formed was nonactin. The oversaturation of nonactin dissolved in the liquid membrane appears to cause crystallization. It has been reported that crystalline ionophore particles inside

the membrane could function as a reservoir of ionophore.[28] Such a buffered carrier concentration within the membrane might prolong the lifetime of nonactin-based sensors.

Table 5.2 Influence of the polymer on the response behavior of NH_4^+-selective CHEMFETs.

polymer	slope (mV dec^{-1}) [a]	linear range (M)
polyurethane (PHB/PTHF 1:1) [b]	17.5 ± 0.7 (n = 2)	0.1 - 10^{-3}
polyurethane (PHB/PTHF 1:5) [c]	37.6 ± 5.7 (n = 14)	0.1 - 10^{-4}
Tecoflex/DOS [d]	57.8 ± 1.5 (n = 6)	0.1 - 10^{-4}
PVC/DOS [e]	61.6 ± 3.1 (n = 9)	0.1 - 10^{-5}

[a] The number of CHEMFETs is n. [b] membrane type 4P (NH_4^+). [c] membrane type 4W1 (double). [d] membrane type 5B (NH_4^+). [e] membrane type 4Q (NH_4^+).

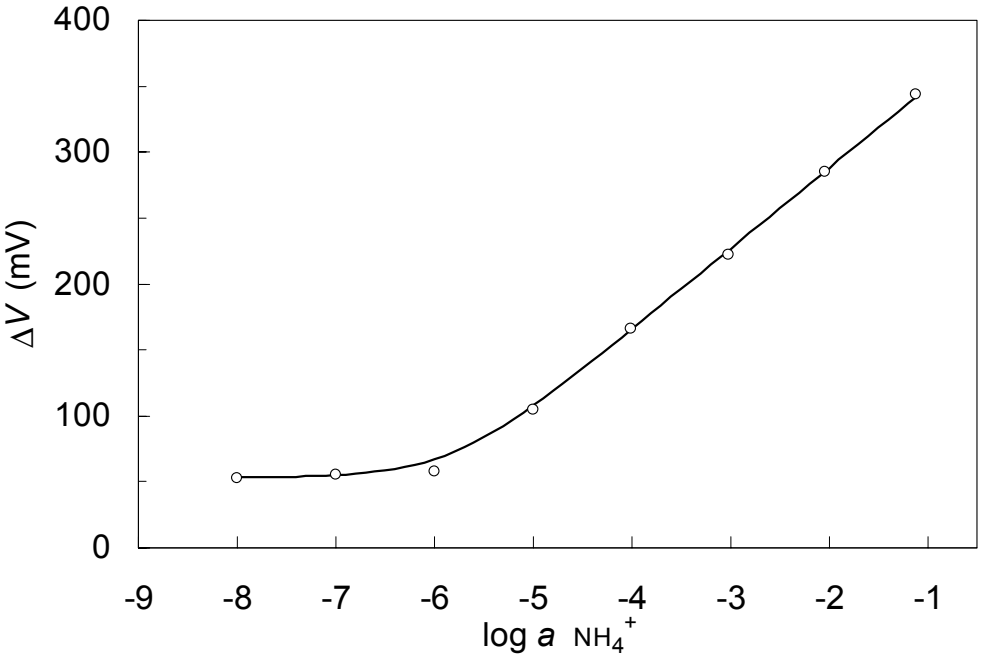

Figure 5.1 Response of an NH_4^+-selective CHEMFET based on nonactin, KTFPB, PVC, and DOS (membrane type 4Q (NH_4^+)).

5.2.2 Hydrogen Ion-Selective CHEMFETs

The hydrogen ion-selective ionophore tridodecylamine is important for the work presented in Chapter 5.3. CHEMFETs based on this mobile carrier showed a slope of 58.6 mV dec^{-1} and a large measuring range,[29, 30] as illustrated in Figure 5.2. The upper detection limit of these devices is controlled by the activity/lipophilicity of the interfering anion and by the basicity of the ionophore.[31]

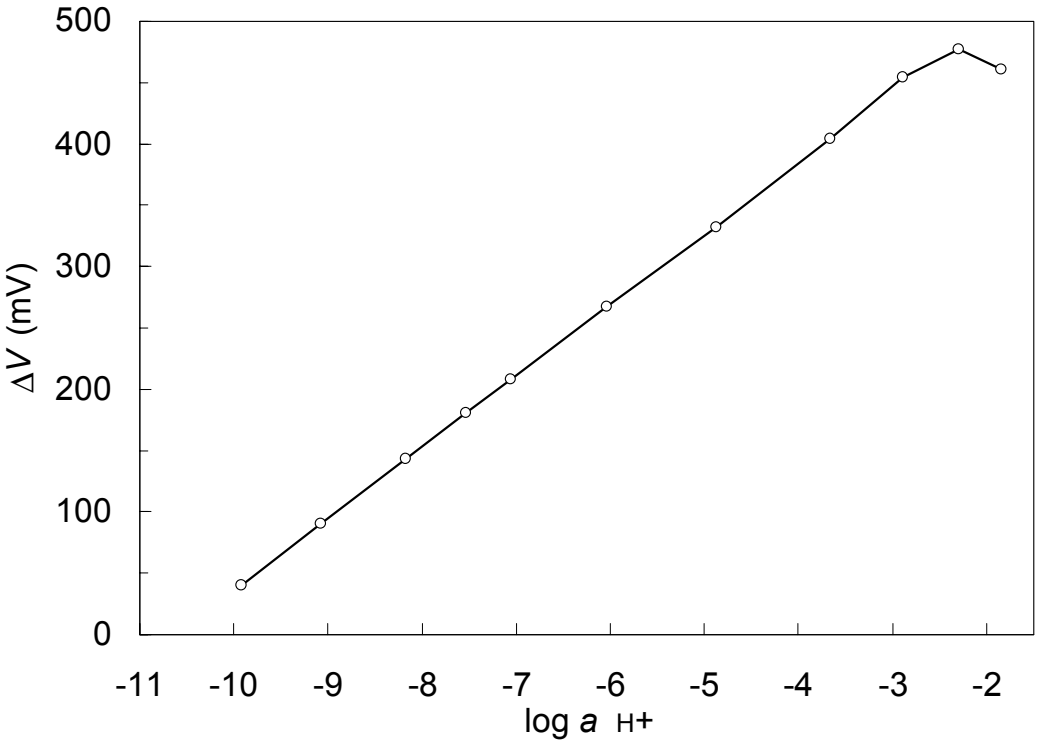

Figure 5.2 Response of an H^+-selective CHEMFET based on tridodecylamine, NaTFPB, ETH 500, and PVC/DOS (membrane type 5D (H^+)). The slope of the CHEMFET was 58.6 mV dec^{-1}.

5.3 Interference from Carbon Dioxide and Organic Acids to CHEMFETs with a Single Membrane Containing a Mobile H^+-Selective Ionophore

The permeation of carbon dioxide across a polymeric membrane was mathematically described in equations 4.3 and 4.4. Figure 5.3 shows a calculated CO_2 uptake curve according to these equations. The theoretical model was experimentally verified using CHEMFETs with an ammonium-selective membrane. Conditioned CHEMFETs were set into the sample solution and, after a few minutes, carbon dioxide was purged into the sample. The response signal of the sensors exhibited a rather large shift within the first few minutes, as shown in Figure 5.4. This potential

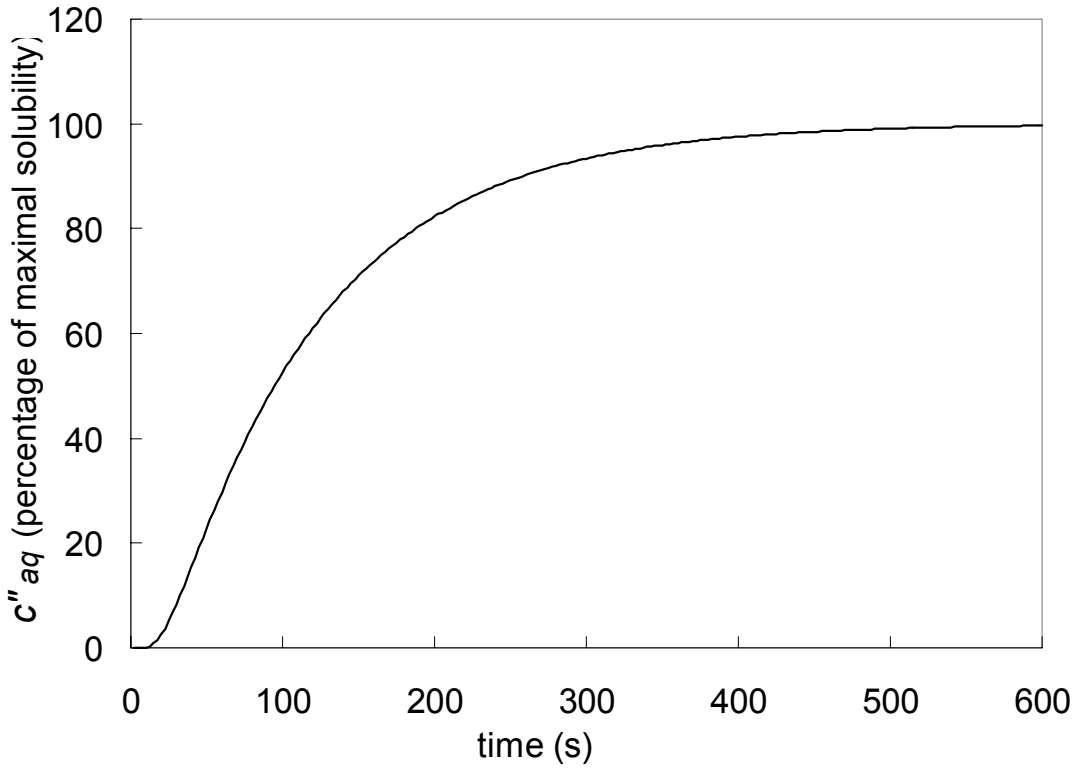

Figure 5.3 Theoretical diffusion kinetic of carbon dioxide across a membrane. The CO_2 level in the sample solution is raised from a background value (no CO_2 added) to a high carbon dioxide concentration. c''_{aq} is the percentage of maximal solubility of CO_2 in the water film between membrane and insulator. These calculations according to equations 4.3 and 4.4 made use of the following parameters: diffusion coefficient of CO_2 within the polymer membrane $D = 10^{-7}$ cm^2 s^{-1}, and membrane thickness $d = 50$ µm.

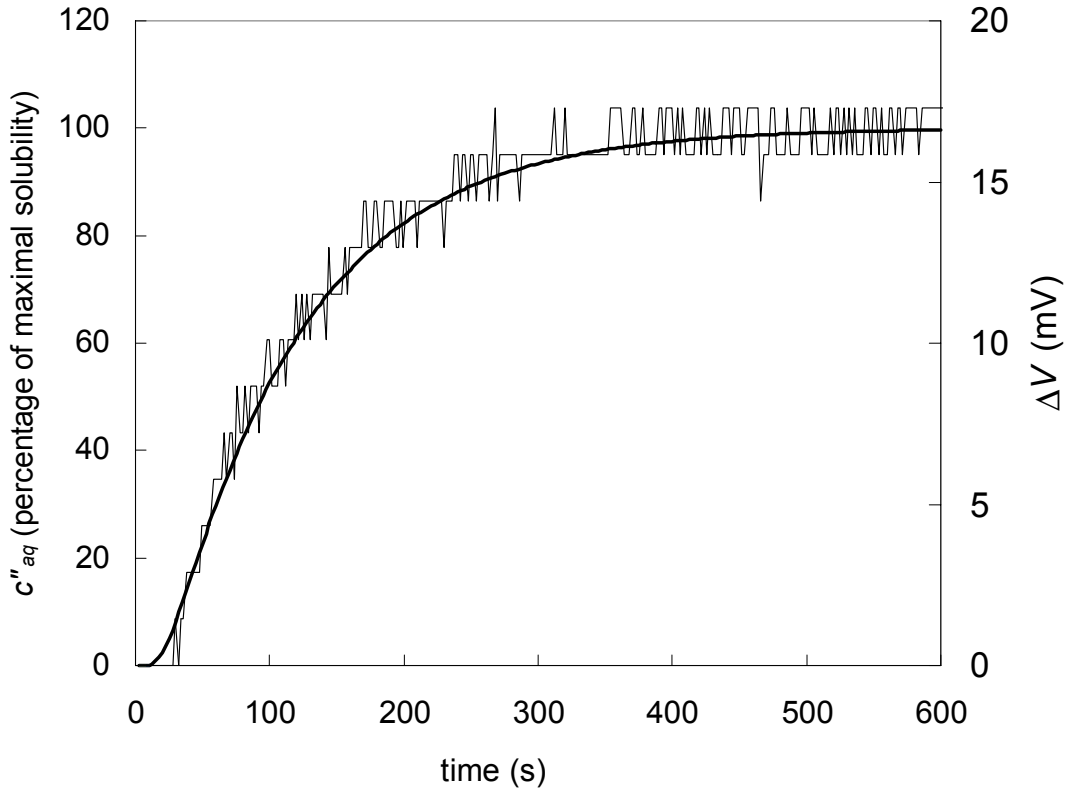

Figure 5.4 Comparison between the theoretical diffusion kinetic of CO_2 across a membrane (according to Figure 5.3) and experimental data measured on an NH_4^+-selective CHEMFET. The CHEMFET based on membrane 5E (NH_4^+) was set into the buffered sample solution (pH 4.5) and, at t = 0 s, CO_2 was purged into the sample solution. The thickness of the membrane was 50 µm.

increase is caused by the decrease of pH in the aqueous film due to the carbon dioxide uptake. The effect proved to be reversible: When N_2 was purged into the sample solution, the response signal decreased.[5] During these experiments, the pH in the sample solution was kept constant using a buffer solution based on citric acid (pH 4.5). The experimental data were in good agreement with the calculated values, as shown in Figure 5.4.

The interference from carbon dioxide and organic acids, respectively, on CHEMFETs was experimentally quantified using the following procedure. Firstly, the sensors were conditioned in an unbuffered solution that had almost the same ionic

composition as the sample solution. Secondly, the CHEMFETs were set into the pH-buffered sample solution and the interfering acid was added 2 –3 min later to minimize the time-dependent influence from the pH buffer on the thin water film. Two CHEMFETs containing an H^+-selective ionophore were always simultaneously measured in the same beaker with two NH_4^+-selective CHEMFETs.

As the carbon dioxide level was raised from a background value (no CO_2 added) to a high CO_2 concentration, the response signal of CHEMFETs based on a mobile H^+-selective ionophore was stable (Table 5.3, first row). The potential change at the phase boundary between membrane and inner water film was the same as the potential shift at the insulator surface. Consequently, changing the pH in the inner

Table 5.3 Effect of the addition of interferents on the response signal of H^+- and NH_4^+-selective CHEMFETs based on a single membrane with one mobile ionophore.

interferent	ionophore (and membrane type)	potential shift (mV) [a]
CO_2 gaseous	tridodecylamine (5D (H^+))	-3.4 ± 2.5 (n = 4)
CO_2 gaseous	nonactin (5E (NH_4^+))	10.2 ± 3.7 (n = 3)
benzoate (30 mM)	tridodecylamine (5D (H^+))	-10.0 ± 1.2 (n = 4)
benzoate (30 mM)	nonactin (5E (NH_4^+))	66.4 ± 7.3 (n = 4)
acetate (20 mM)	tridodecylamine (5D (H^+))	-2.5 ± 1.8 (n = 2)
acetate (20 mM)	nonactin (5E (NH_4^+))	72.1 ± 12.3 (n = 2)

[a] The potential shift is the ΔV of the CHEMFET caused by the addition of interfering species into the sample solution (citrate buffer (pH 4.5) with a constant NH_4Cl concentration of 10^{-3} M). CHEMFETs based on tridodecylamine were measured with CHEMFETs based on nonactin in the same beaker simultaneously. The number of CHEMFETs is n.

water film does not alter the response signal of the sensor. NH_4^+-selective CHEMFETs, which were in the same sample solution as the H^+-selective CHEMFETs, showed a large response towards carbon dioxide (Table 5.3, second row). This potential change is solely caused by an increase of the boundary potential at the interface between the thin water film and the Al_2O_3 surface. Adding carbonic acid into the sample solution in form of gaseous CO_2 gave more reproducible potential shifts than the addition in form of $NaHCO_3$.

Figure 5.5 illustrates the influence of the addition of benzoic acid into the sample solution on the response behavior of several H^+-selective sensors. The organic acid slightly decreased the potential of an H^+-selective glass electrode and of an ISFET which was not covered with a membrane. The response curve of the ISFET showed

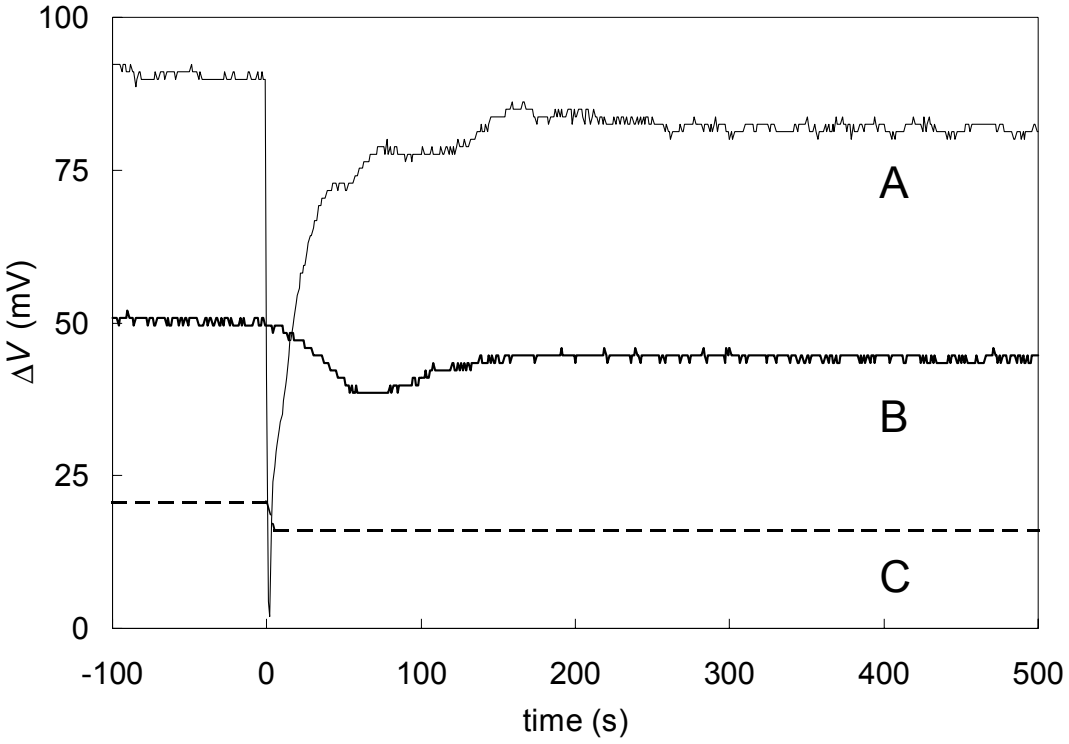

Figure 5.5 Response to benzoic acid of an H^+-selective CHEMFET (A) based on tridodecylamine (membrane type 5D (H^+)), an ISFET (B), and an H^+-selective glass electrode (C). At t = 0 s, benzoate (30 mM) was added into the sample solution (50 mM citric acid (pH 4.5), 76 mM NaOH, and 1 mM NH_4Cl).

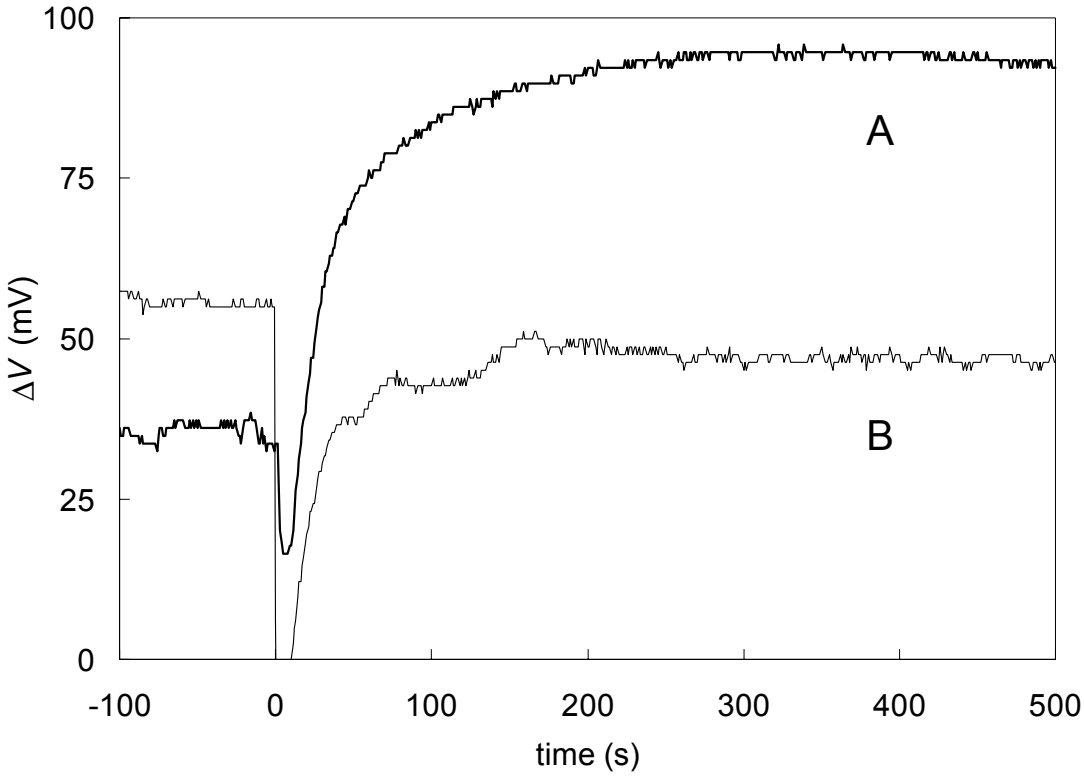

Figure 5.6 Response to benzoic acid of an NH_4^+-selective CHEMFET (A) based on nonactin (membrane type 5E (NH_4^+)) and an H^+-selective CHEMFET (B) containing tridodecylamine (membrane type 5D (H^+)). At t = 0 s, benzoate (30 mM) was added into the sample solution (50 mM citric acid (pH 4.5), 76 mM NaOH, and 1 mM NH_4Cl).

first a large decrease and afterwards an increase of the potential. This dip of the response signal may be caused by interaction of the aromatic compound with Al_2O_3 at the gate surface. A CHEMFET based on an H^+-selective membrane showed the same potential dip. UV-spectroscopic studies[32] indicated that benzoic acid permeates easily through plasticized PVC membranes in the neutral acid form. The potential change at the phase boundary between membrane and inner water layer (-59 mV / pH) was not exactly compensated by the potential shift at the gate insulator surface (53 mV / pH). Hence, a decrease of the pH in the inner water film causes a small total potential decrease of the H^+-selective CHEMFET. In contrast, NH_4^+-selective CHEMFETs,

which were in the same sample solution as the hydrogen ion-selective CHEMFETs, showed a large response towards benzoate, as illustrated in Figure 5.6.

Figure 5.7 illustrates the influence of the addition of acetic acid into the sample solution on the response behavior of several H^+-selective sensors. The response signal of the H^+-selective CHEMFET was stable like the potential of the other sensors. This demonstrates the pH compensating effect of the hydrogen ion-selective membrane. In contrast, the addition of acetic acid into the sample solution caused an increase of the potential of the NH_4^+-selective CHEMFET, as shown in Figure 5.8. The predominant form of transport across the membrane is likely the diffusion of acetate as associated acid.[33] It was reported that the diffusion of acetic acid through the polymeric membrane of an ISE, which was 200 μm thick, occurs within a few minutes.[33]

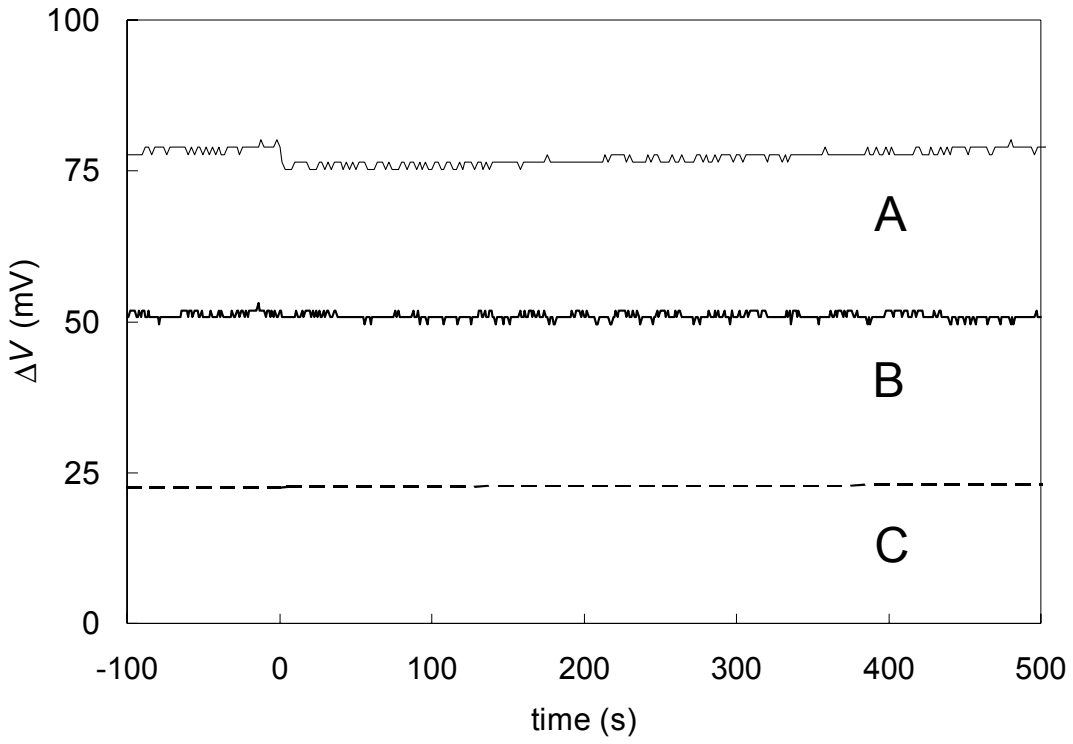

Figure 5.7 Response to acetic acid of an H^+-selective CHEMFET (A) based on tridodecylamine (membrane type 5D (H^+)), an ISFET (B), and an H^+-selective glass electrode (C). At t = 0 s, acetate (20 mM) was added into the sample solution (50 mM citric acid (pH 4.5), 76 mM NaOH, and 1 mM NH_4Cl).

The shift of the response signal of CHEMFETs caused by different acids is summarized in Table 5.3. The NH_4^+-selective CHEMFETs typically had a larger response towards benzoate and acetate than towards CO_2,[5] since benzoic acid and acetic acid are stronger acids than H_2CO_3. These compounds have the following acid dissociation constants (pK_a): benzoic acid 4.2, acetic acid 4.8, and carbonic acid (H_2CO_3/HCO_3^-) 6.4.

In conclusion, the H^+-selective CHEMFETs compensated pH changes in the water film at the membrane/insulator interface. Carbon dioxide and organic acids did not interfere with the measurement of the analyte ion in the sample solution.

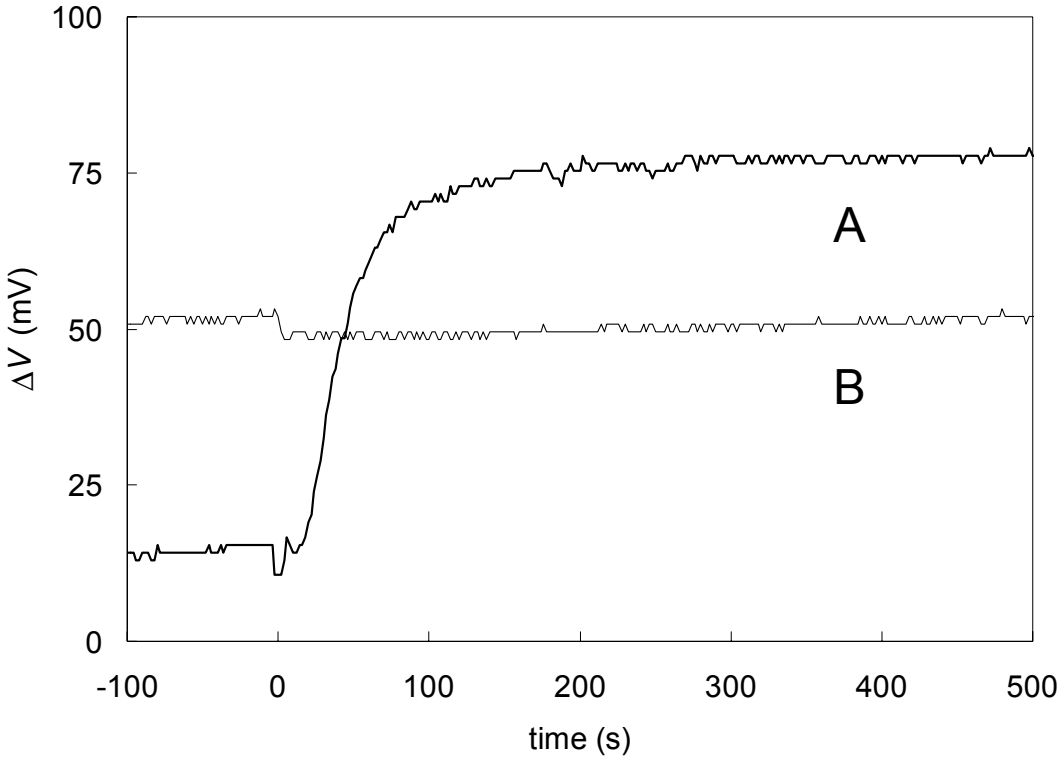

Figure 5.8 Response to acetic acid of an NH_4^+-selective CHEMFET (A) based on nonactin (membrane type 5E (NH_4^+)) and an H^+-selective CHEMFET (B) containing tridodecylamine (membrane type 5D (H^+)). At t = 0 s, acetate (20 mM) was added into the sample solution (50 mM citric acid (pH 4.5), 76 mM NaOH, and 1 mM NH_4Cl).

5.4 Interference from Carbon Dioxide and Organic Acids to CHEMFETs with a Single Membrane Containing Two Ionophores

Membranes containing both nonactin and covalently bound *N*-butyldiethanolamine are much more selective to H^+ than to NH_4^+, as shown in curve B of Figure 4.13.[34, 35] The polymer matrix of CHEMFETs was optimized in order to obtain a good adhesion of the membrane on the ISFET. Plasticized PVC membranes containing two ionophores had a better adhesion than the corresponding membranes made from plasticized Tecoflex. Therefore, plasticized PVC was used as the polymer matrix of the present CHEMFET membranes.

Table 5.4 Effect of the addition of interferents on the response signal of H^+- and NH_4^+-selective CHEMFETs based on a single membrane with two ionophores and with one ionophore, respectively.

interferent	ionophores (membrane type)	potential shift (mV) [a]
CO_2 gaseous	*N*-butyldiethanolamine and nonactin (5F (H^+))	-10.3 ± 16.9 (n = 2)
CO_2 gaseous	nonactin (5E (NH_4^+))	57.8 ± 16.1 (n = 4)
benzoate (30 mM)	*N*-butyldiethanolamine and nonactin (5F (H^+))	48.6 ± 17.8 (n = 7)
benzoate (30 mM)	nonactin (5E (NH_4^+))	97.8 ± 33.3 (n = 7)

[a] The potential shift is the ΔV of the CHEMFET caused by the addition of interfering species into the sample solution (citrate buffer (pH 4.5) with a constant NH_4Cl concentration of 10^{-3} M). CHEMFETs based on two ionophores were measured with CHEMFETs based on nonactin in the same sample solution simultaneously. The number of CHEMFETs is n.

The CHEMFETs based on two ionophores were almost stable against the interference from carbon dioxide, as shown in the first row of Table 5.4. The ammonium-selective CHEMFETs showed a large potential shift due to the response to carbon dioxide Table 5.4, second row). Adding benzoate to the sample solution caused a smaller response shift to the CHEMFETs made from the membrane containing two ionophores (Table 5.4, third row) than to the NH_4^+-selective CHEMFETs (Table 5.4, fourth row). The difference between the influence of CO_2 and benzoic acid might be explainable by the fact that H_2CO_3 is a weaker acid than benzoic acid. The potential stability against the interference by carbon dioxide is more important than the stability towards benzoate, because CO_2 is present in almost all sample solutions in practical applications of ion-selective sensors. The difference in the potential shifts of NH_4^+-selective CHEMFETs based on membrane type 5D (NH_4^+) between Tables 5.3 and 5.4 can be explained by the different conditioning times for these devices, as described in the next chapter.

5.5 Interference from Carbon Dioxide and Organic Acids to CHEMFETs with a Double Membrane

CHEMFETs based on a double membrane were used in the following experiments. The schematic set-up of such a double membrane is shown in Figures 4.4 and 4.5, and the response mechanism is explained in Chapter 4.7. For the deposition of the double membrane onto an ISFET, the inner membrane was cast first onto the gate oxide resulting in a layer with a diameter of 2 mm. Secondly, a disk of the outer membrane with a diameter of 6 mm was glued with tetrahydrofuran onto the CHEMFET covered with the inner membrane. The resulting NH_4^+-selective CHEMFETs had a Nernstian slope, as shown in Figure 5.9. The addition of sulfuric acid to the sample solution (pH 1) had no effect on the stability of the response signal of these CHEMFETs during two hours. This was clear evidence that the inner membrane did not contact the measuring solution. The double membrane was based on plasticized Tecoflex.

The influence of the addition of organic acids and CO_2 into the sample solution, respectively, on the response signal was studied. CHEMFETs based on a double membrane, which contained immobilized *N*-butyldiethanolamine in the inner membrane (Table 5.5, first row), showed an improved stability towards the

interference from carbon dioxide in comparison with single membrane NH_4^+-selective CHEMFETs (Table 5.5, second row). Figure 5.10 illustrates the response behavior of these sensors towards carbon dioxide. The addition of benzoate into the sample solution caused a large potential shift to both the CHEMFETs based on the double membrane (Table 5.5, row 3) and the CHEMFETs made from the single membrane (Table 5.5, row 4). The response of all devices towards benzoate was larger in comparison to the interference by carbon dioxide.

These results might be explained as follows. Firstly, carbonic acid is a weaker acid than benzoic acid. Secondly, the stabilizing effect of the double membrane is partially limited by the measuring range of the inner membrane, which contains two

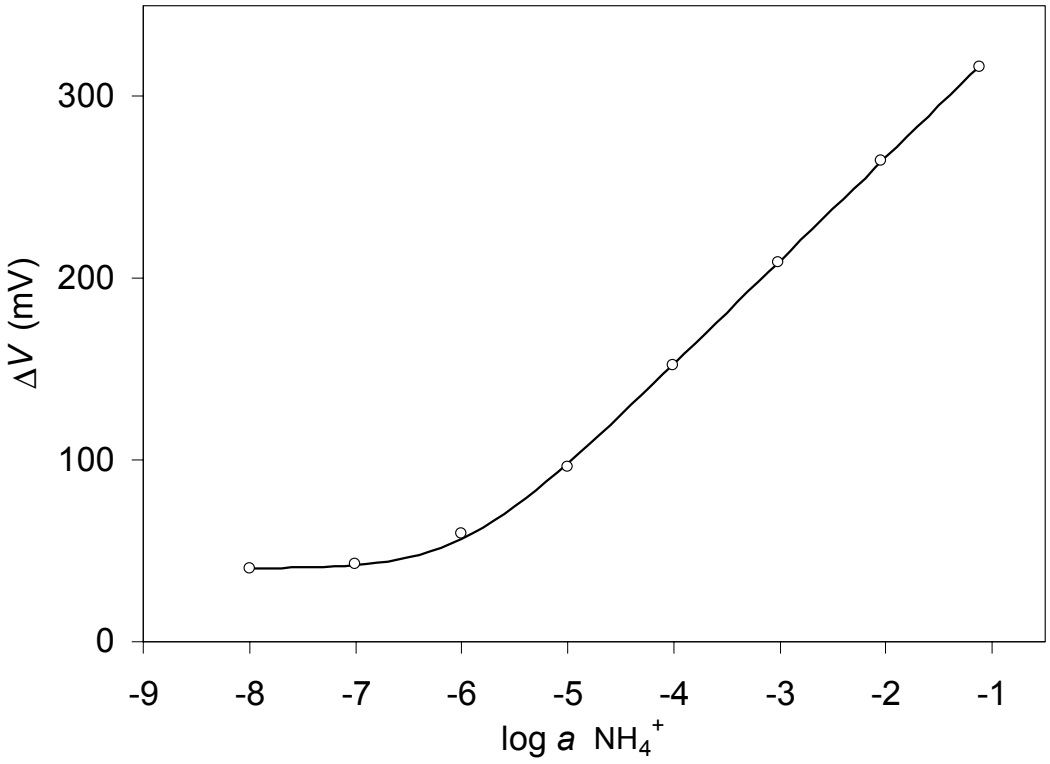

Figure 5.9 Response to NH_4^+ of a CHEMFET covered with a double membrane as a function of the logarithm of the ammonium ion activity in the sample solution. The average slope of three CHEMFETs was 58.1 ± 0.9 mV dec^{-1}. The outer membrane in contact with the sample solution contained nonactin, NaTFPB, ETH 500, and Tecoflex/DOS (membrane type 5G1 (double)). The inner membrane contained covalently bound *N*-butyldiethanolamine, nonactin, NaTFPB, ETH 500, and Tecoflex/DOS (membrane type 5G2 (double)).

ionophores, as shown in curve B of Figure 4.13. Finally, there could be an additional potential at the interface between the outer and the inner membrane. This additional phase boundary potential would decrease the stabilizing effect of the propagated double membrane mechanism.

Double membranes based on the covalently bound bis-2,6-hydroxymethyl pyridine yielded no improved signal stability against interference from carbon dioxide, as shown in row 5 of Table 5.5. This may be explained by the lower detection limit of the inner membrane towards hydrogen ions, as shown in curve C of Figure 4.15. Other workers who buffered the pH of the thin water layer[36] or changed the solid part of the system[32] observed signal stability against the interference from carbonic acid.

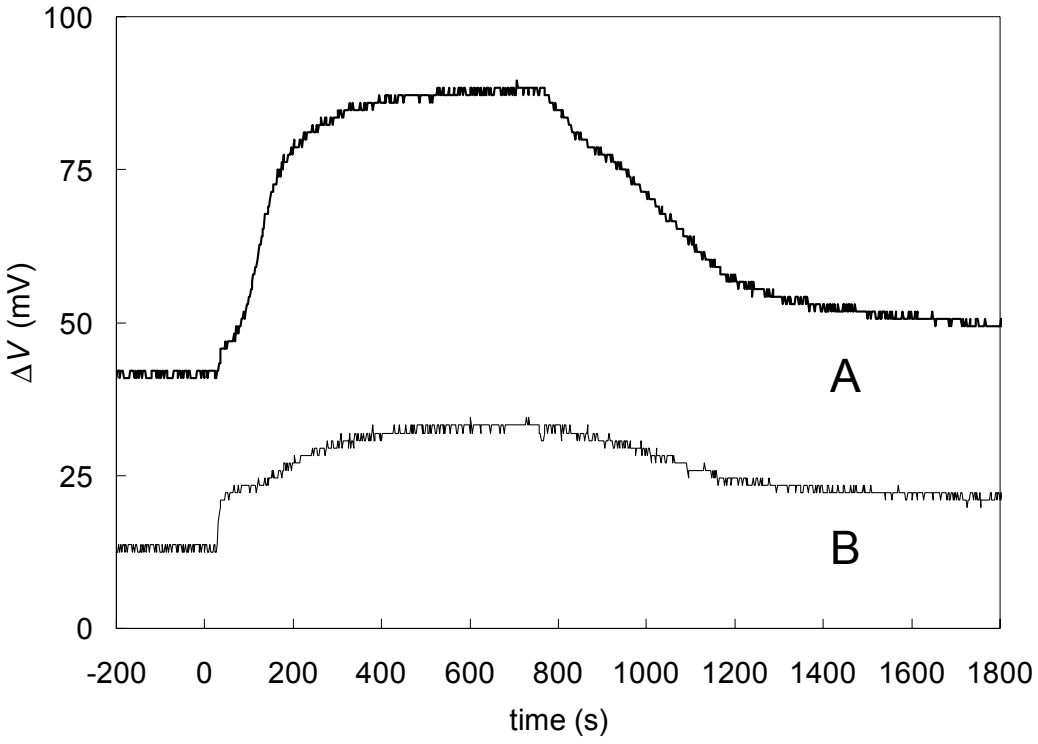

Figure 5.10 Response to carbon dioxide of an NH_4^+-selective CHEMFET (A) based on a single membrane (membrane type 5B (NH_4^+)) and an NH_4^+-selective CHEMFET (B) made from a double membrane (membrane type 5G (double)). At t = 0 s, CO_2 was purged into the sample solution (0.1 M citrate buffer at pH 4.2 and 10^{-3} M NH_4Cl). At t = 720 s, N_2 was purged into the sample solution.

Table 5.5 Effect of the addition of interferents on the response signal of NH_4^+-selective CHEMFETs based either on a single or on a double membrane.

interferent	membrane	potential shift (mV) [a]
CO_2 gaseous	double membrane containing *N*-butyldiethanolamine in the inner membrane (membrane type 5G (double))	18.0 ± 2.0 (n = 6)
CO_2 gaseous	single membrane based on nonactin (membrane type 5B (NH_4^+))	35.6 ± 11.0 (n = 6)
benzoate (30 mM)	double membrane containing *N*-butyldiethanolamine in the inner membrane (membrane type 5G (double))	84.9 ± 25.1 (n = 4)
benzoate (30 mM)	single membrane based on nonactin (membrane type 5B (NH_4^+))	109.0 ± 27.1 (n = 4)
CO_2 gaseous	double membrane containing bis-2,6-hydroxymethyl pyridine in the inner membrane (membrane 5H (double))	39.3 ± 18.2 (n = 4)
CO_2 gaseous	single membrane based on nonactin (membrane type 5B (NH_4^+))	31.3 ± 0.7 (n = 3)

[a] The potential shift is the ΔV of the CHEMFET caused by the addition of interfering species into the sample solution (citrate buffer (pH 4.2) with a constant NH_4Cl concentration of 10^{-3} M). CHEMFETs based on a double membrane were measured with CHEMFETs made from a single membrane in the same sample solution simultaneously. The number of CHEMFETs is n.

In this work, the extent of the potential shift due to the response towards carbon dioxide (Tables 5.3 – 5.5) was not always constant. Table 5.6 shows that a prolongation of the conditioning time increased the potential shift. This effect can be

partially explained by the growing of the inner water layer. The thickness of the water film between membrane and insulator depends on the conditioning time.[5] In the initial period, the water layer is very thin and inhomogeneous. The longer the conditioning time is, the thicker is the water layer and the higher its influence on the phase-boundary potential formation. The diffusion coefficient in the membrane was also shown to depend on the conditioning time.[2, 3] Furthermore, thin plasticized PVC membranes can incorporate very high water concentrations.[4, 37]

Table 5.6 Influence of the conditioning time on the interference from carbon dioxide to the response signal of CHEMFETs.

conditioning time (days)	membrane	potential shift (mV) [a]
1	double membrane containing *N*-butyldiethanolamine in the inner membrane (membrane type 5G (double))	14.2 ± 3.9 (n = 6)
1	single membrane based on nonactin (membrane type 5B (NH_4^+))	22.3 ± 6.4 (n = 6)
5	double membrane containing *N*-butyldiethanolamine in the inner membrane (membrane type 5G (double))	18.0 ± 2.0 (n = 6)
5	single membrane based on nonactin (membrane type 5B (NH_4^+))	35.6 ± 11.0 (n = 6)

[a] The potential shift is the ΔV of the CHEMFET caused by the addition of carbon dioxide into the sample solution (citrate buffer (pH 4.2) with a constant NH_4Cl concentration of 10^{-3} M). CHEMFETs based on the double membrane were measured with CHEMFETs made from a single membrane in the same sample solution simultaneously. The number of CHEMFETs is n.

5.6 Conclusions

Plasticized PVC membranes showed a better adhesion to ISFETs in comparison with different polyurethane membranes. NH_4^+-selective CHEMFETs respond towards carbon dioxide and several organic acids in the sample solution. CHEMFETs based on a mobile H^+-selective ionophore showed signal stability towards CO_2 and organic acids in the sample solution. These effects can be completely explained by the different phase-boundary potentials of the CHEMFET. The propagated double membrane improved the stability of CHEMFETs against interference by CO_2 and organic acids. The stabilizing effect of the double membrane is partially limited by the pH measuring range of the inner membrane, which contained two ionophores, and by an additional potential contribution arising at the interface between the outer and the inner membrane.

Other ionophores than nonactin could be incorporated into the double membrane. It should be easily possible to measure with these modified double membranes other analytes than ammonium in the sample solution. Furthermore, the lifetime of CHEMFETs based on the double membrane might be prolonged by a covalent binding of both ionophores. Such novel microdevices could be useful for a wide range of industrial applications, measurements in environmental samples, and *in vivo* measurements.

References

(1) Schneider, B. Diffusionsprozesse und Phasengleichgewichte in ionenselektiven Flüssigmembranen und -optoden, Doctoral Dissertation No. 11255, ETH, Zurich, 1995.

(2) Li, Z.; Li, X.; Petrovic, S.; Harrison, D. J. Dual-Sorption Model of Water Uptake in Poly(vinyl Chloride)-Based Ion-Selective Membranes: Experimental Water Concentration and Transport Parameters. *Anal. Chem.* **1996,** *68*, 1717-1725.

(3) Li, Z.; Li, X.; Rothmaier, M.; Harrison, D. J. Comparison of Numerical Modeling of Water Uptake in Poly(vinyl chloride)-Based Ion-Selective Membranes with Experiment. *Anal. Chem.* **1996,** *68*, 1726-1734.

(4) Chan, A. D. C.; Li, X.; Harrison, D. J. Evidence for a Water-Rich Surface Region in Poly(vinyl chloride)-Based Ion-Selective Electrode Membranes. *Anal. Chem.* **1992,** *64*, 2512-2517.

(5) Fogt, E. J.; Untereker, D. F.; Norenberg, M. S.; Meyerhoff, M. E. Response of Ion-Selective Field Effect Transistors to Carbon Dioxide and Organic Acids. *Anal. Chem.* **1985,** *57*, 1995-1998.

(6) Telting-Diaz, M.; Collison, M. E.; Meyerhoff, M. E. Simplified Dual-Lumen Catheter Design for Simultaneous Potentiometric Monitoring of Carbon-Dioxide and pH. *Anal. Chem.* **1994,** *66*, 576-583.

(7) Sekiguchi, T.; Nagai, Y.; Makino, T.; Ohno, K.; Nakamura, M.; Hosaka, H.; Sakio, H. S. B.; Ohtsu, S.; Takahashi, H. Gastric P-CO_2 Monitoring System Based on a Double Membrane Type P-CO_2 Sensor. *Sens. Actuators, B* **1998,** *49*, 171-178.

(8) Lundström, I.; van den Berg, A.; van der Schoot, B. H.; van den Vlekkert, H. H.; Armgarth, M.; Nylander, C. J. In *Chemical and Biochemical Sensors: Part I*; Göpel, W., Jones, T. A., Kleitz, M., Lundström, J., Seiyama, T., Eds.; VCH: Weinheim, 1991; Vol. 2, pp 467-528.

(9) Cha, G. S.; Liu, D.; Meyerhoff, M. E.; Cantor, H. C.; Midgley, A. R.; Goldberg, H. D.; Brown, R. B. Electrochemical Performance, Biocompatibility and Adhesion of New Polymer Matrices for Solid-State Ion Sensors. *Anal. Chem.* **1991,** *63*, 1666-1672.

(10) Clechet, P.; Jaffrezic-Renault, N.; Martelet, C. In *Chemical Sensor Technology*; Yamauchi, S., Ed.; Kodansha and Elsevier: Tokyo, 1992; Vol. 4, pp 205-225.

(11) van der Wal, P.; de Rooij, N. F.; Koudelka-Hep, M. *Covalently Bound Plasticized PVC Membranes for Solid State Ion-Selective Devices*: Proceedings of the 196th Meeting of The Electrochemical Society, Inc. - Chemical Sensors IV; Honolulu, Hawaii, 1999.

(12) Reinhoudt, D. N. Durable Chemical Sensors Based on Field-Effect Transistors. *Sens. Actuators, B* **1995,** *24-25*, 197-200.

(13) Högg, G.; Lutze, O.; Cammann, K. Novel Membrane Material for Ion-Selective Field-Effect Transistors with Extended Lifetime and Improved Selectivity. *Anal. Chim. Acta* **1996,** *335*, 103-109.

(14) Bratov, A.; Abramova, N.; Munoz, J.; Dominguez, C.; Alegret, S.; Batroli, J. Optimization of Photocurable Polyurethane Membrane Composition for Ammonium Ion Sensor. *J. Electrochem. Soc.* **1997,** *144*, 617-621.

(15) Ufer, S.; Cammann, K. Ion-Sensitive Field-Effect Transistor with Improved Membrane Adhesion. *Sens. Actuators, B* **1992,** *7*, 572-575.

(16) Meyerhoff, M. E.; Cha, G. S.; Ma, S. C.; Goldberg, H. D.; Brown, R. B.; Midgley, A. R.; Cantor, H. C. New Polymeric Membrane Materials for Fabricating Potentiometric Ion- and Bioselective Sensors. *Polym. Mater. Sci. Eng.* **1991,** *64*, 292-293.

(17) Sakong, D. S.; Cha, M. J.; Shin, J. H.; Cha, G. S.; Ryu, M. S.; Hower, R. W.; Brown, R. B. Asymmetric Membrane-Based Potentiometric Solid-State Ion Sensors. *Sens. Actuators, B* **1996,** *32*, 161-166.

(18) Bergveld, P.; Sibbald, A. *Analytical and Biomedical Applications of Ion-Selective Field-Effect Transistors*; Elsevier: Amsterdam, 1988.

(19) Yun, S. Y.; Hong, Y. K.; Oh, B. K.; Cha, G. S.; Nam, H.; Lee, S. B.; Jin, J. Potentiometric Properties of Ion-Selective Electrode Membranes Based on Segmented Polyether Urethane Matrices. *Anal. Chem.* **1997,** *69*, 868-873.

(20) Iordanskii, A. L.; Razumovskii, L. P.; Krivandin, A. V.; Lebedeva, T. L. Diffusion and Sorption of Water in Moderately Hydrophilic Polymers: From Segmented Polyetherurethanes to Poly-3-hydroxybutyrate. *Desalination* **1996,** *104*, 27-35.

(21) Bratov, A. V.; Abramova, N.; Munoz, J.; Dominguez, C.; Alegret, S.; Bartoli, J. Ion Sensor with Photocurable Polyurethane Polymer Membrane. *J. Electrochem. Soc.* **1994,** *141*, L111-L112.

(22) Oesch, U.; Caras, S.; Janata, J. Field Effect Transistors Sensitive to Sodium and Ammonium Ions. *Anal. Chem.* **1981,** *53*, 1983-1986.

(23) Munoz, J.; Jimenez, C.; Bratov, A.; Bartroli, J.; Alegret, S.; Dominguez, C. Photosensitive Polyurethanes Applied to the Development of CHEMFET and ENFET Devices for Biomedical Sensing. *Biosens. Bioelectron.* **1997,** *12*, 577-585.

(24) Jimenez, C.; Bartroli, J. Development of an Ion-Sensitive Field Effect Transistor (ISFET) Based on PVC Membrane Technology with Improved Long-Term Stability. *Electroanalysis* **1997,** *9(4)*, 316-319.

(25) Senillou, A.; Jaffrezic-Renault, N.; Martelet, C.; Griffe, F. A Miniaturized Ammonium Sensor Based on the Integration of Both Ammonium and Reference FETs in a Single Chip. *Mater. Sci. Eng., C* **1998**, 59-63.

(26) Jimenez, C.; Marques, I.; Bartroli, J. Continuous-Flow System for Online Water Monitoring Using Back-Side Contact ISFET-Based Sensors. *Anal. Chem* **1996,** *68*, 3801-3807.

(27) Brzozka, Z.; Dawgul, M.; Pijanowska, D.; Torbicz, W. Durable NH_4^+-Sensitive CHEMFET. *Sens. Actuators, B* **1997,** *44*, 527-531.

(28) van der Wal, P. The Development of a Durable Potassium Sensor Based on FET-Technology, Doctoral Dissertation, University of Twente, 1991.

(29) PuigLleixa, C.; Jimenez, C.; Fabregas, E.; Bartroli, J. Potentiometric pH Sensors Based on Urethane-Acrylate Photocurable Polymer Membranes. *Sens. Actuators, B* **1998,** *49*, 211-217.

(30) Bühlmann, P.; Pretsch, E.; Bakker, E. Carrier-Based Ion-Selective Electrodes and Bulk Optodes. 2. Ionophores for Potentiometric and Optical Sensors. *Chem. Rev.* **1998,** *98*, 1593-1687.

(31) Bakker, E.; Xu, A.; Pretsch, E. Optimum Composition of Neutral Carrier Based pH Electrodes. *Anal. Chim. Acta* **1994,** *295*, 253-262.

(32) Li, X.; Verpoorte, E. M. J.; Harrison, D. J. Elimination of Neutral Species Interferences at the Ion-Sensitive Membrane/Semiconductor Device Interface. *Anal. Chem.* **1988,** *60*, 493-498.

(33) Jadhav, S.; Bakker, E. Acetic Acid Release from Polymeric Membrane pH Electrodes for Generating Local pH Gradients at Ion-Selective Membranes. *Electrochem. and Solid-State Letters* **1998,** *1*, 194-196.

(34) Chaniotakis, N. A.; Moschou, E. A.; Constantinidis, G. Highly Selective Two-Ion-Carrier Chemically Modified FETs. *Microelectron. Eng.* **1998,** *41/42*, 481-484.

(35) Moschou, E. A.; Chaniotakis, N. A. Ion-Partitioning Membrane-Based Electrochemical Sensors. *Anal. Chem.* **2000,** *72*, 1835-1842.

(36) Sudhölter, E. J. R.; van der Wal, P. D.; Skowronska Ptasinska, M.; van den Berg, A.; Bergveld, P.; Reinhoudt, D. N. Modification of ISFETs by Covalent Anchoring of Poly(hydroxyethylmethacrylate) Hydrogel: Introduction of a Thermodynamically Defined Semiconductor-Sensing Membrane Interface. *Anal. Chim. Acta* **1990,** *230*, 59-65.

(37) Zwickl, T.; Schneider, B.; Lindner, E.; Sokalski, T.; Schaller, U.; Pretsch, E. Chromoionophore-Mediated Imaging of Water Transport in Ion-Selective Membranes. *Anal. Sciences* **1998,** *14*, 57-61.

6 Photochemical Immobilization of Biotin on the Surface of Ion-Selective Electrode Membranes and Binding of Streptavidin

6.1 Introduction

In the past years, there has been a great development in the field of biosensors, driven by a huge demand for biomedical applications such as immunoassays, drug screening and discovery, functional genomics, and tissue engineering.[1] Most bioanalytical sensors have a surface with patterned biomolecules like peptides, proteins, or oligonucleotides. Over the years, a wide variety of immobilization strategies have been developed for creating selective reaction layers. The most important techniques are adsorption, gel entrapment, cross-linking and direct covalent coupling to the surface.[2] In this work, photo-cross-linking based on activation of introduced light-sensitive reagents is used for immobilizing biomolecules on surfaces. The immobilized biomolecules serve as host molecules for the complexation with guest molecules dissolved in the sample solution.

In this doctoral dissertation, the synthesis of a novel, highly effective photoreactive cross-linker bearing a biotin moiety is reported. This biotin derivative, immobilized on a polyurethane membrane, specifically binds a protein called streptavidin in the sample. Furthermore, the influence of immobilized photoreagents on the response behavior of ISEs was investigated with and without bound protein. The aim of this work was to achieve a change in the potentiometric signal due to the specifically bound protein on the membrane surface.

6.2 A Working Vocabulary

6.2.1 Photo-Cross-Linking

Although a great number of techniques is available to covalently bind organic compounds to various substrates in order to create selective reaction layers, there are only comparatively few contributions to modify the surface of soft polymers. In such substrates, diffusion coefficients of water or organic molecules are in the order of 10^{-8}

cm^2 s^{-1}.[3, 4] Therefore, several of the established procedures of covalent immobilization to solid surfaces cannot be applied with such membranes. For example, one frequently used method for improving the biocompatibility of soft polyurethanes is plasma etching,[5] which generates an uncontrolled mixture of functional groups which extend into the interior of the polymer. Plasma etching is, therefore, not considered to be adequate for pure surface modifications. In contrast, photo-cross-linking has been shown to be applicable for the surface modification of polyurethane membranes. It has been used to modify the surface of the membranes in order to improve their biocompatibility. For example, poly(ethylene oxide)[6] and theophylline[7] were attached to the surface of the polyurethanes Tecoflex and Pellethane by photo-cross-linking using dicumyl peroxide as photoinitiator or an azidobenzene derivative of theophylline, respectively. In both cases, a significant reduction of surface platelet formation was achieved.[6, 7] However, we are not aware of any work that attempted to immobilize selective complexing agents on the surface of sensor membranes.

On activation by light, photoreactive cross-linkers can be covalently bound to surfaces. This technique is often used for biointerfaces that have become essential components of sensor devices, bioelectronic elements, diagnostic systems, and medical equipment.[8] The preferred mediating photosensitive reagents are substituted arylazides, trifluoromethylaryldiazirines, and benzophenones. In this work, trifluoromethylaryldiazirines are used, which absorb light of wavelength 350 nm and are remarkably stable under a range of different physical and chemical conditions, including heat (80 ^{o}C), strong bases and acids.[9] They can be handled under normal laboratory conditions, and no precautions are required to avoid exposure to light, since they have low extinction coefficients.

Highly reactive carbenes are formed according to Figure 6.1 on photoactivation of trifluoromethylaryldiazirines[10], which react preferably with C-H, C-C, C=C, N-H, O-H, or S-H bonds. Photogenerated carbenes are short living species with half-lifetimes on the order of microseconds. They form covalent bonds with substrates or molecules that are within their molecular vicinity. Thus, the removal of solvent on surface is necessary before light activation.[8] Photoimmobilizing mostly does not hamper the biological functions of biomolecules.[11] In contrast to thermochemical target molecule immobilization, light activatable cross-linking is a noninvasive coupling procedure requiring mild reaction conditions, which retain native biomolecule structures. Photo-

cross-linking is excellently suited for biological molecules because it does not demand heating. Moreover, topical addressability is an important property of photoactivatable reagents.

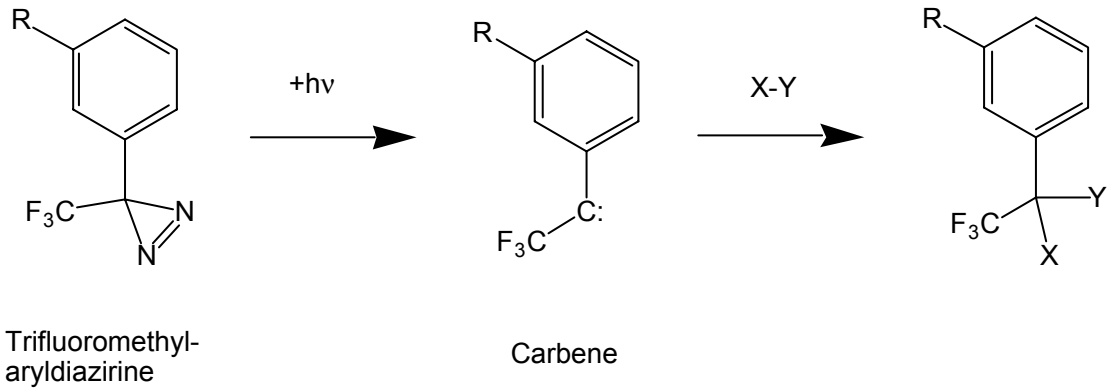

Figure 6.1 Chemical structures of a light-induced reaction to a polymer surface.[8]

In this work, heterobifunctional cross-linkers are used. They have a trifluoromethylaryldiazirine as photoreactive group and either a maleimide or biotin as an additional functional group. There is a commercially available photobiotin with arylazide as photoreactive group,[12] but the formation of cross-links with trifluoromethylaryldiazirines is much more efficient than with their arylazide counterparts. Furthermore, the covalent adducts of trifluoromethylaryldiazirines are stable enough for purification and following reaction steps.[13] As no carbene-generating biotin derivative was available when we started the project, we designed and synthesized a novel trifluoromethylaryldiazirine derivative bearing a biotin moiety biotin in order to generate patterned surfaces with biotin-streptavidin. More recently, carbene-generating photobiotins were used on the one hand for the segregation of micrometer-sized domains of glassy-carbon, quartz, and polymer surfaces,[14] and on the other hand in bioprobes, such as a photoaffinity taxoid probe[15] or for photoaffinity labeling of a glycosyltransferase.[16]

6.2.2 Biotin-Streptavidin System

Biotin-streptavidin was chosen for immobilization on ISE membranes because it is a very well characterized bioconjugation. The corresponding interaction (K_d = 10^{-14} M) is one of the strongest known noncovalent biological recognitions between protein and ligand.[17, 18] Streptavidin has a significant higher affinity for biotin in solution than for immobilized biotin on planar layers.[19] Bond formation between biotin and streptavidin is very rapid, and once formed, it is unaffected by wide ranges of pH, temperature, organic solvents, or other denaturing agents.[20] Outside these parameters, the loss of biotin-binding capacity is largely due to the denaturation of streptavidin. The half-life of the biotin-streptavidin complex in solution is 9.2 d at pH 5.0, 2.9 d at pH 7.0, and 1.3 d at pH 9.2.[18] It was found that the rate constants of dissociation of the streptavidin-biotin bond were larger on surfaces than in solutions.[21, 22]

Streptavidin is a 60 000 Da, tetrameric, biotin-binding protein isolated from culture broth of *Streptomyces avidinii*.[23] Streptavidin has four biotin-binding sites, and cooperative binding of biotin occurs.[20] In contrast to avidin, streptavidin does not possess carbohydrate and has a slightly acid isoelectric point of approximately 5-6.[18] Streptavidin is interchangeable with avidin in many applications, but streptavidin is usually preferred due to its lower nonspecific binding characteristics.[24] Unlike avidin,[18] streptavidin retains its ability to bind to biotin in the presence of common detergents.[20]

Biotin is a naturally occurring vitamin found in every living cell. The tissues with the highest amounts of biotin are liver, kidney, and pancreas. Biotin has a very small extinction coefficient at the absorption maximum (λ = 250 nm).[20] The biotin-streptavidin technology is widely used for biosensors. Biotin has been immobilized for example on gold surfaces using self-assembled monolayers,[21, 25-29] on solid-contacts by photo-cross-linking,[12, 30, 31] on Langmuir-Blodgett films,[32] and on electrodes by entrapment.[33] Spacers enhance the accessibility of the biotin moiety for holding streptavidin, thereby improving binding characteristics.[22] The choice of the spacer arm is crucial. A length of eleven atoms or more is necessary to ensure unrestricted recognition of biotin by streptavidin.[34] In addition, its chemical composition is important in order to guarantee solubility of biotin during the preparation of the active layer.[28] Most spacers have a hydrophobic/hydrophilic balance originating from oxygen atoms and methylene groups.[34]

The density of the immobilized biotin layer is crucial, as the surface density of bound streptavidin reaches a maximum at low biotin concentration.[32] It has been hypothesized that a too closely packed layer of biotin on the surface could sterically inhibit biotin entry into one of the streptavidin binding pockets.[28] As the amount of the biotin ligand on the surface increases, there is a greater likelihood that streptavidin may bind to the surface *via* tow binding sites.[29] Furthermore, the composition and density of the immobilized biotin layer influence the binding kinetics of streptavidin.[24-26, 35, 36] Adsorption of streptavidin was found to occur at a diffusion-limited rate.[21]

6.2.3 Super-Nernstian Response of Ion-Selective Electrodes

Referring to data of Sokalsky *et al*.,[37-40] the detection limit of ISEs can be extended into the picomolar range by eliminating the leaching of primary ions into the sample boundary zone, which is in contact with the membrane surface.[41-43] This can be achieved by creating a concentration gradient in the membrane that drives primary ions backwards, through the membrane, into the inner filling. Therefore, a large improvement of the lower detection limit was obtained with inner solutions, whose concentration of analyte ions was buffered to a low level while keeping that of the interfering ions high. However, the net fluxes of ions through the membrane have to be very small in order to guarantee a Nernstian slope. By applying a very low direct current during the measurement, the lower detection limit was also extended by several orders of magnitude.[44]

In this work, a photosensitive biotin derivative was cross-linked on a polyurethane ISE membrane. The influence of the immobilized biotin-streptavidin on the sensor behavior was evaluated. In contrast to the systems studied by Sokalsky *et al*.,[38-40] ISEs with a super-Nernstian response were used in this dissertation. Large gradients in the membrane (Figure 6.2) lead to considerate depletion of analyte ions in the sample boundary region next to the sample/membrane and thus to a super-Nernstian response, as shown in Figure 6.3. In order to obtain a pronounced super-Nernstian response, which is kinetically controlled, it is necessary to maximize the diffusion fluxes at the sample/membrane interface. Therefore, the ion concentration gradients in the membrane have to be sufficiently high which results in high transmembrane ion

fluxes. At very low activities of the primary ions in the sample, interfering ions are released from the membrane. In this case, the ISE response is mainly dictated by the interfering ions and therefore the resulting potentials appear at very low values. In contrast, the flux-induced deviations between boundary and bulk activity values turn out to be negligible for activities above the super-Nernstian step. In this activity range, the ISE reaches an equilibrium response to the analyte ions, which leads to much higher potentials. The intermediate super-Nernstian step yields extremely large potential excursions for very small changes of the sample activity in the bulk.

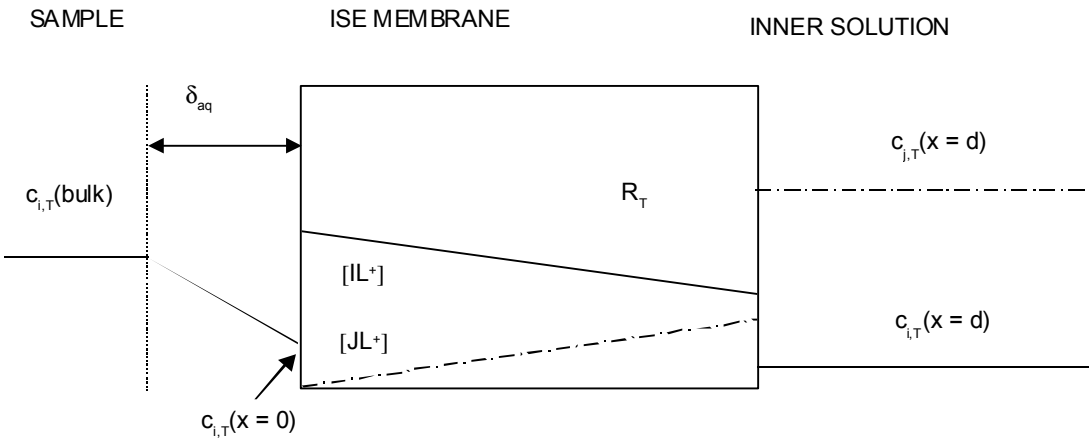

Figure 6.2 Schematic representation of the processes influencing the lower detection limit of ISEs. Gradients are generated in the aqueous boundary layer (thickness δ_{aq}) between sample and membrane because of transmembrane fluxes and partial exchange of primary ions by interfering ones at the inner membrane side.[40] $c_{i,T}$(bulk) is the total concentration of the free ion I^{zi} in the bulk sample solution.

The sample activity range where the super-Nernstian step occurs might be shifted under the influence of reactions taking place at the membrane surface, as shown in Figure 6.3. Host molecules (photosensitive biotin) covalently bound to the membrane surface can complex guest molecules (streptavidin) from the sample solution. These immobilized biomolecules might decrease the diffusion rate at the surface.

So far, only a few chemical sensor systems are known that are based on a change of fluxes at the interface. First, a potentiometric sensor responsive to the polyanion heparin[45] works on the principle of a nonequilibrium change of the phase boundary potential at the sample/membrane interface. Second, examples of ion-channel-mimetic sensors were described.[46] Redox reactions of electroactive species in the sample occur at the surface of these electrodes. The reaction rates can be controlled by selectively binding of analytes from the sample to the electrode surface, which is

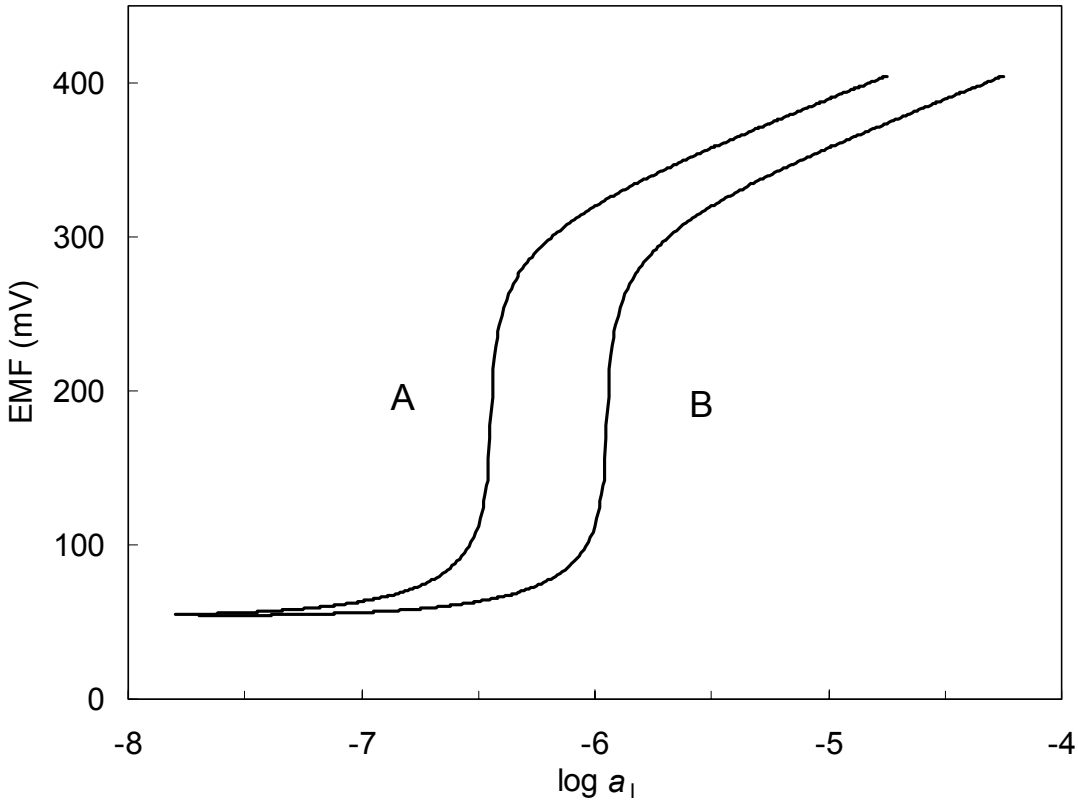

Figure 6.3 Membranes with a large ion uptake from the sample solution usually show a step-like change in the emf response function. The measuring ion acticity in the sample solution at which the ion uptake induces a large potential change might be significantly shifted when biological molecules from the sample bind to the membrane surface. In contrast to response curve A of a conventional system, response curve B refers to a system where biological guest molecules from the sample solution are complexed by covalently bound host molecules on the membrane surface.

chemically modified with receptors. The sterical blocking of the interface thus permits an indirect determination of the electroinactive analytes with the inherent possibility for chemical signal amplification. Furthermore, early studies by Rechnitz[47] indicated that by immobilizing of immunogen conjugates in the bulk of a liquid membrane matrix, antibody-selective potentiometric responses are obtained.

6.3 Surface Analyses of a Photoimmobilized Trifluoromethylaryldiazirine Derivative

The aim of the following surface analyses was to obtain evidence for the cross-linking of a photoactivatable reagent to a polyurethane surface. The photoreagent used was N-{3-[3-(trifluoromethyl)diazirine-3-yl]phenyl}-4-maleimidobutyramide (MAD). This MAD carries a diazirine, which will be lost during light activation leading to carbene-mediated binding to solid-supports and a maleimide function for thermochemical reactions with thiolated reagents.[48] Tecoflex membranes without plasticizers were used for all photoimmobilizations.

6.3.1 Atomic Force Microscopy

First, the aptitude of the polyurethane surface for photo-cross-linking was tested. To this end, the morphology of a pure Tecoflex membrane without MAD was mapped out using atomic force microscopy (AFM). The AFM images are shown in Figures 6.4–6.6. The surface structure of the Tecoflex membrane was featureless with a root-mean-square (r.m.s) roughness of about 0.7 nm. The height differences between the lower and higher spots were around 3 nm, as depicted in Figure 6.7. Nurdin *et al*.[49] found for a similar polyurethane surface, after drying in the vacuum, a peak-to-valley distance of about 15 nm. The Tecoflex membrane turns out to be very plain in comparison with an evaporated gold layer on a glass plate, as used for a self-assembled monolayer.[50] Accordingly, the smooth and homogenous morphology of the investigated polyurethane is well suited for immobilization of biomolecules.

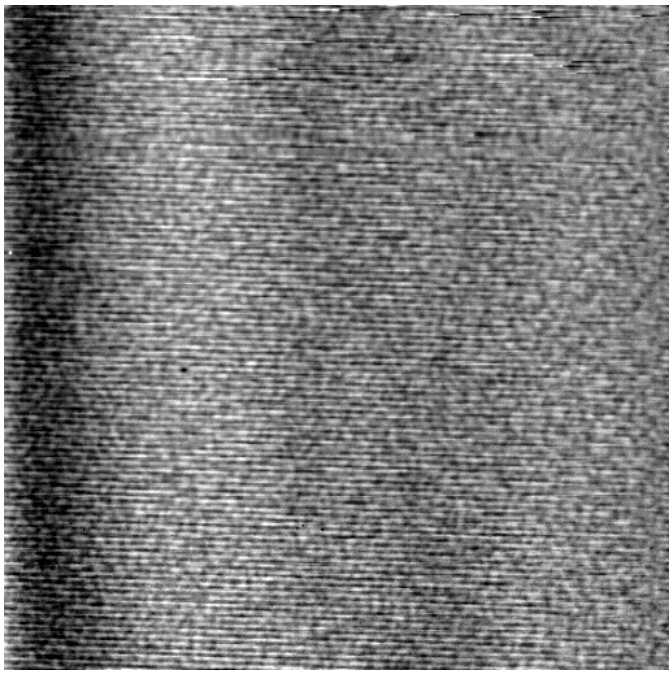

Figure 6.4 50 x 50 μm^2 AFM image (first order flattening) of a pure Tecoflex membrane.

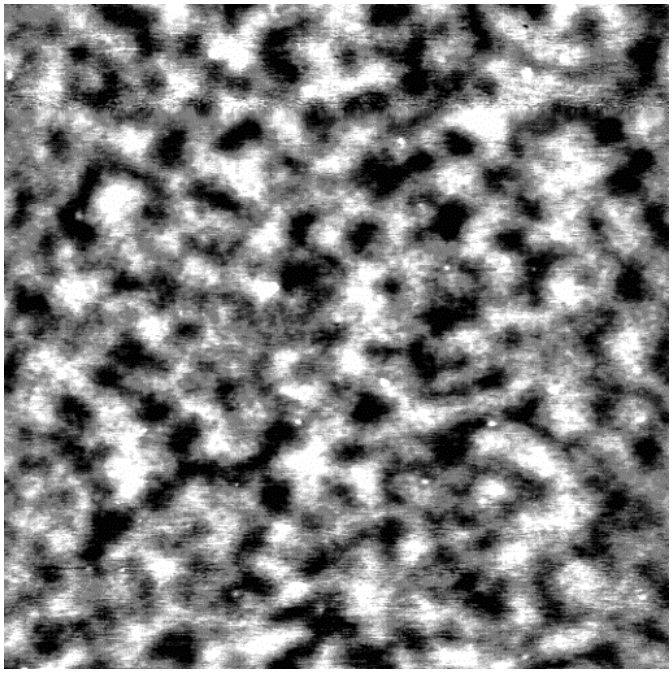

Figure 6.5 10 x 10 μm^2 AFM image (first order flattening) of a pure Tecoflex membrane. This picture is a blow-up of Figure 6.4. The z-range was 4 nm.

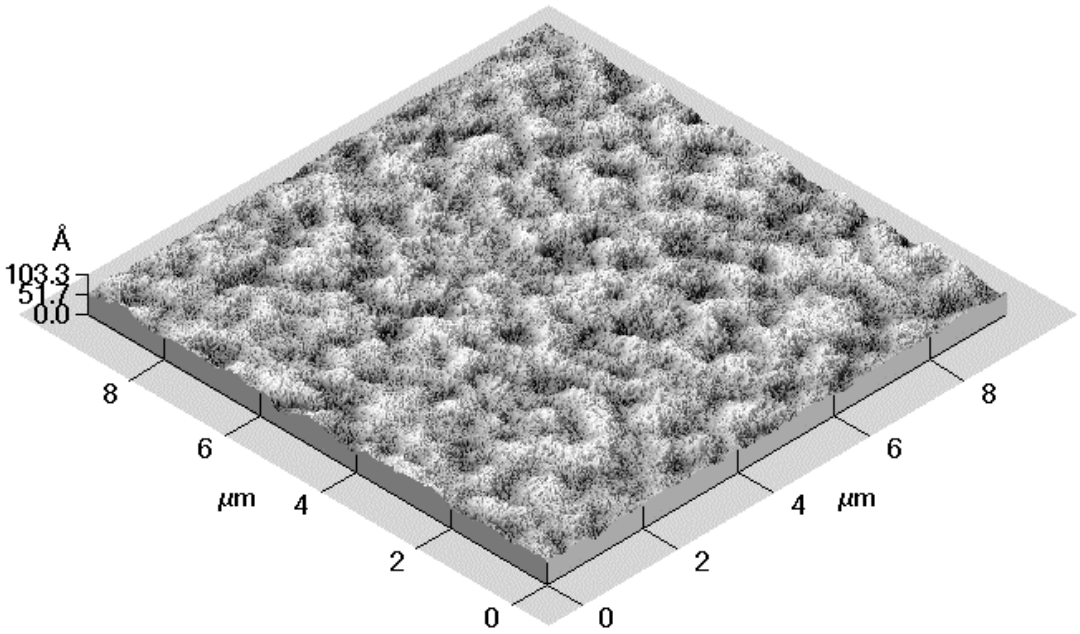

Figure 6.6 10 x 10 µm^2 AFM image (first order flattening) of a pure Tecoflex membrane. This picture is a 3-d view of Figure 6.5

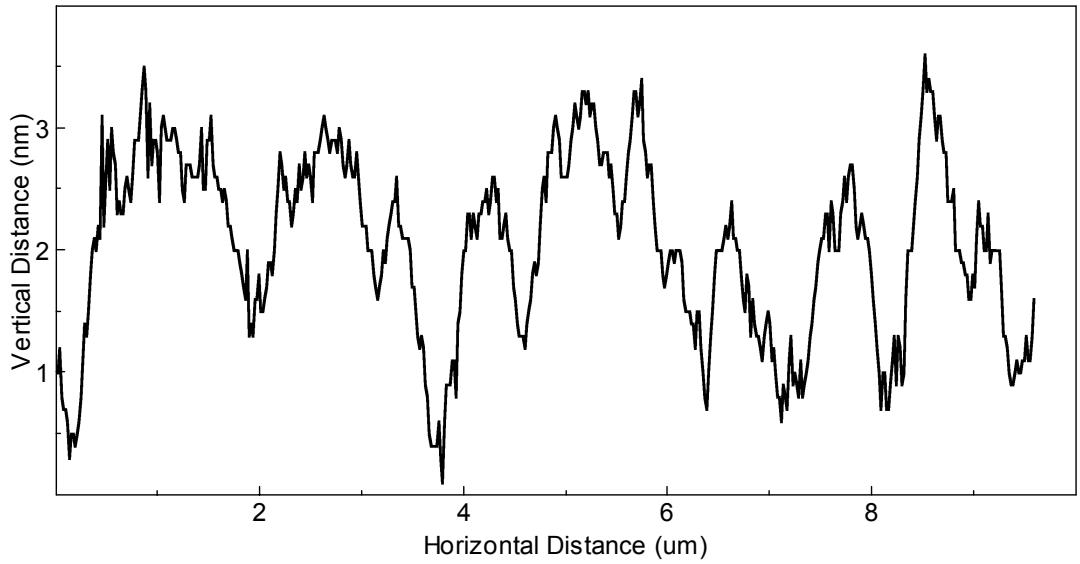

Figure 6.7 AFM depth profile of a pure Tecoflex membrane.

6.3.2 Fourier Transformation Infrared Reflection Absorption Spectroscopy

The surfaces of some membranes with and without MAD, respectively, were investigated using Fourier transformation infrared reflection absorption spectroscopy (FT-IRAS).[51, 52] For the photoimmobilization, an ethanol solution of MAD was deposited on a Tecoflex membrane, dried under high vacuum and irradiated by a UV-lamp immediately. Ethanol and other solvents like water, methanol, acetonitrile, diethyl ether, cyclohexane, petroleum ether, and hexane neither dissolved nor swelled Tecoflex. The added borate in the membrane does not disturb the photoimmobilization, because it absorbs at 250 nm.

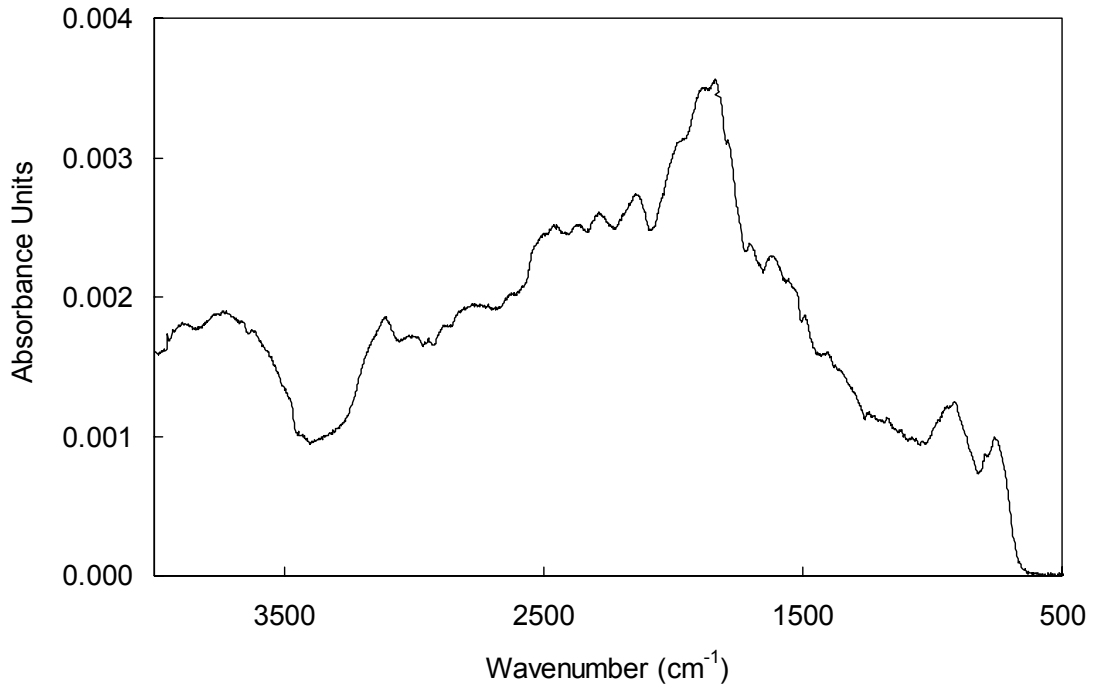

Figure 6.8 FT-IRAS spectra of a Tecoflex membrane without photoimmobilized MAD on the membrane surface.

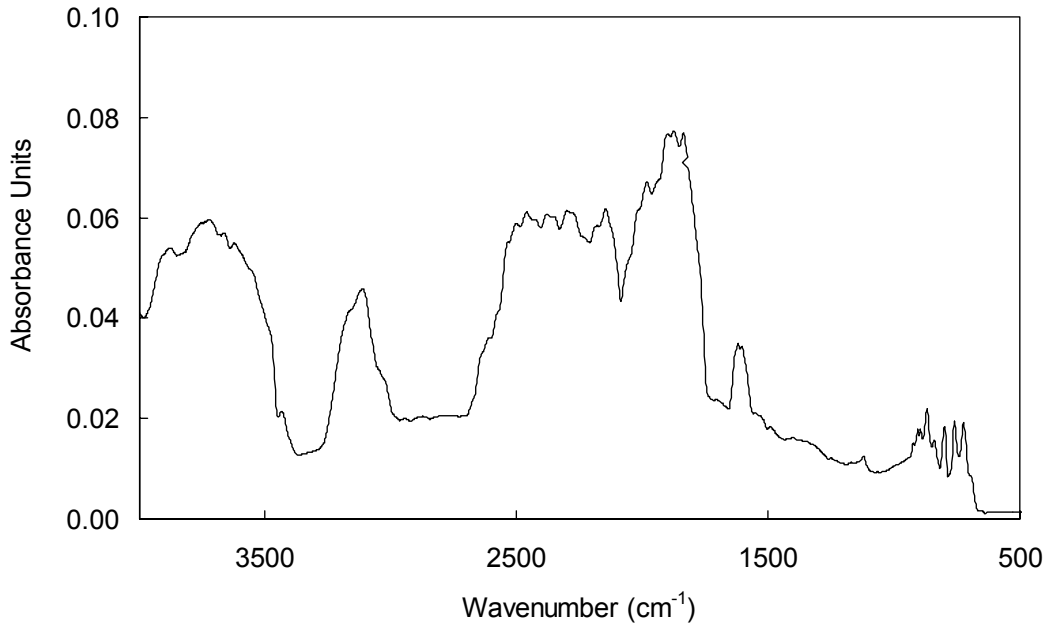

Figure 6.9 FT-IRAS spectra of a Tecoflex membrane with photoimmobilized MAD on the membrane surface.

In contrast to Tecoflex, MAD possesses a trifluoromethyl-group with two characteristic IR-peaks.[53] The FT-IRAS spectra of membranes without MAD (Figure 6.8) were significantly different from the ones with MAD (Figure 6.9), but there were no typical trifluoromethyl peaks recorded. Consequently, there was no evidence for the photoimmobilization of MAD using FT-IRAS. The orientation of MAD on the surface might be non-uniform and the surface concentration of MAD was perhaps too small.

6.3.3 X-Ray Photoelectron Spectroscopy

Pure Tecoflex membranes with and without MAD were examined by X-ray photoelectron spectroscopy (XPS) for providing a qualitative and quantitative analysis of their surface.

Table 6.1 Composition (atomic percentage) of pure Tecoflex membranes with and without MAD.

analytical method	C [%]	O [%]	N [%]	F [%]
elemental analysis[a]	78.57	19.05	2.38	-
XPS[a]	78.07	20.98	0.95	-
XPS[b]	78.25	19.59	1.81	0.35

[a] MAD was not photoimmobilized on the membrane surface.

[b] MAD was photoimmobilized on the membrane surface.

Membranes without MAD do not contain fluorine, as shown in Table 6.1. There are small differences between the surface concentrations determined from the XPS analysis (Table 6.1, second row) and the bulk membrane composition found from the elemental analysis (Table 6.1, first row). This can be explained by phase separation

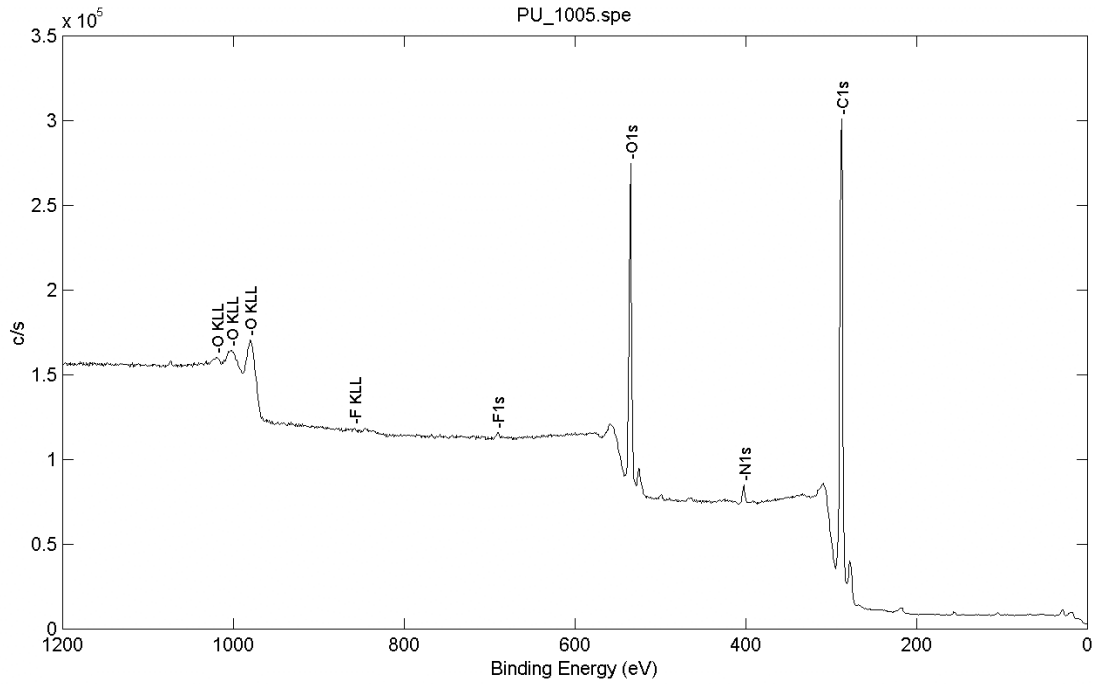

Figure 6.10 XPS wide-scan spectra of a pure Tecoflex membrane with photoimmobilized MAD. There is a weak fluorine signal at 689.5 eV.

that takes place at the few outermost molecular layers of the polyurethane, where little or no hard segments were found in earlier studies.[54-56] For the membrane with MAD, the spectrum in Figure 6.10 displays a weak photoelectron peak for F 1s, which is a clear evidence for the successful photoimmobilization of MAD.[57] Consequently, MAD was definitely cross-linked on the membrane surface.

Referring to the data of Sigrist,[57, 58] MAD was photoimmobilized on diamond, silicon, and silicon nitride. Diamond had the highest grafting efficiency, and it was shown that C-O bonds were formed when diazirine photoactivation was involved. Besides, a MAD-derivative was immobilized on diamond with a density of 1 x 10^{12} molecules cm^{-2}, and the efficiency of the immobilization was found to be below one percent.[59, 60]

6.4 Radiochemical Surface Analysis of Photoimmobilized Biotin-Streptavidin

6.4.1 Syntheses

For the immobilization of biotin-streptavidin on polyurethane, the light activatable compound **1** was synthesized, as shown in Figure 6.11. This novel photoreagent is based on MAD and bears a biotin moiety. The thiol group of the synthesized biotin derivate **3** reacted with the maleimide function of MAD resulting in compound **1**. Some biotin derivatives bearing a thiol group were described in the literature,[21, 25, 27-29, 61-63] but all of them either had a too long chain length or were rather cumbersome to synthesize. In addition, the synthesis of heterobifunctional cross-linking reagents with a biotin and a trifluoromethylaryldiazirine moiety has been described.[13, 15, 16] However, the syntheses of these compounds are very cumbersome and include at least eight reaction steps. After completing this work, the use of a similar compound was reported,[14] but the synthesis of this compound has not yet been described.

The first task of the synthesis of MAD-biotin **1** was the esterification of biotin. Bromo-biotin **2** was prepared by reaction of biotin with five equivalents of 11-bromo-undecanol in toluene heated to reflux, catalyzed by *p*-toluenesulphonic acid.[64] Filtration to remove unreacted biotin and chromatography gave the ester **2** in a yield of 70%. Preliminary esterfication experiments demonstrated that this reaction is also possible with shorter alkyl chains and might be useful for biotin immobilization on functionalized surfaces.

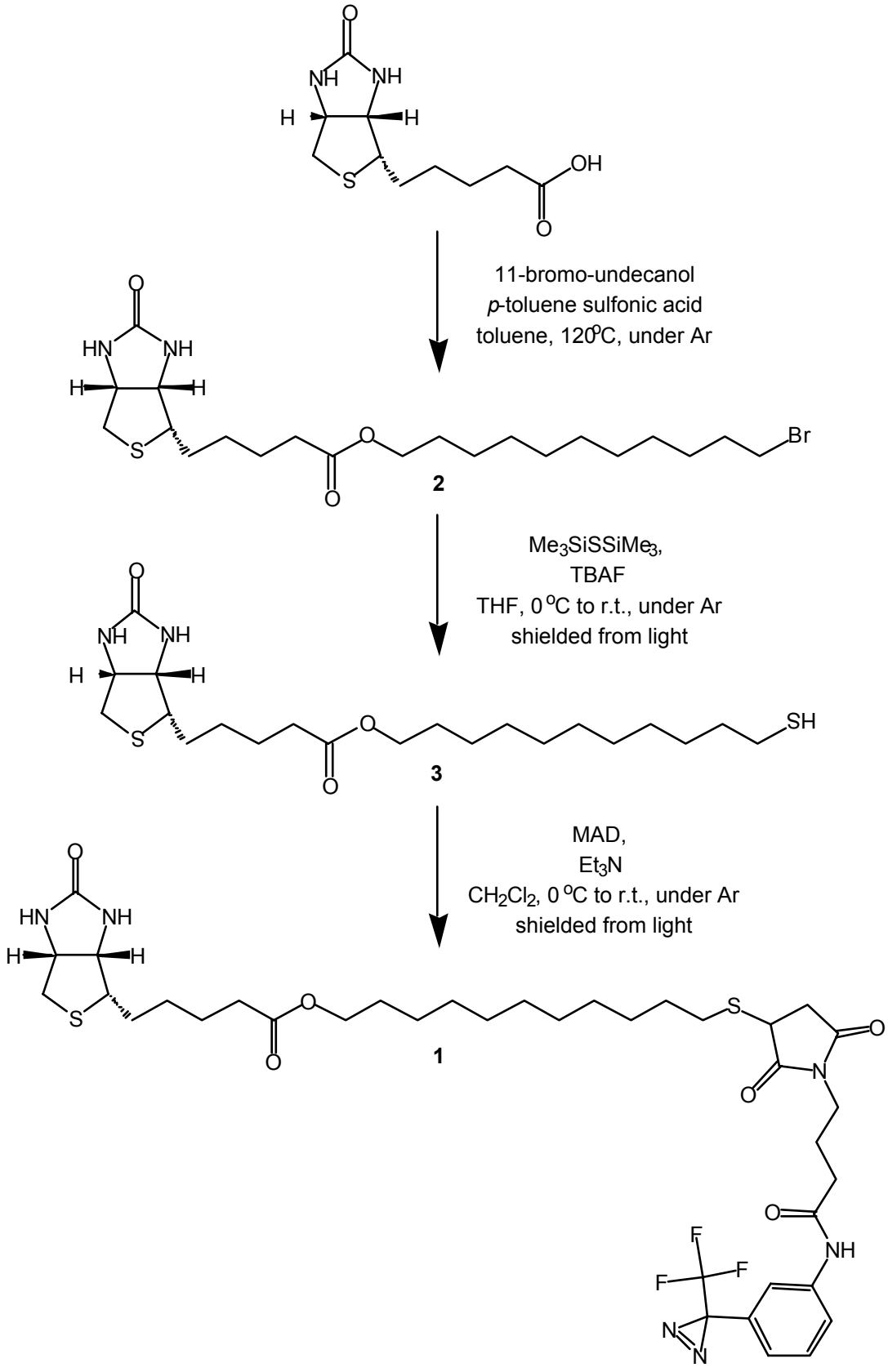

Figure 6.11 Synthetic pathway to biotin derivative **1**.

The second reaction step was the thiolization of the bromo-biotin **2**. For this purpose, tetrabutylammonium trimethylsilylthiolate ($Me_3SiS^-Bu_4N^+$) was generated in situ by adding a solution of tetrabutylammonium fluoride (TBAF) to hexamethyldisilathiane ($Me_3SiSSiMe_3$) in THF.[65] Tetrabutylammonium trimethylsilylthiolate reacted rapidly with the bromo-biotin **2** to form on aqueous workup and purification by reprecipitation the thiol-biotin **3** in a yield of 75 %. This procedure represents one of the mildest available methods for thiol synthesis. Since the reaction is conducted under near neutral reaction conditions for a short period of time, autooxidation of thiol products to disulfides and/or sulfonic acids becomes less severe compared to methodologies that require basic hydrolysis.[65] The synthesis of exactly the same thiol-biotin **3** was already described by Knoll *et al.*[61] However, their procedure with a disulfide intermediate including four reaction steps was cumbersome and had very poor yields. The novel and simpler reaction presented here requires only two simple reaction steps and gives better yields.

The reaction with MAD gave the final product **1**. Adding thiol-biotin **3** to MAD in the presence of a catalytic amount of triethylamine resulted in the succinimide MAD-biotin **1** as a 1:1-mixture of diastereoisomers.[66-68] The disappearance of the maleimide function at λ = 330 nm during this reaction and the loss of the diazirine function of the MAD-biotin during irradiation at λ = 350 nm were observed by UV/VIS spectroscopy.[69]

6.4.2 Radiochemistry

Some factors governing the binding reaction between surface-attached MAD-biotin and streptavidin from solution were elucidated by radiochemical methods. Most of the surface analyses of the biotin-streptavidin system done to date were based on fluorescence, which yields qualitative results with very high spatial resolution.[12, 22, 30-32, 34, 70, 71] In contrast, autoradiographic methods provide quantitative results[72] and two-dimensional images with a resolution of 88 μm. The soft β-emitter [^{35}S]-streptavidin was used as radiolabel. First, MAD-biotin was photoimmobilized on small glass plates that were covered with a membrane of type 6B (Ca^{2+}). After conditioning several series of the glass plates in water and treating them with a

surfactant, all samples were contacted with a [^{35}S]-streptavidin solution. Finally, the adsorbed radiolabel on the membrane was quantified using autoradiography.

According to Figures 6.12 – 6.14, the samples with photoimmobilized MAD-biotin bound stronger [^{35}S]-streptavidin than the ones without MAD-biotin. Consequently, the cross-linked MAD-biotin was able to bind [^{35}S]-streptavidin on the polyurethane surface. Furthermore, the MAD-biotin activation by light did not impair the biological activity. The distribution of [^{35}S]-streptavidin on the membranes with MAD-biotin was non-uniform, as depicted in Figure 6.14. This was caused by irregular photoimmobilization of MAD-biotin, because the [^{35}S]-streptavidin coverage on membranes without MAD-biotin was homogenous. The deposition of MAD-biotin droplets and the vacuum treatment resulted in a heterogeneous coverage that could even be observed with a magnifying glass. In previous AFM studies, the immobilization of photobiotin on solid contact was not uniform either.[12] AFM images also indicated that the adsorption of streptavidin on biotinylated surfaces is non-uniform, and that the proteins tend to cluster.[30] More than 80% of the adsorbed proteins were found in clusters of three or more molecules.[21] Additionally, avidin does not bind fully towards immobilized biotin.[12] Cosnier[33] investigated several techniques for stable immobilization of macromolecular biomolecules on polymers with complete retention of their biological recognition properties. Cross-linking was characterized as a rarely reproducible deposition technique with a poor spatial control.

The surface densities of the adsorbed [^{35}S]-streptavidin are shown in Table 6.2. These calculations are based on the density of a two-dimensional crystalline streptavidin (C2,2,2) monolayer, which is 262 ng cm^{-2} or 3780 angstrom^2 molecule^{-1}.[19, 29] The density of this streptavidin crystal is not very high. The area of the holes between the streptavidin molecules amount to 34% of the monolayer surface.[28] Most Tecoflex membranes in this work were not fully covered with [^{35}S]-streptavidin, although the quantity of applied [^{35}S]-streptavidin would have been enough to cover the membrane surface 100 times. It is difficult to get a complete surface coverage because of repulsion. For example, self-assembled monolayers showed the highest streptavidin density, when only 5-10 % of the surface was biotinylated.[28]

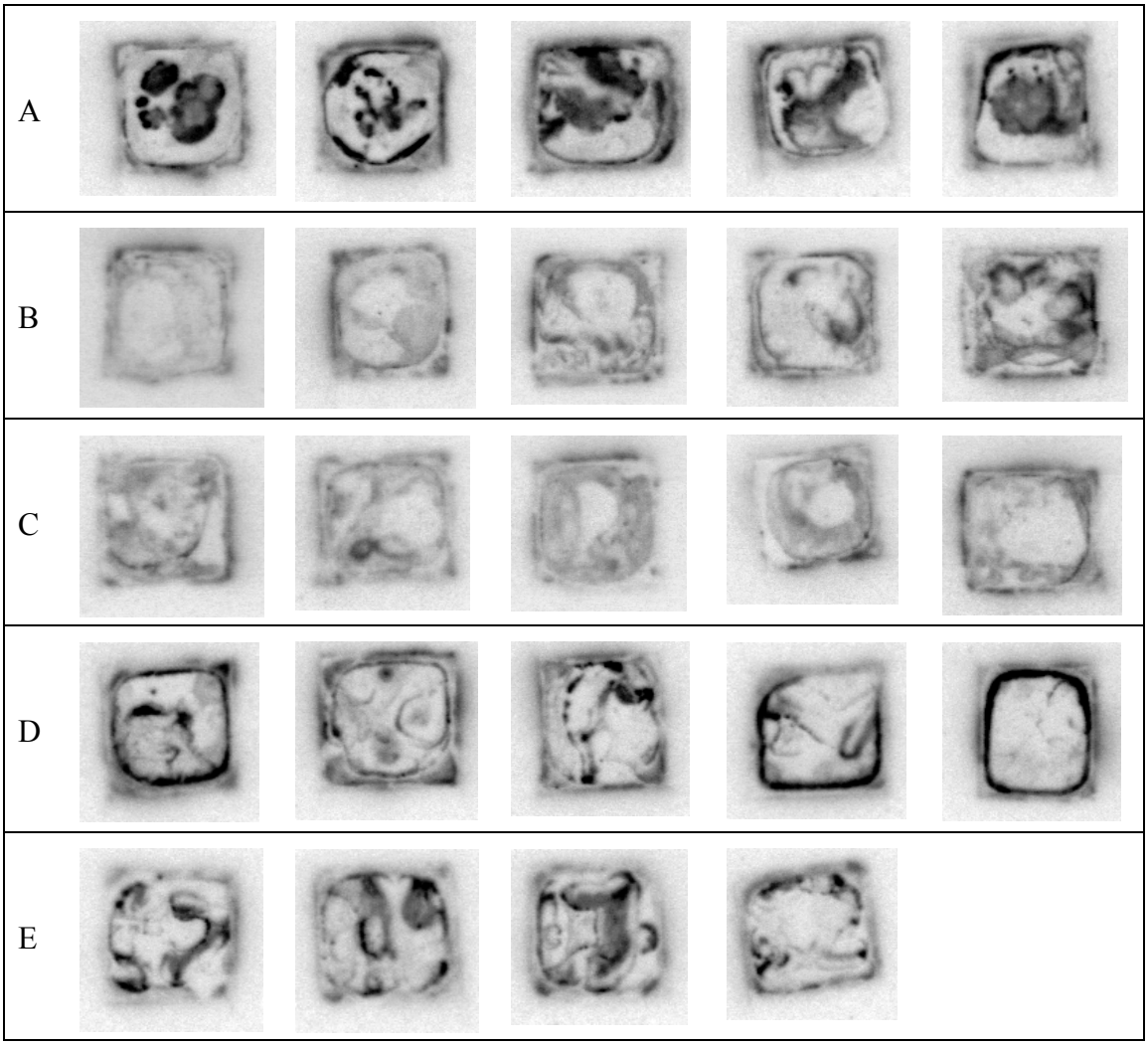

Figure 6.12 Autoradiography of membranes poured onto quadratic glass slides, which were incubated into a solution of [^{35}S]-streptavidin. The intensity of the coloring is proportional to the density of adsorbed [^{35}S]-streptavidin. MAD-biotin was photoimmobilized on all samples, whereas the pretreatment was different: A, 10 min in vacuum and without any surfactant incubation; B, 10 min in vacuum and surfactant (Tween) treatment before the streptavidin incubation; C, 20 min in vacuum and Tween treatment before the streptavidin incubation; D, 80 min in vacuum and without any Tween incubation; E, 80 min in vacuum and Tween treatment after the streptavidin incubation.

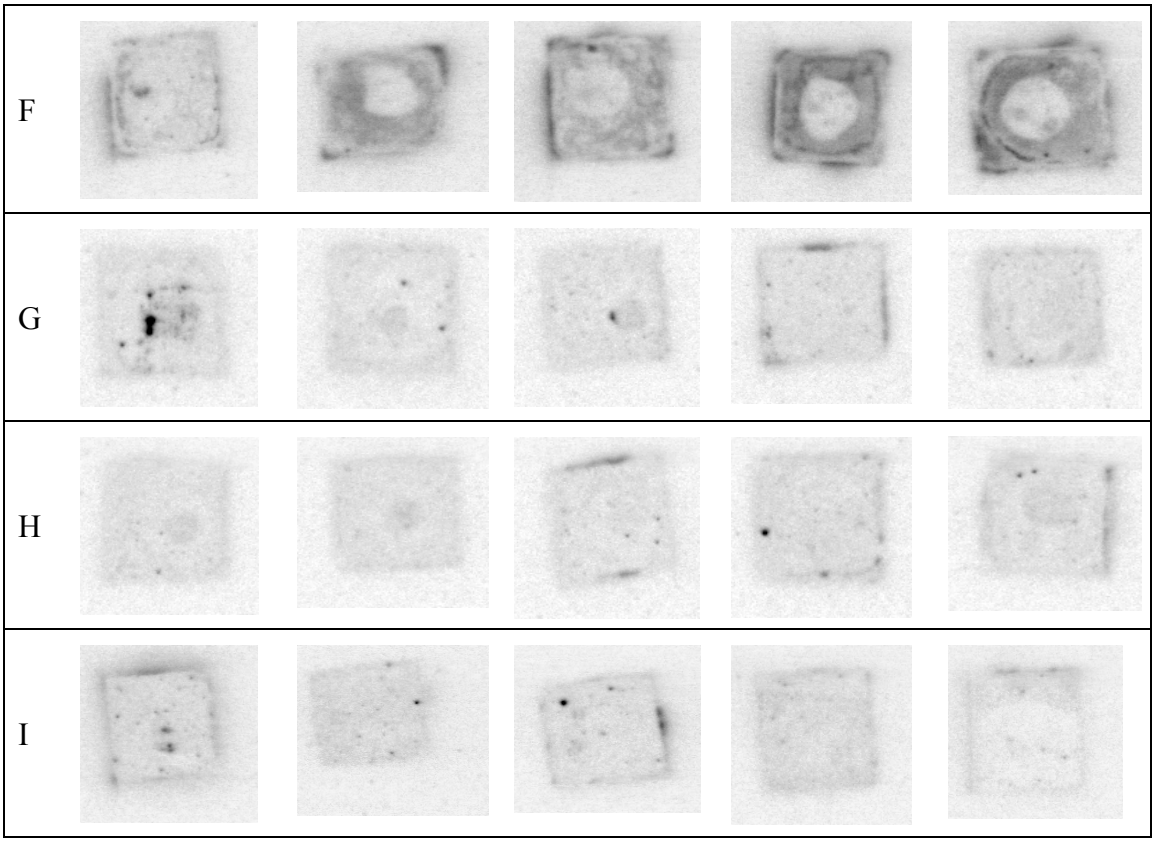

Figure 6.13 Autoradiography of membranes poured onto quadratic glass slides, which were incubated into a solution of [^{35}S]-streptavidin. The intensity of the coloring is proportional to the density of adsorbed [^{35}S]-streptavidin. MAD-biotin was photoimmobilized only on the samples of series F. The samples had the following pretreatment: F, 80 min in vacuum and Tween treatment before the streptavidin incubation; G, without any pretreatment; H, deposition of a pure acetonitrile drop, 80 min vacuum and no Tween treatment; I, Tween treatment before the streptavidin incubation.

As a result, photoimmobilizing of MAD-biotin was non-uniform and might have a poor efficiency. In previous studies, the photo coupling efficiency of MAD-[^{35}S]Cys to Polystyrene was 7%.[48] Furthermore, diffusion of MAD-biotin into the PUR membrane before cross-linking may have a certain effect. Assuming that MAD-biotin is sufficiently soluble in Tecoflex, the diffusion of MAD-biotin into Tecoflex can be estimated with the help of the following equation:[73]

$$d = \sqrt{2Dt}$$

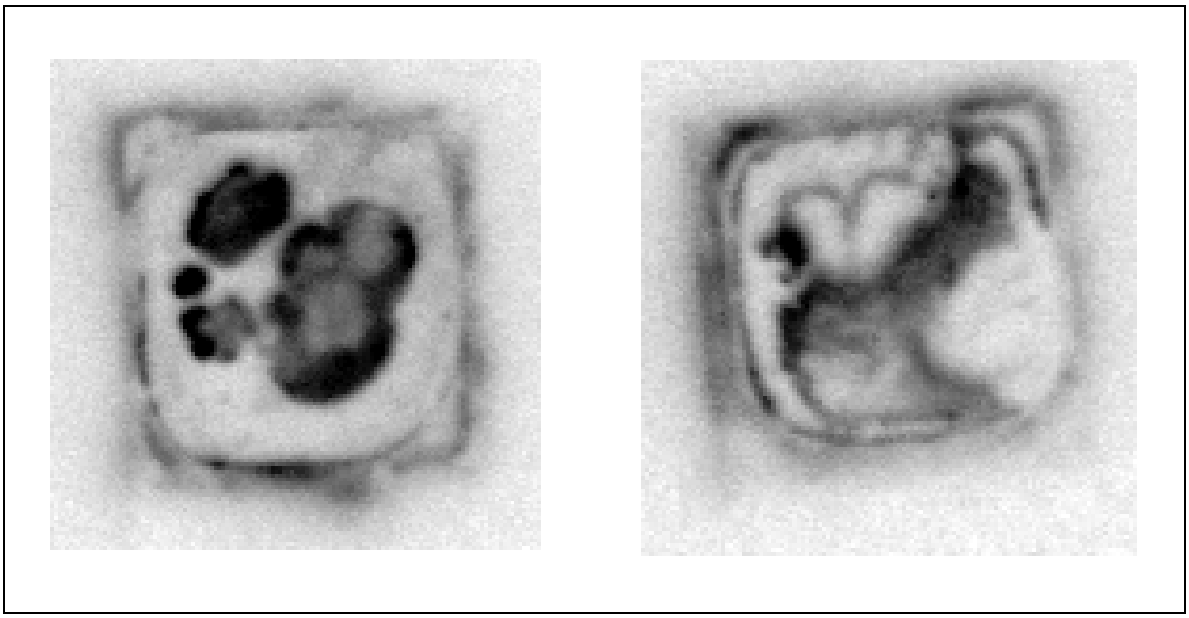

Figure 6.14 Enlargement of autoradiography of membranes poured onto quadratic glass slides from series A in Figure 6.12. The samples were incubated into a solution of [^{35}S]-streptavidin. The intensity of the coloring is proportional to the density of adsorbed [^{35}S]-streptavidin.

These calculations were done using an approximative diffusion coefficient D in Tecoflex of 10^{-8} cm^{-2} s^{-1}.[40] The distance d of the diffusion for a time t of 5 min is 35 µm. Therefore most of MAD-biotin diffused inside the membrane and was not available for immobilization on the surface. The recovery of [^{35}S]-streptavidin on the membrane surface was higher when the evacuation time was shorter. Actually, a short evacuation time of 10 min led to a smaller diffusion length in the membrane. Furthermore, a long vacuum time can modify the interaction forces present at the surface of polyurethanes.[49, 56]

Samples which were conditioned in water for 2 d showed the same [^{35}S]-streptavidin recoveries as samples without conditioning (data not shown). After exposure to water, the surface layer of polyurethane can be restructured. The hydrophobic end groups of polyurethane or biotin can submerge while the hydrophilic polyurethane backbone can emerge.[54] This energetical optimization of the surface is

Table 6.2 [^{35}S]-streptavidin densities on the surfaces of Tecoflex membranes (a).

series[b]	vacuum time (min)	cross-linking of MAD-biotin	time of treatment with Tween	density of streptavidin and STDEV (ng cm^{-2})[c]	percentage of a streptavidin-monolayer and STDEV
A	10	yes	no Tween	311 ± 43	119 ± 16
B	10	yes	before streptavidin	45 ± 9	17 ± 3
C	20	yes	before streptavidin	42 ± 19	16 ± 7
D	80	yes	no Tween	134 ± 33	51 ± 13
E	80	yes	after streptavidin	152 ± 81	58 ± 31
F	80	yes	before streptavidin	30 ± 9	12 ± 3
G	0	no	no Tween	26 ± 17	10 ± 7
H	80	no	no Tween	17 ± 3	7 ± 1
I	0	no	before streptavidin	22 ± 14	8 ± 5

[a] All membranes were of type 6B (Ca^{2+}) and were incubated into a solution of [^{35}S]-streptavidin.

[b] The capital letters correspond to the series in Figures 6.12 - 6.13 and are described in the experimental part. Five samples were examined for each series.

[c] The radiolabel densities were quantified using autoradiography and compared with the density of a two-dimensional crystalline streptavidin (C2,2,2) monolayer.[19, 29]

called volume exclusion effect.[56] However, this process had no significant influence on the binding of [^{35}S]-streptavidin to the immobilized MAD-biotin.

A nonionic surfactant called Tween 20, which is a polyoxyethylene derivative, was used for reducing non-specific adsorption of [^{35}S]-streptavidin. The membranes which were treated before the [^{35}S]-streptavidin incubation with Tween 20 showed lower recoveries than the other membranes. Therefore, Tween 20 decreased the [^{35}S]-streptavidin adsorption. On the account of binding of Tween 20 to streptavidin,[74] this

surfactant should not be applied during the streptavidin incubation. In previous studies, the reduction of noncovalently attached protein was more efficient when the surfactant was present during the covalent attachment than when it was only used for removing the protein after the linkage.[75] Besides, surfactants like Tween[76] or Triton[77] disturb the response of ISEs.

6.5 Influence of Photoimmobilized Molecules on the Response of Ion-Selective Electrodes

6.5.1 Influence of MAD

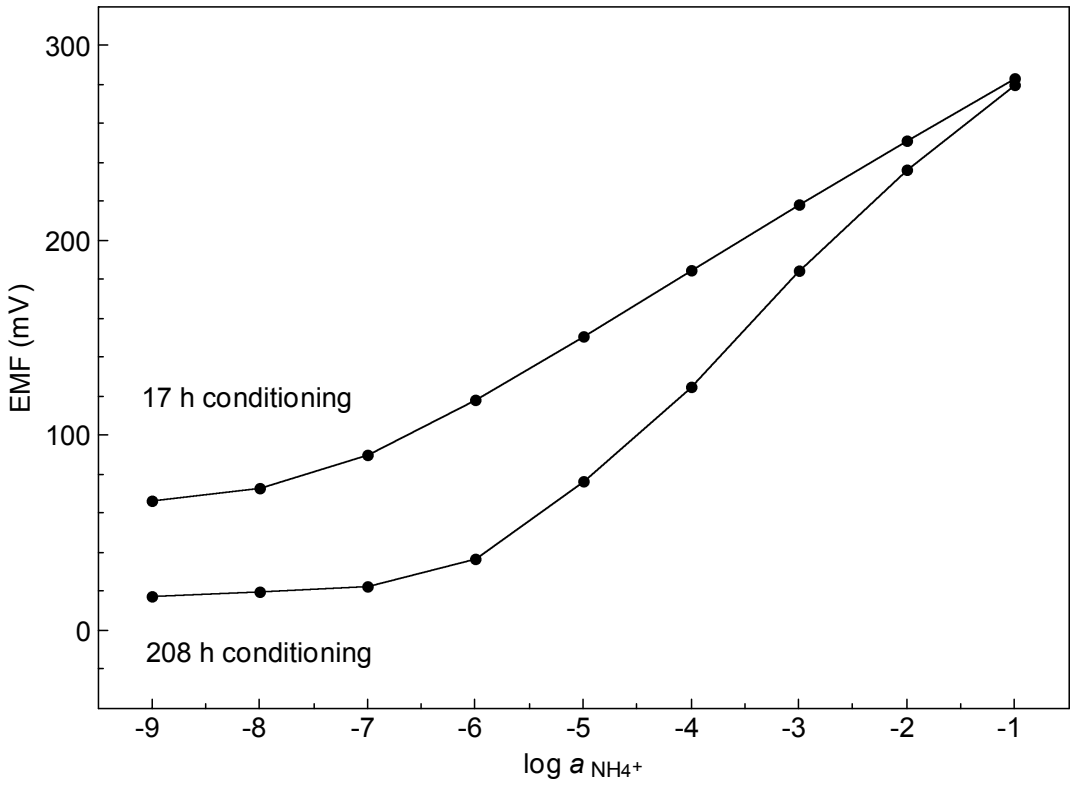

Figure 6.15 EMF responses of ammonium selective Tecoflex membrane ISEs containing nonactin and NaTFPB; the membranes were prepared without any plasticizer. After a conditioning time of 17 h, a slope of 33.3 ± 0.6 mV decade^{-1} (n = 4, 10^{-2}–10^{-5} M) was determined, whereas the slope was 53.6 ± 1.1 mV decade^{-1} (n = 5, 10^{-2}–10^{-5} M) after a conditioning time of 208 h.

The influence of photoimmobilized MAD on the response of ISEs was investigated using polyurethane membranes. As shown in Figure 6.15, Tecoflex membranes without plasticizer (type 6C (NH_4^+)) need a long conditioning time in order to obtain a close to Nernstian slope. The diffusion fluxes in these membranes without plasticizer and the establishment of a steady state between aqueous and organic phase are extremely slow.[78] The response curves of corresponding ISEs for monovalent or divalent ions were linear, but they usually showed sub-Nernstian slopes, except for the H^+-selective ISEs, which gave a Nernstian slope, as shown in Table 6.3. The latter phenomenon was due to protonation of the Tecoflex matrix,[79, 80] as explained in Chapter 4. This is confirmed by Figure 6.16, where the calibration curves of a cation-exchanger membrane ISE (type 6A ($N(CH_3)_4^+$))[81, 82] showed that the membrane

Table 6.3 Response characteristics of ISE membranes containing NaTFPB, different ionophores, and Tecoflex, without the addition of a plasticizer. MAD was immobilized on the surface of some membranes using photo-cross-linking.[48]

Measuring ion	MAD [mM]	UV-irradiation	Slope (mV/decade)	Linear range [M]	Membrane type
NH_4^+	0	no	53.6 ± 1.1 (n = 5)	10^{-2} to 10^{-5}	6C (NH_4^+)
H^+	0	no	58.2 ± 0.5 (n = 4)	10^{-2} to 10^{-5}	6D (H^+)
Ca^{2+}	0	no	19.7 ± 0.6 (n = 5)	10^{-2} to 10^{-5}	6E (Ca^{2+})
$N(CH_3)_4^+$	0	no	45.5 ± 0.8 (n = 5)	10^{-1} to 10^{-3}	6A ($N(CH_3)_4^+$)
$N(CH_3)_4^+$	0.027	no	44.8 (n = 1)	10^{-1} to 10^{-3}	6A ($N(CH_3)_4^+$)
$N(CH_3)_4^+$	0.27	no	43.6 (n = 1)	10^{-1} to 10^{-3}	6A ($N(CH_3)_4^+$)
$N(CH_3)_4^+$	2.7	no	44.9 (n = 1)	10^{-1} to 10^{-3}	6A ($N(CH_3)_4^+$)
$N(CH_3)_4^+$	0.027	yes	45.9 ± 0.7 (n = 4)	10^{-1} to 10^{-3}	6A ($N(CH_3)_4^+$)
$N(CH_3)_4^+$	0.27	yes	45.8 ± 1.1 (n = 4)	10^{-1} to 10^{-3}	6A ($N(CH_3)_4^+$)
$N(CH_3)_4^+$	2.7	yes	45.6 ± 0.8 (n = 4)	10^{-1} to 10^{-3}	6A ($N(CH_3)_4^+$)

was actually more selective to hydrogen ions than to tetramethylammonium ions. The selectivities are in good accordance with data reported by Lindner *et al*.[83]

MAD was photoimmobilized on cation-exchanger membranes of type 6A ($N(CH_3)_4^+$). Calibration curves were recorded for tetramethylammonium and calcium ions (data not shown) as measuring ions. Table 6.3 shows that the ISEs with immobilized MAD (irradiated) had the same slopes and measuring ranges, as the ISEs without MAD (not irradiated). Hence, the surface-immobilized MAD did not influence the potentiometric response of these ISEs. In addition, there was no difference in the response behavior between membranes with low and high MAD concentrations.

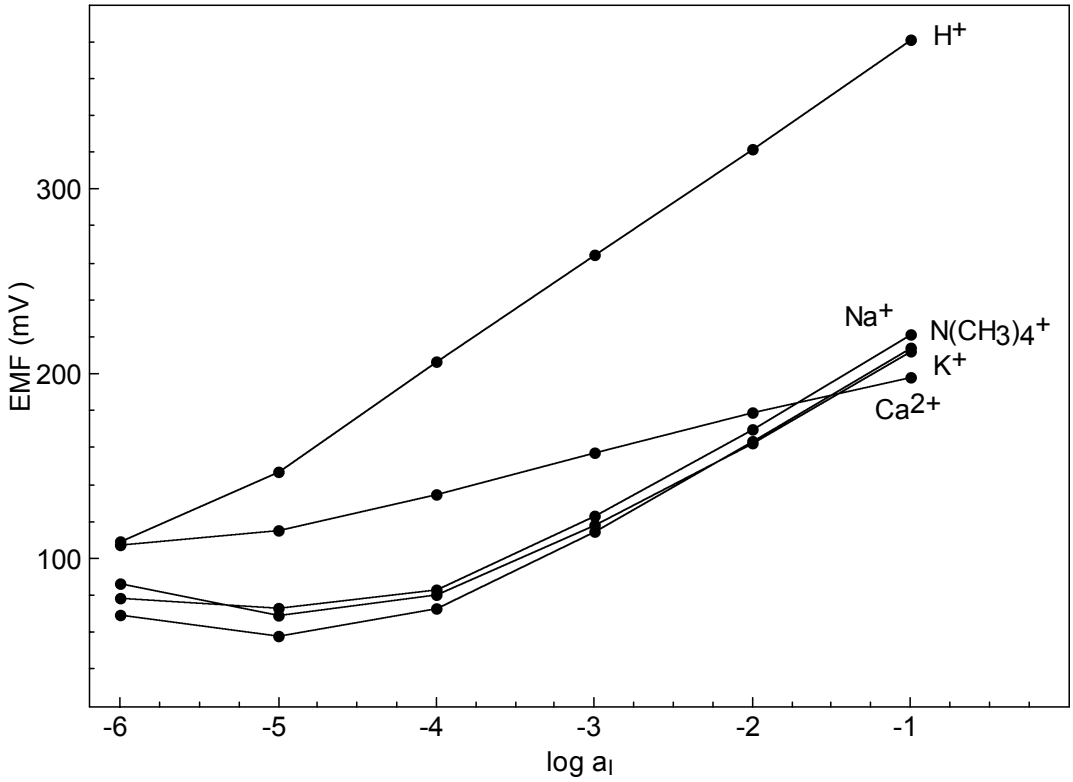

Figure 6.16 EMF response curves for different ions obtained with an ISE based on an ion-exchanger membrane (NaTFPB, Tecoflex). The following slopes were determined: $N(CH_3)_4^+$ 49.0 ± 1.3 mV decade^{-1}; H^+ 58.3 ± 0.3 mV decade^{-1}; K^+ 46.4 ± 0.4 mV decade^{-1}; Na^+ 48.5 ± 0.5 mV decade^{-1} and Ca^{2+} 21.1 ± 0.1 mV decade^{-1}. The standard deviations were calculated from measurements with four identically prepared ISEs.

6.5.2 Tecoflex-Based Ion-Selective Electrodes with a Super-Nernstian Response

The influence of the immobilized MAD-biotin-streptavidin system on the super-Nernstian response of ISEs was investigated in the following experiments. To get a reproducible super-Nernstian response, the parameters were optimized for calcium-selective Tecoflex electrodes. The selectivity value log $K^{pot}_{Ca,\,H}$ of these ISEs (membrane type 6B (Ca^{2+})) was 0.4.[84] Membranes with high diffusion fluxes exhibit a more pronounced super-Nernstian response.[41] Hence, the membranes used in the following experiments contained a high ionophore concentration and a high borate concentration (membrane type 6F (Ca^{2+})). In addition, the inner filling solution of all

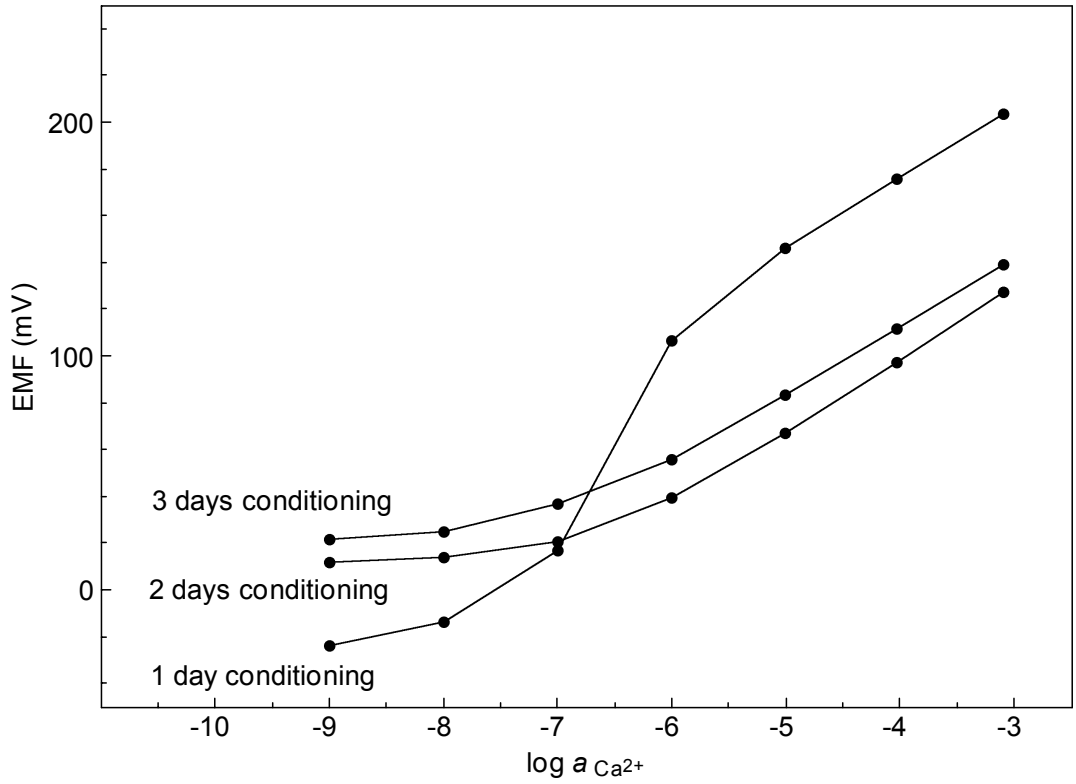

Figure 6.17 Influence of the conditioning time on the response of Ca^{2+}-ISEs containing ETH 5234, NaTFPB and Tecoflex without plasticizer (number of ISE: n = 5). The conditioning solution was 10^{-3} M $CaCl_2$, and the inner electrolytes were 0.05 M Na_2EDTA, 10^{-3} M $CaCl_2$, and 0.06 M NaOH (pH 8.9).

these ISEs contained a high sodium activity and the calcium activity was kept low by using an ion buffering system (e.g., EDTA).[38]

Figure 6.17 illustrates the influence of the conditioning of ISEs in 10^{-3} M $CaCl_2$. After a relatively short conditioning period, the electrodes showed a super-Nernstian behavior induced by Ca^{2+} flux from the sample into and through the membrane. A longer conditioning time caused an enrichment of calcium ions in the major part of the membrane. Consequently, this led to an equilibrium response to the analyte ion. Hence, ISEs which were conditioned in a high Ca^{2+} concentration did not show a

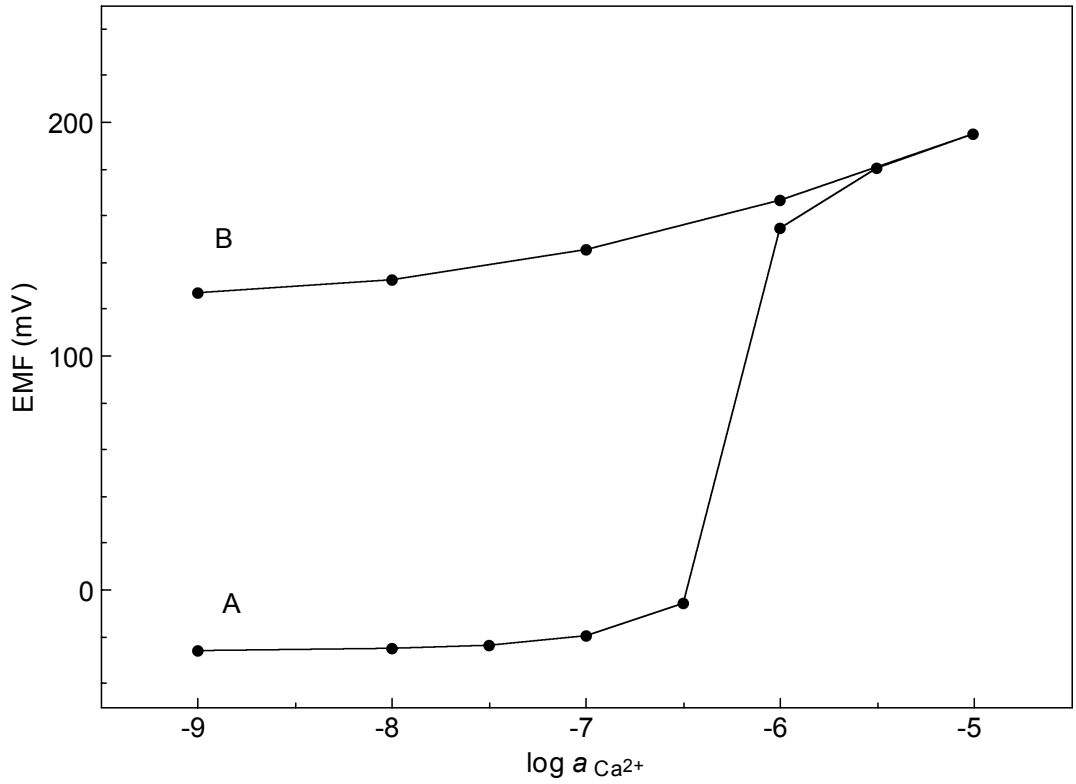

Figure 6.18 Response of Ca^{2+}-ISEs (n = 6) containing ETH 5234, NaTFPB and Tecoflex without plasticizer. The ISEs and their inner electrolytes were the same for both curves: 0.05 M Na_2EDTA, 10^{-3} M $CaCl_2$, and 0.06 M NaOH (pH 8.9). The conditioning solution used before experiments A had the same composition as the inner filling solution, whereas the conditioning solution for experiments B was 10^{-3} M $CaCl_2$. The conditioning times amounted to 1- 3 d throughout.

reproducible super-Nernstian behavior. In contrast, ISEs conditioned in a solution similar to the one in the inner compartment showed a strong super-Nernstian response, as depicted in Figure 6.18. Here, the ISE response at low analyte concentrations was mainly dictated by the release of interfering ions from the membrane. All following experiments were performed with ISEs whose conditioning solution was the same as the inner filling solution. ISEs with a membrane thickness of 40 µm, 70 µm, and 100 µm, respectively, showed the same response behavior (data not shown). In order to obtain mechanically stable ISEs, a membrane thickness of 100 µm was used for the subsequent experiments.

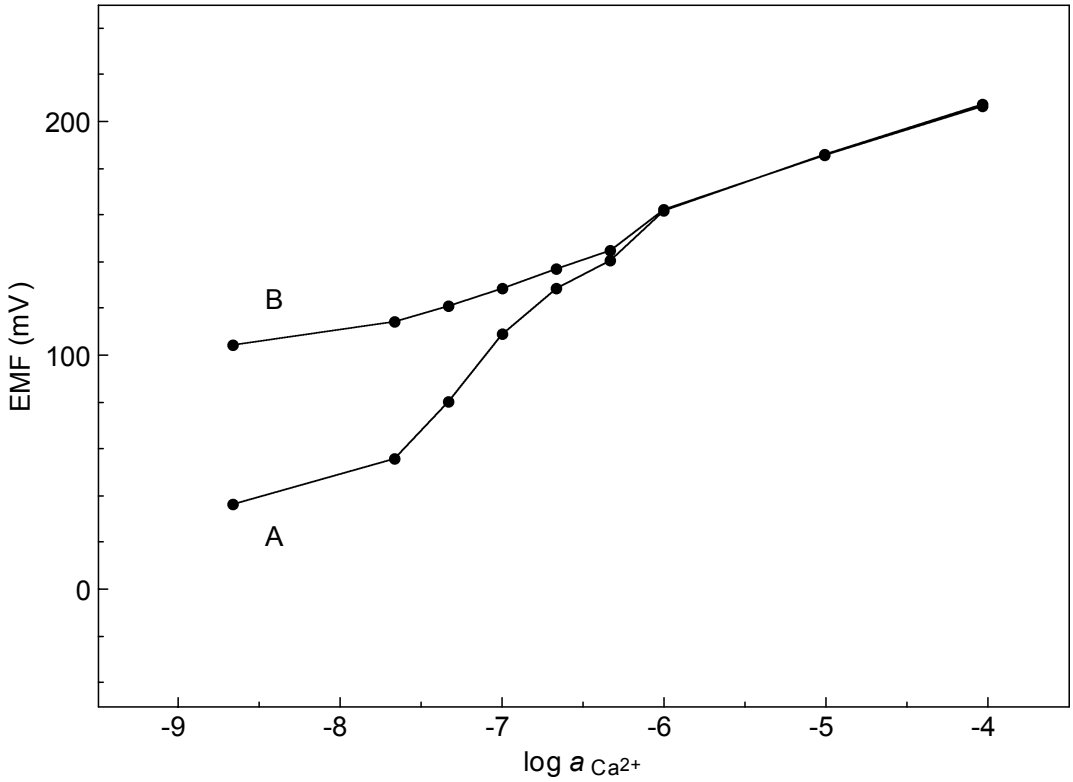

Figure 6.19 Response of Ca^{2+}-ISEs (n = 6) containing ETH 5234, NaTFPB, Tecoflex without plasticizer. Results are given for two systems with different pH values of the inner filling solution: A, 5 x 10^{-3} M Na_2EDTA, 10^{-3} M $CaCl_2$ and 5 x 10^{-3} M NaOH (pH 8.9); B, 5 x 10^{-3} M Na_2EDTA, 10^{-3} M $CaCl_2$ and 1.4 x 10^{-3} M NaOH (pH 6.0). The conditioning solution for both sets of experiments was the same as the inner solution of ISE A.

The curves in Figure 6.19 show the influence of the calcium activity in the conditioning solution and in the inner solution, respectively. Evidently, a relatively high calcium concentration leads to a reduction of the diffusion flux inside the membrane and results in a weaker super-Nernstian behavior.[39] In a further set of experiments, the concentration of the interfering ion in the inner filling was varied, as depicted in Figure 6.20. An increase of the sodium concentration from 0.01 M to 0.1 M causes a stronger super-Nernstian response, which effect is favored by moderate coextraction of Cl^- from the sample into the membrane during the conditioning phase and by an outflow of Na^+ from the membrane into the sample during the

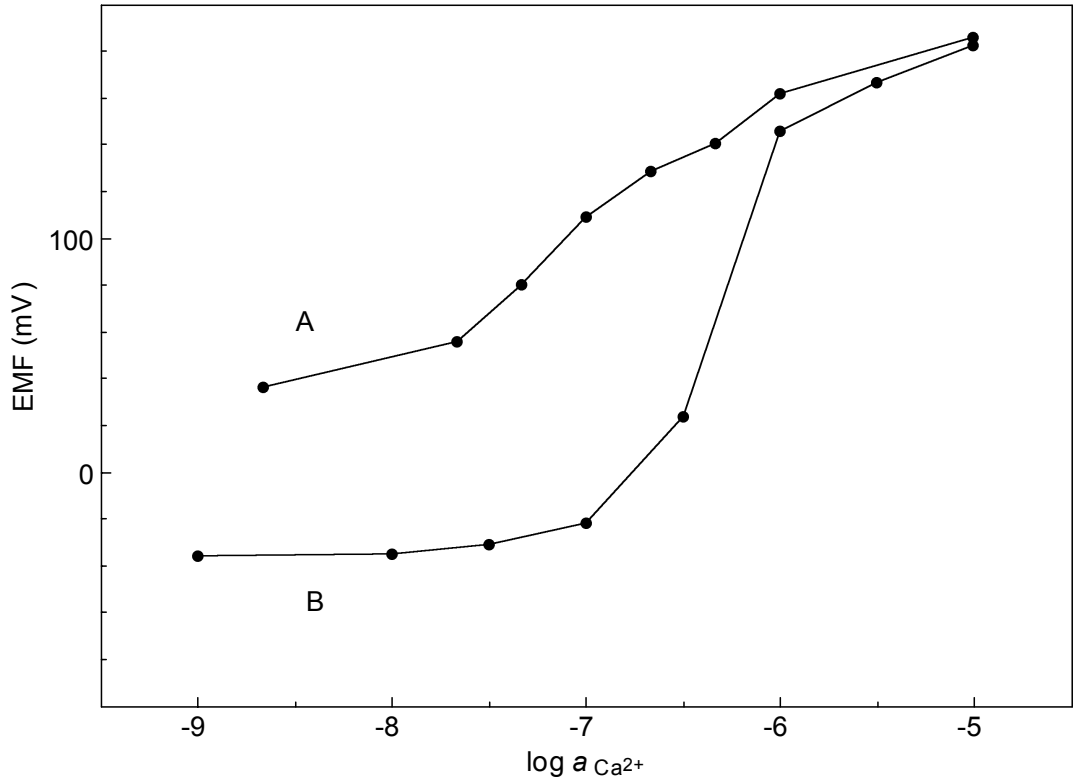

Figure 6.20 EMF response of Ca^{2+} - ISEs (n = 6) containing ETH 5234, NaTFPB and Tecoflex without plasticizer. Composition of the conditioning solution and the inner filling solution of ISE A: 5 x 10^{-3} M Na_2EDTA, 10^{-3} M $CaCl_2$ and 5 x 10^{-3} M NaOH (pH 8.9). Composition of the conditioning solution and the inner filling solution of ISE B: 0.05 M Na_2EDTA, 10^{-3} M $CaCl_2$, and 0.06 M NaOH (pH 8.9).

measurement. However, a further increase of the Na^+ concentration in the conditioning solution reduced the super-Nernstian response because of a predominant salt extraction (data not shown).

Figure 6.21 shows the influence of an ion buffer, 2-morpholinoethanesulfonic acid (MES), on the response behavior. When the MES-buffer was added to the conditioning solution and to the sample, a reproducible super-Nernstian response was no longer observed.

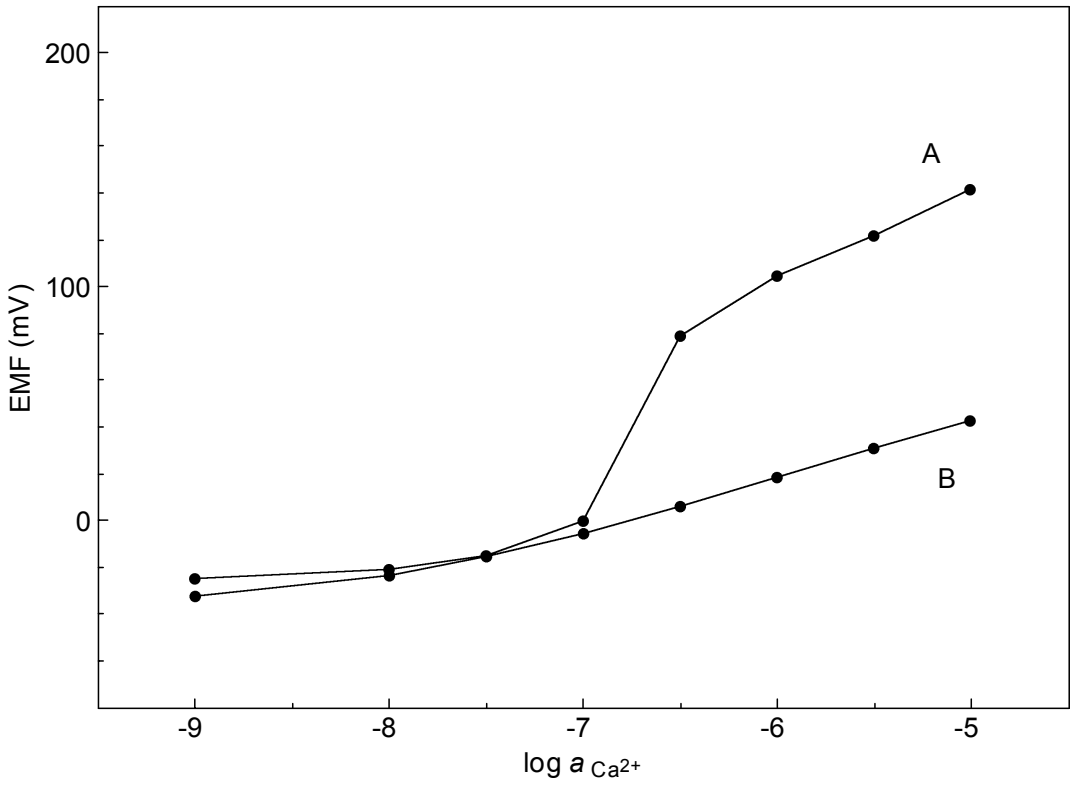

Figure 6.21 Influence of an additional ion buffer (MES) on the response of Ca^{2+}-ISEs (n = 5) containing ETH 5234, NaTFPB and Tecoflex without plasticizer. All inner fillings consisted of 0.05 M Na_2EDTA, 10^{-3} M $CaCl_2$, and 0.06 M NaOH (pH 8.9). The conditioning solution of ISE A had the same composition as the inner filling, whereas the conditioning solution of ISE B was a MES-buffer, which was kept constant during the calibration of ISE B. The sample solution of ISE A did not contain a MES-buffer.

The most reproducible super-Nernstian responses were observed at a moderate stirring rate. In this case, the thickness of the aqueous boundary layer remained constant and the response times were short. In addition, the super-Nernstian responses were most reproducible when all ISEs were centered in the measuring beaker and were exposed to the same convection fluxes. The incubation of the ISEs in a Tween 20 solution had no observable influence on the super-Nernstian response behavior.

The influence of immobilized MAD-biotin-streptavidin on the response behavior of ISEs was investigated using the ISEs which showed the most reproducible super-Nernstian response. The ISEs were calibrated, set back into the conditioning solution

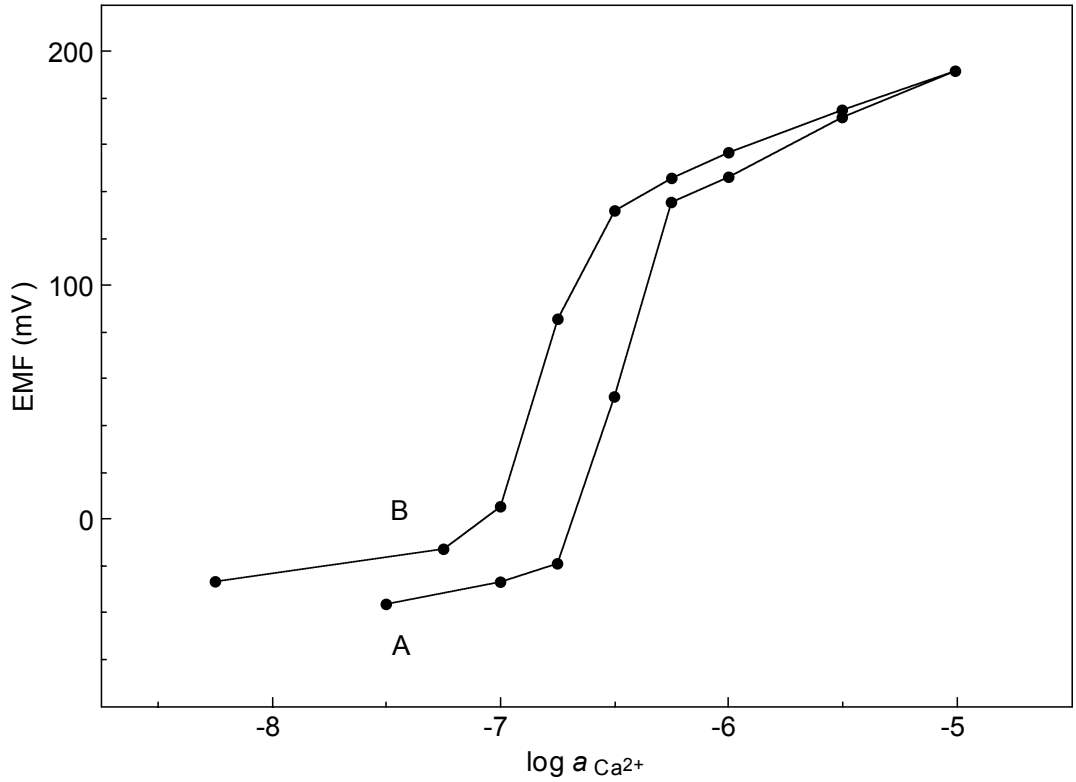

Figure 6.22 Response of Ca^{2+}-ISEs (n = 20) containing ETH 5234, NaTFPB and Tecoflex without plasticizer. All conditioning solutions and inner filling solutions contained 0.05 M Na_2EDTA, 10^{-3} M $CaCl_2$, and 0.06 M NaOH (pH 8.9). Curve B was measured one day after curve A. Before the recording of curve B, the ISE was incubated with streptavidin solution.

for one night, incubated in a streptavidin solution, and finally calibrated again. For ISEs without immobilized MAD-biotin, which do not bind streptavidin specifically, there was a small shift of the super-Nernstian response, as shown in Figure 6.22. Essentially, the super-Nernstian response was found at a lower calcium activity on the second day. This clear shift toward lower activities was verified with more than 20 ISEs. There was no significant difference in the response behavior of ISEs without photoimmobilized MAD-biotin in comparison with ISEs with cross-linked MAD-biotin. Therefore, the bound streptavidin had no visible influence on the response behavior of these ISEs. The exchange of calcium ions at the phase boundary between membrane and sample solution is evidently not blocked by the binding of streptavidin. The lack of the expected effect is probably explained by the heterogeneity of the MAD-biotin-streptavidin layer, as shown in the previous radiochemistry experiments.

6.6 Conclusions

The morphology of Tecoflex membranes is characterized by a uniform structure, which is very smooth with a roughness of about 0.7 nm. This featureless surface is well suited for photoimmobilizing biomolecules. A novel, highly efficient photoreactive cross-linker bearing a biotin moiety was synthesized. This MAD-biotin was photo-cross-linked on membranes of ISEs. Surface analyses showed that streptavidin was bound to the cross-linked MAD-biotin successfully although the immobilized MAD-biotin layer turned out to be non-uniform. None of the immobilized biomolecules, neither MAD nor MAD-biotin-streptavidin had an influence on ISEs with a Nernstian slope or with a super-Nernstian response.

In order to obtain a reproducible super-Nernstian response of ISEs made from polyurethane membranes without plasticizer, the following conditions have to be met. First, it is absolutely indispensable to lower the analyte activity through an ion buffer in the inner filling solution and to add a high concentration of interfering ions into the inner compartment. Second, the conditioning solution ought to have a similar composition as the inner filling. Third, there should be no additional ion buffering systems in the sample during the measurement. Finally, the stirring rate and the geometrical position of the ISEs have to be carefully adjusted.

References

(1) Yang, S.; Pérez-Luna, V. H.; Lopez, G. P. In *Protein Architecture*; Marcel Dekker: New York, 2000, pp 355-389.

(2) Cunningham, A. J. *Introduction to Bioanalytical Sensors*; Wiley-Interscience, 1998.

(3) Li, X.; Harrison, D. J. Measurements of Concentration Profiles Inside a Nitrite Ion-Selective Electrode Membrane. *Anal. Chem.* **1991,** *63*, 2168-2174.

(4) Schneider, B.; Zwickl, T.; Federer, B.; E. Pretsch; Lindner, E. Spectro-Potentiometry: A New Method for *in situ* Imaging of Concentration Profiles in Ion-Selective Membranes with Simultaneous Recording of Potential-Time Transients. *Anal. Chem.* **1996,** *68*, 4342-4350.

(5) Klee, D.; Hocker, H. *Polymers for Biomedical Applications: Improvement of the Interface Compatibility*; Springer: Berlin, 1999.

(6) Espadas-Torre, C.; Meyerhoff, M. E. Thrombogenic Properties of Untreated and Poly(ethylene oxide)-Modified Polymeric Matrices Useful for Preparing Intraarterial Ion-Selective Electrodes. *Anal. Chem.* **1995,** *67*, 3108-3114.

(7) Kuijpens, J. M. H.; Kardaun, G. A.; Blezer, R.; Pijpers, A. P.; Koole, L. H. Immobilization of Theophylline on Medical-Grade Polyurethane Inhibits Surface-Induced Activation of blood platelets. *J. Am. Chem. Soc.* **1995,** *117*, 8691-8697.

(8) Sigrist, H.; Collioud, A.; Clémence, J. F.; Gao, H.; Luginbühl, R.; Sänger, M.; Sundarababu, G. Surface Immobilization of Biomolecules by Light. *Opt. Eng.* **1995,** *34*, 2339-2348.

(9) Weber, T.; Brunner, J. 2-(tributylstannyl)-4-(3-(trifluoromethyl)-3H-diazirin-3-yl)benzyl Alcohol: A Building Block for Photolabeling and Cross-Linking Reagents of Very High Specific Radioactivity. *J. Am. Chem. Soc.* **1995,** *117*, 3084-3095.

(10) Hermanson, G. T. *Bioconjugate Techniques*; Academic Press: San Diego, 1995.

(11) Brunner, J. New Photolabeling and Crosslinking Methods. *Annu. Rev. Biochem.* **1993,** *62*, 483-514.

(12) Brooks, S. A.; Ambrose, W. P.; Kuhr, W. G. Micrometer Dimension Derivatization of Biosensor Surfaces Using Confocal Dynamic Patterning. *Anal. Chem.* **1999,** *71*, 2558-2563.

(13) Hatanaka, Y.; Hashimoto, M.; Kanaoka, Y. A Novel Biotinylated Heterobifunctional Cross-linking Reagent Bearing an Aromatic Diazirine. *Bioorg. Med. Chem.* **1994,** *2*, 1367-1373.

(14) Brooks, S.; Dontha, N.; Davis, C.; Stuart, J.; O'Neill, G.; Kuhr, W. Segregation of Micrometer-Dimension Biosensor Elements on a Variety of Substrate Surfaces. *Anal. Chem.* **2000,** *72*, 3253-3259.

(15) Lin, S. N.; Fang, K.; Hashimoto, M.; Nakanishi, K.; Ojima, I. Design and Synthesis of a Novel Photoaffinity Taxoid as a Potential Probe for the Study of Paclitaxel-Microtubules Interactions. *Tetrahedron Letters* **2000,** *41*, 4287-4290.

(16) Hatanaka, Y.; Hashimoto, M.; Nishihara, S.; Narimatsu, H.; Kanaoka, Y. Synthesis and Characterization of a Carbene-Generating Biotinylated *N*-Acetylglucosamine for Photoaffinity Labelling of beta-(1-4)-Galactosyltransferase. *Carbohydr. Res.* **1996,** *294*, 95-108.

(17) Bayer, E. A.; Wilchek, M. In *Methods of Biochem. Anal.*, 1980; Vol. 26, pp 1-45.

(18) Green, N. M. In *Avidin-Biotin Technology*; Wilchek, M., Bayer, E. A., Eds.; Academic Press: San Diego, 1990; Vol. 184, pp 51-67.

(19) Darst, S. A.; Ahlers, M.; Meller, P. H.; Kubalek, E. W.; Blankenburg, R.; Ribi, H. O.; Ringsdorf, H.; Kornberg, R. D. Two-Dimensional Crystals of Streptavidin on Biotinylated Lipid Layers and Their Interactions with Biotinylated Macromolecules. *Biophys. J.* **1991,** *59*, 387-396.

(20) Savage, M. D. In *A Laboratory Guide to Biotin-Labeling in Biomolecule Analysis*; Meier, T., Fahrenholz, F., Eds.; Birkhäuser: Basel, 1996; Vol. 7, pp 1-28.

(21) Perez Luna, V. H.; O Brien, M. J.; Opperman, K. A.; Hampton, P. D.; Lopez, G. P.; Klumb, L. A.; Stayton, P. S. Molecular Recognition Between Genetically Engineered Streptavidin and Surface-Bound Biotin. *J. Am. Chem. Soc.* **1999,** *121*, 6469-6478.

(22) Wang, Y. L.; Bobbitt, D. R. Binding Characteristics of Avidin and Surface Immobilized Octylbiotin - Implications for the Development of Dynamically Modified Optical-Fiber Sensors. *Anal. Chim. Acta* **1994,** *298*, 105-112.

(23) Savage, D.; Mattson, G.; Desai, S.; Nielander, G.; Morgensen, S.; Conklin, E. *Avidin-Biotin Chemistry: A Handbook*; Pierce Chemical Company, 1992.

(24) Stamm, C.; Lukosz, W. Integrated Optical Difference Interferometer as Biochemical Sensor. *Sens. Actuators, B* **1994,** *18-19*, 183-187.

(25) Busse, S.; Kashammer, J.; Kramer, S.; Mittler, S. Gold and Thiol Surface Functionalized Integrated Optical Mach-Zehnder Interferometer for Sensing Purposes. *Sens. Actuators, B.* **1999,** *60*, 148-154.

(26) Stayton, P. S.; Nelson, K. E.; McDevitt, T. C.; Edwards, T.; Castner, D. G.; Shimoboji, T.; Ding, Z. L.; Hoffman, A. In *Protein Architecture*; Marcel Dekker: New York, 2000, pp 287-309.

(27) Spinke, J.; Liley, M.; Schmitt, F.-J.; Guder, H.-J.; Angermaier, L.; Knoll, W. Molecular Recognition at Self-Assembled Monolayers: Optimization of Surface Functionalization. *J. Chem. Phys.* **1993,** *99*, 7012-7019.

(28) Knoll, W.; Zizlsperger, M.; Liebermann, T.; Arnold, S.; Badia, A.; Liley, M.; Piscevic, D.; Schmitt, F. J.; Spinke, J. Streptavidin Arrays as Supramolecular Architectures in Surface-Plasmon Optical Sensor Formats. *Colloids Surf., A* **2000,** *161*, 115-137.

(29) Jung, L. S.; Nelson, K. E.; Campbell, C. T.; Stayton, P. S.; Yee, S. S.; Perez-Luna, V.; Lopez, G. P. Surface Plasmon Resonance Measurement of Binding and Dissociation of Wild-Type and Mutant Streptavidin on Mixed Biotin-Containing Alkylthiolate Monolayers. *Sens. Actuators, B* **1999,** *54*, 137-144.

(30) Dontha, N.; Nowall, W. B.; Kuhr, W. G. Generation of Biotin/Avidin/Enzyme Nanostructures with Maskless Photolithography. *Anal. Chem.* **1997,** *69*, 2619-2625.

(31) Nowall, W. B.; Dontha, N.; Kuhr, W. G. Electron Transfer Kinetics at a Biotin/Avidin Patterned Glassy Carbon Electrode. *Biosens. Bioelectron.* **1998,** *13*, 1237-1244.

(32) Zhao, S.; Reichert, W. M. Influence of Biotin Lipid Surface-Density and Accessibility on Avidin Binding to the Tip of an Optical Fiber Sensor. *Langmuir* **1992,** *8*, 2785-2791.

(33) Cosnier, S. Biomolecule Immobilization on Electrode Surfaces by Entrapment or Attachment to Electrochemically Polymerized Films. A Review. *Biosens. Bioelectron.* **1999,** *14*, 443-456.

(34) Torres-Rodriguez, L. M.; Roget, A.; Billon, M.; Bidan, G. Synthesis of a Biotin Functionalized Pyrrole and Its Electropolymerization: Toward a Versatile Avidin Biosensor. *Chem. Commun.* **1998,** *21*, 1993-1994.

(35) Anicet, N.; Bourdillon, C.; Moiroux, J.; Saveant, J. M. Electron Transfer in Organized Assemblies of Biomolecules. Step-by-Step Avidin/Biotin Construction and Dynamic Characteristics of a Spatially Ordered Multilayer Enzyme Electrode. *J. Chem. Phys. B.* **1998,** *102*, 9844-9849.

(36) Romero, J. M. F.; Stiene, M.; Kast, R.; deCastro, M. D. L.; Bilitewski, U. Application of Screen-Printed Electrodes as Transducers in Affinity Flow-Through Sensor Systems. *Biosens. Bioelectron.* **1998,** *13*, 1107-1115.

(37) Zwickl, T.; Sokalski, T.; Pretsch, E. Steady-State Model Calculations Predicting the Influence of Key Parameters on the Lower Detection Limit and Ruggedness of Solvent Polymeric Membrane Ion-Selective Electrodes. *Electroanalysis* **1999,** *11*, 673-680.

(38) Sokalski, T.; Ceresa, A.; Zwickl, T.; Pretsch, E. Large Improvement of the Lower Detection Limit of Ion-Selective Polymer Membrane Electrodes. *J. Am. Chem. Soc.* **1997,** *119*, 11347-11348.

(39) Sokalski, T.; Ceresa, A.; Fibbioli, M.; Zwickl, T.; Bakker, E.; Pretsch, E. Lowering the Detection Limit of Solvent Polymeric Ion-Selective Membrane Electrodes. 2. Influence of Composition of Sample and Internal Electrolyte Solution. *Anal. Chem.* **1999,** *71*, 1210-1214.

(40) Sokalski, T.; Zwickl, T.; Bakker, E.; Pretsch, E. Lowering the Detection Limit of Solvent Polymeric Ion-Selective Electrodes. 1. Modeling the Influence of Steady-State Ion Fluxes. *Anal. Chem.* **1999,** *71*, 1204-1209.

(41) Morf, W. E.; Badertscher, M.; Zwickl, T.; de Rooij, N. F.; Pretsch, E. Effects of Ion Transport on the Potential Response of Ionophore-Based Membrane Electrodes: A Theoretical Approach. *J. Phys. Chem. B* **1999**, 11346-11356.

(42) Qin, W.; Zwickl, T.; Pretsch, E. Improved Detection Limits and Unbiased Selectivity Coefficients Obtained by Using Ion-Exchange Resins in the Inner Reference Solution of Ion-Selective Polymeric Membrane Electrodes. *Anal. Chem.* **2000,** *72*, 3236-3240.

(43) Mathison, S.; Bakker, E. Effect of Transmembrane Electrolyte Diffusion on the Detection Limit of Carrier-Based Potentiometric Ion Sensors. *Anal. Chem.* **1998,** *70*, 303-309.

(44) Lindner, E.; Gyurcsanyi, R. E.; Buck, R. P. Tailored Transport Through Ion-Selective Membranes for Improved Detection Limits and Selectivity Coefficients. *Electroanalysis* **1999,** *11*, 695-702.

(45) Fu, B.; Bakker, E.; Yun, J. H.; Yang, V. C.; Meyerhoff, M. E. Response Mechanism of Polymer Membrane-Based Potentiometric Polyion Sensors. *Anal. Chem.* **1994,** *66*, 2250-2259.

(46) Bühlmann, P.; Aoki, H.; Xiao, K. P.; Amemiya, S.; Tohda, K.; Umezawa, Y. Chemical Sensing with Chemically Modified Electrodes that Mimic Gating at Biomembranes Incorporating Ion-Channel Receptors. *Electroanalysis* **1998,** *10*, 1149-1158.

(47) Solsky, R. L.; Rechnitz, G. A. Antibody-Selective Membrane Electrodes. *Science* **1979,** *204*, 1308-1309.

(48) Collioud, A.; Clémence, J. F.; Sänger, M.; Sigrist, H. Oriented and Covalent Immobilization of Target Molecules to Solid Supports: Synthesis and Application of a Light-Activatable and Thiol-Reactive Cross-Linking Reagent. *Bioconjugate Chem.* **1993,** *4*, 528-536.

(49) Nurdin, N.; Descouts, P. Effect of Toluene Extraction on Biomer TM Surface: II. An Atomic Force Microscopy Study. *J. Biomater. Sci. Polymer.* **1995,** *7*, 425-438.

(50) Fibbioli, M. New Types of Ion-Selective Electrodes: Hydrophilic Anions and Solid-Contacted Membranes, Doctoral Dissertation No. 13789, ETH, Zurich, 2000.

(51) Bandekar, J.; Klima, S. FT-IR Spectroscopic Studies of Polyurethanes Part I. *J. Mol. Struct.* **1991,** *263*, 45-57.

(52) Bandekar, J.; Sawyer, A. FT-IR Spectroscopic Studies of Polyurethanes Part IV. Studies of the Effect of the Presence of Processing Aids on the Hemocompatibility of Polyurethanes. *J. Biomater. Sci. Polymer* **1995,** *7*, 485-501.

(53) Pretsch, E.; Clerc, T.; Seibl, J.; Simon, W. *Tabellen zur Strukturaufklärung organischer Verbindungen mit spektroskopischen Methoden*: Berlin, 1990.

(54) Chen, Z.; Ward, R.; Tian, Y.; Eppler, A. S.; Shen, Y. R.; Somorjai, G. A. Surface Composition of Biopolymer Blend Biospan-SP/Phenoxy and Biospan-F/Phenoxy Observed with SFG, XPS, and Contact Angle Goniometry. *J. Phys. Chem. B* **1999,** *103*, 2935-2942.

(55) Hearn, M. J.; Briggs, D.; Yoon, S. C.; Ratner, B. D. SIMS and XPS Studies of Polyurethane Surfaces 2. Polyurethanes with Fluorinated Chain Extenders. *Surf. Interface Anal.* **1987,** *10*, 384-391.

(56) Herbert, C. B.; Hernandez, A. M.; Hubbell, J. A. Platelet Adhesion to Polyurethane Blended with Polytetramethylene Oxide. *Biotechnol. Bioeng.* **1996,** *52*, 81-88.

(57) Leonard, D.; Chevolot, Y.; Bucher, O.; Sigrist, H.; Mathieu, H. J. ToF-SIMS and XPS Study of Photoactivatable Reagents Designed for Surface Glycoengineering - Part I. N-(m-(3-(trifluoromethyl)diazirine-3-yl)phenyl)-4-maleimidobutyramide (MAD) on Silicon, Silicon Nitride and Diamond. *Surf. Interface Anal.* **1998,** *26*, 783-792.

(58) Leonard, D.; Chevolot, Y.; Bucher, O.; Haenni, W.; Sigrist, H.; Mathieu, H. J. ToF-SIMS and XPS Study of Photoactivatable Reagents Designed for Surface Glycoengineering - Part 2. N-[m-(3-(trifluoromethyl)diazirine-3-yl)phenyl]-4-(-3-thio(-1 -D-galactopyrannosyl)-maleimidyl)butyramide (MAD-Gal) on Diamond. *Surf. Interface Anal.* **1998,** *26*, 793-799.

(59) Chevolot, Y.; Bucher, O.; Léonard, D.; Mathieu, H. J.; Sigrist, H. Synthesis and Characterization of a Photoactivatable Glycoaryldiazirine for Surface Glycoengineering. *Bioconjugate Chem.* **1999,** *10*, 169-175.

(60) Gao, H.; Luginbühl, R.; Sigrist, H. Bioengineering of Silicon Nitride. *Sens. Actuators, B* **1997,** *38-39*, 38-41.

(61) Knoll, W.; Schmitt, F.-J.; Klein, C. *German Patent Application DE 4039677*; Boehringer Mannheim GmbH, BRD, 1992.

(62) Dubrovsky, T. B. In *Protein Architecture*; Marcel Dekker: New York, 2000, pp 25-54.

(63) He, P. G.; Ye, J. N.; Fang, Y. Z.; Anzai, J.; Osa, T. Self-Assembled Biotinylated Disulfide Derivative Monolayer on Gold Electrode for Immobilizing Enzymes. *Talanta* **1997,** *44*, 885-890.

(64) Crisp, G. T.; Gore, J. Biotin Derivates as Gelators of Organic Solvents. *Synth. Commun.* **1997,** *27*, 2203-2216.

(65) Hu, J.; Fox, M. A. A Convenient Trimethylsilylthioxy-Dehalogenation Reaction for the Preparation of Functionalized Thiols. *J. Org. Chem.* **1999,** *64*, 4959-4961.

(66) Arai, Y.; Matsui, M.; Fujii, A.; Kontani, T.; Ohno, T.; Koizumi, T.; Shiro, M. Asymmetric Diels-Alder Reaction of Optically Active alpha-(2-exo-Hydroxy-10-bornyl) sulfinylmaleimides and Its Application to Optically Active 5-Functionalised Pyrrolines via Retro-Diels-Alder Reaction. *J. Chem. Soc. Perkin Trans. 1* **1994**, 25-37.

(67) Partis, M. D.; Griffiths, D. G.; Roberts, G. C.; Beechey, R. B. Cross-Linking of Protein by w-Maleimido Alkanoyl N-Hydroxysuccinimido Esters. *J. Protein Chem.* **1983,** *2*, 263-277.

(68) Heitz, J. R. e. a. Inactivation of Yeast Alcohol Dehydrogenase by N-Alkylmaleimides. *Arch. Biochem. Biophys.* **1968,** *127*, 627-636.

(69) Clémence, J. F.; Ranieri, J. P.; Aebischer, P.; Sigrist, H. Photoimmobilization of a Bioactive Laminin Fragment and Pattern-Guided Selective Neuronal Cell Attachment. *Bioconjugate Chem.* **1995,** *6*, 411-417.

(70) Anzai, J.; Kobayashi, Y.; Suzuki, Y.; Takeshita, H.; Chen, Q.; Osa, T.; Hoshi, T.; Du, X. Y. Enzyme Sensors Prepared by Layer-by-Layer Deposition of Enzymes on a Platinum Electrode Through Avidin-Biotin Interaction. *Sens. Actuators, B* **1998,** *52*, 3-9.

(71) Asanov, A. N.; Wilson, W. W.; Oldham, P. B. Regenerable Biosensor Platform: A Total Internal Reflection Fluorescence Cell with Electrochemical Control. *Anal. Chem.* **1998,** *70*, 1156-1163.

(72) Sytkowski, A. J. In *Avidin-Biotin Technology*; Wilchek, M., Bayer, E. A., Eds.; Academic Press: San Diego, 1990; Vol. 184, pp 353-356.

(73) Atkins, P. W. *Physikalische Chemie*; VCH: Weinheim, 1990.

(74) Duhamel, R. C.; Whitehead, J. S. In *Avidin-Biotin Technology*; Wilchek, M., Bayer, E. A., Eds.; Academic Press: San Diego, 1990; Vol. 184, pp 201-207.

(75) Wahlgren, M.; Welin-Klintström, S.; Karlsson, C. A.-C. In *Biopolymers at Interfaces: Surfactant Science Series*; Malmsten, M., Ed.; Marcel Dekker, 1998; Vol. 75.

(76) Ye, Q.; Vincze, A.; Horvai, G.; Leermakers, F. A. M. Partial Blocking of Ion Transport at the Interface of an Ion-Selective Liquid Membrane Electrode by Neutral Surfactants. Experimental and Computer Simulation. *Electrochimica Acta* **1998,** *44*, 125-132.

(77) Malinowska, E.; Meyerhoff, M. E. Influence of Nonionic Surfactants on the Potentiometric Response of Ion-Selective Polymeric Membrane Electrodes Designed for Blood Electrolyte Measurements. *Anal. Chem.* **1998,** *70*, 1477-1488.

(78) Schneider, B. Diffusionsprozesse und Phasengleichgewichte in ionenselektiven Flüssigmembranen und -optoden, Doctoral Dissertation No. 11255, ETH, Zurich, 1995.

(79) Cosofret, V. V.; Nahir, T. M.; Lindner, E.; Buck, R. P. New Neutral Carrier-Based H+ Selective-Membrane Electrodes. *J. Electroanal. Chem.* **1992,** *327*, 137-146.

(80) Bakker, E.; Lerchi, M.; Rosatzin, T.; Rusterholz, B.; Simon, W. Synthesis and Characterization of Neutral Hydrogen Ion-Selective Chromoionophores for Use in Bulk Optodes. *Anal. Chim. Acta* **1993,** *278*, 211-225.

(81) Schaller, U. Ionenselektive Makro- und Mikroelektroden auf der Basis von geladenen oder neutralen Ionophoren mit ionischen Additiven, Doctoral Dissertation No 10948, ETH, Zurich, 1994.

(82) Ceresa, A.; Pretsch, E. Determination of Formal Complex Formation Constants of Various Pb2+ Ionophores in the Sensor Membrane Phase. *Anal. Chim. Acta* **1999,** *395*, 41-52.

(83) Lindner, E.; Cosofret, V. V.; Ufer, S.; Buck, R. P.; Kao, W. J.; Neuman, M. R.; Anderson, J. M. Ion-Selective Membranes with Low Plasticizer Content: Electroanalytical Characterization and Biocompatibility Studies. *J. Biomed. Mater. Res.* **1994,** *28*, 591-601.

(84) Cosofret, V. V.; Erdosy, M.; Raleigh, J. S.; Johnson, T. A.; Neuman, M. R.; Buck, R. P. Aliphatic Polyurethane as a Matrix for pH Sensors: Effects of Native Sites and Added Proton Carrier on Electrical and Potentiometric Properties. *Talanta* **1996,** *43*, 143-151.

7 Experimental

7.1 Reagents

Tecoflex SG-80A was purchased from Thermedics Inc. (Woburn, MA). *N*,*N*-Dicyclohexyl-*N'*,*N'*-dioctadecyl-3-oxapentanediamide (ETH 5234), tridodecylamine, valinomycin, sodium tetrakis[3,5-bis(trifluoromethyl)phenyl]borate (NaTFPB), potassium tetraphenylborate (KTPB), tetradodecylammonium tetrakis-(4-chlorophenyl)borate (ETH 500), bis(2-ethylhexyl) sebacate (DOS), *ortho*-nitrophenyl octyl ether (*o*-NPOE), and poly(vinyl chloride) (PVC) were obtained from Fluka AG (CH-9471 Buchs, Switzerland). 4-{[9-(Dimethylamino)-5*H*-benzo[a]phenoxin-5-ylidene]amino}phenyl-acetic acid 11-[(1-butylpentyl)oxy]-11-oxoundecyl ester (ETH 2439) was synthesized in the ETHZ group laboratory.[1] Figure 7.1 shows the ammonium ionophore, which was a mixture of 75% nonactin and 25% monactin (Novartis).

The soft and the hard polyurethane as well as all in polyurethane immobilized compounds (bis-2,6-hydroxymethyl pyridine, *N*-butyldiethanolamine, and *o*-NPOE) were synthesized in the ETHZ group laboratory.[2, 3] Soft polyurethane consisted of 17% poly[3-(R)-hydroxybutyric acid] diol (PHB) (hard segment) and of 83% poly(tetrahydrofurane) diol (PTHF) (soft segment), which were polymerized with the coupling reagent 2,2,4-trimethylhexamethylene diisocyanate (TMDI). Hard polyurethane consisted of 50% PHB, 50% PTHF, and TMDI.[2]

N-{3-[3-(Trifluoromethyl)diazirine-3-yl]phenyl}-4-maleimido-butyramide (MAD) was a gift from H. Sigrist.[4] Polyoxyethylenesorbitan monolaurate (Tween 20) was purchased from Sigma - Aldrich (CH-9471 Buchs, Switzerland). 3-(*N*-morpholino)ethanesulfonic acid (MES), tris(hydroxymethyl)aminomethane (Tris), biotin, 3-bromo-1-propanol, 11-bromo-1-undecanol, hexamethyldisilathiane, tetrabutylammonium fluoride (TBAF), *p*-toluene sulphonic acid and streptavidin from *Streptomyces avidinii* were obtained from Fluka. [^{35}S]-Streptavidin from Amersham (CH-8600 Dübendorf, Switzerland) had a specific activity of 7.4 – 74 TBq mmol^{-1}.

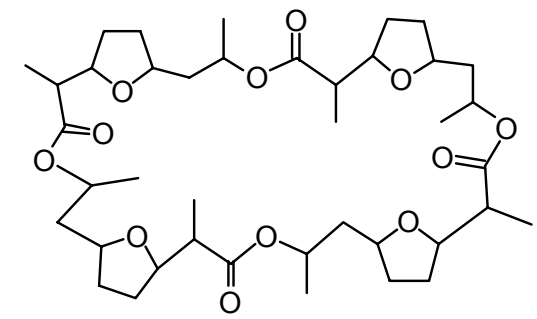

NH_4^+ (Nonactin)

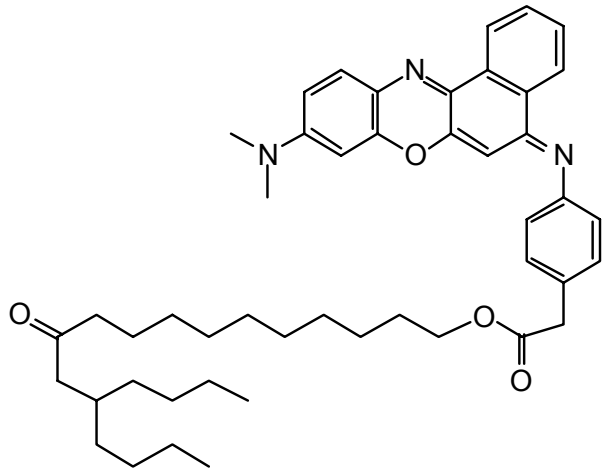

H^+ (ETH 2439)

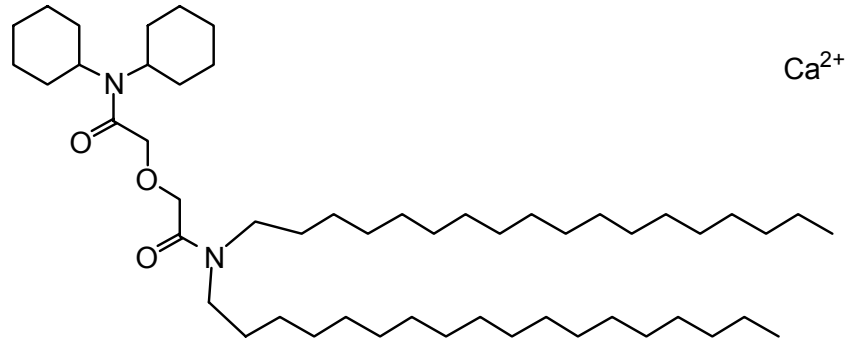

Ca^{2+} (ETH 5234)

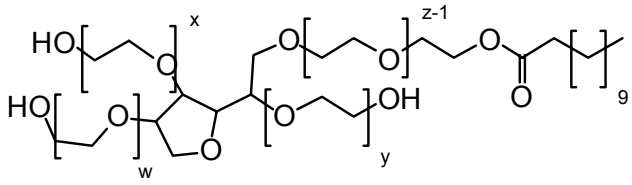

polyoxyethylenesorbitan monolaurate (Tween 20)
w + x + y + z = 20

Figure 7.1 Chemical structures of some mobile ionophores and Tween 20.

All solvents (Fluka, Merck, Baker or Riedel-de Haën) were purchased reagent-grade and used without further purification, except for tetrahydrofuran (THF), which was distilled. Gold (99.99%) was obtained from Balzers AG (FL-9496 Balzers, Liechtenstein).

The acids and salts were of puriss p.a. or Microselect quality from Fluka. Aqueous solutions were prepared with freshly deionized water (18.0 MΩ cm specific resistance) obtained with a NANOpure reagent-grade water system (SKAN, CH-4009 Basle, Switzerland).

7.2 Organic Syntheses

All reactions were performed in standard glassware. Evaporation and concentration *in vacuo* were done at water aspirator pressure, and compounds were dried at 10^{-2} mbar.

Column Chromatography. SiO_2 60 (220 – 440 mesh, 0.035 – 0.070 mm) from Fluka. TLC aluminum plates coated with SiO_2 60 F_{254} from E. Merck, visualization by UV light (254 or 366 nm). TLC glass plates coated with SiO_2 (Silgur-25 UV_{254}) from Macherey-Nagel (CH-4702 Oensingen, Switzerland).

Melting Points. Büchi melting point apparatus (CH-9239 Flawil, Switzerland).

IR Spectra. 883 infrared spectrophotometer from Perkin Elmer.

UV/VIS Spectra. Uvikon 940 from Kontron Instruments.

EI-MS: VG Tribid instrument, 70 eV. ESI-MS: Finnigan TSQ 7000 instrument.

NMR Spectra.[5] Varian Gemini 200 (200 MHz) or Bruker AMX-2-500 (500 MHz) spectrometer at 300 K, with solvent peaks as reference.

Elemental Analyses were performed by the Microlaboratory at the Institute of Organic Chemistry, ETH Zurich.

(3a*S*, 4*S*, 6a*R*) 11-bromoundecyl 5-(hexahydro-2-oxo-1*H*-thieno[3,4-*d*]imidazol-4*t*-yl) pentanoate **(2)**

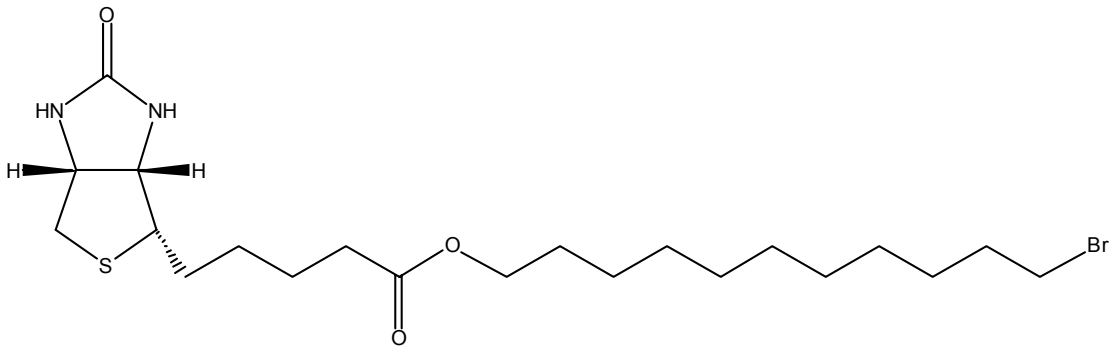

A mixture of biotin (1.350 g, 5.5 mmol), 11-bromo-1-undecanol (6.940 g, 27.6 mmol), *p*-toluene sulfonic acid (0.105 g, 0.55 mmol) and toluene (34 mL) was stirred and refluxed at 120 ^{o}C for 48 h under argon. The reaction mixture was cooled to room temperature. Precipitated unreacted biotin was removed by filtration, the solvent was removed *in vacuo* and the residue was purified by flash chromatography (MeOH/CH_2Cl_2 5:95) to give compound **2** as a white solid (1.970 g, 70 %).

Anal. Calculated for $C_{21}H_{37}N_2O_3SBr$: C, 52.82; H, 7.81; N, 5.87; O, 10.05; S, 6.72; Br, 16.73. Found: C, 52.59; H, 7.74; N, 5.62; O, 10.32; S, 6.82; Br, 16.70; mp 103.5 – 104.0 ^{o}C; IR ν_{max} (cm^{-1}): 3462, 2929, 2853, 1705, 1597; ^{1}H NMR (500 MHz, CD_2Cl_2, δ): 1.28 – 1.47 (m, 16H), 1.57 – 1.74 (m, 6H), 1.85 (m, -C*H*$_2$CH$_2$Br, 2H), 2.31 (t, *J* = 7.4 Hz, -C*H*$_2$C(O)OCH$_2$-, 2H), 2.71 (d, *J* = 12.6 Hz, -CHC*H*$_2$S-, 1H), 2.90 (dd, *J* = 12.7 Hz, *J* = 5.0 Hz, -CHC*H*$_2$S-, 1H), 3.17 (m, -SC*H*-, 1H), 3.42 (t, *J* = 6.9 Hz, -C*H*$_2$Br, 2H), 4.03 (t, *J* = 6.9 Hz, -OC*H*$_2$-, 2H), 4.30 (m, -NHC*H*CH$_2$-, 1H), 4.48 (m, -NHC*H*(CH-)$_2$, 1H), 5.43 (s, -N*H*CH(CH-)$_2$, 1H), 5.73 (s, -N*H*CHCH$_2$-, 1H); ^{13}C NMR (125 MHz, CD_2Cl_2, δ): 25.28, 26.33, 28.57, 28.70, 28.78, 29.07, 29.15, 29.65, 29.81, 29.86, 29.88, 33.31 (-*C*H$_2$CH$_2$Br), 34.31, 34.68, 41.04 (-*C*H$_2$S-), 55.90 (-S*C*H-), 60.54 (-N*C*CH2), 62.28 (-N*C*(CH-)$_2$), 64.82 (-C(O)O*C*-), 163.94 (-N*C*(O)N-), 173.95 (-*C*(O)O-); EI-MS *m*/*z* (relative intensity): M^+ 476.1 (1), 418.1 (3), 227.1 (10), 166.1 (19).

(3a*S*, 4*S*, 6a*R*) 11-sulfanylundecyl 5-(hexahydro-2-oxo-1*H*-thieno[3,4-*d*]imidazol-4*t*-yl) pentanoate **(3)**

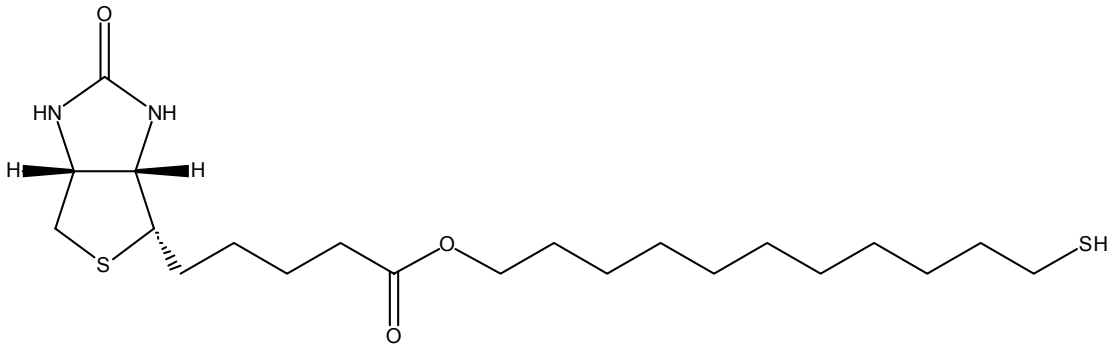

A stirred solution of compound **2** (1.000 g, 2.09 mmol) in THF was cooled to –10 ^{o}C, and hexamethyldisilathiane (2.20 mL, 10.45 mmol)) and TBAF (10.5 mL, 1.0 M solution in THF with 5% water, 10.45 mmol) were added. The resulting reaction mixture was allowed to warm to room temperature while it was stirred. The reaction was shielded from ambient light in order to avoid photoinduced side reactions and was carried out under argon. After 20 min, the reaction mixture was washed with 20 mL aqueous ammonium chloride (saturated) and 10 mL CH_2Cl_2. Recrystallization from CH_2Cl_2 and hexane gave compound **3** as white solid (0.673 g, 75 % yield).

Anal. Calculated for $C_{21}H_{38}N_2O_3S_2$: C, 58.57; H, 8.89; N, 6.50; S, 14.89. Found: C, 57.94; H, 8.50; N, 6.16; S, 14.31 (The ^{1}H-NMR spectrum indicated that some disulfides occurred as impurities in the product); mp 99.5 – 101.0 ^{o}C; IR ν_{max} (cm^{-1}): 3462, 2929, 2853, 1705, 1597; UV (CH_2Cl_2) λ_{max} (log ε): 219 (0.48); ^{1}H NMR (500 MHz, CD_2Cl_2, δ): 1.28 – 1.47 (m, 17H), 1.57 – 1.74 (m, 6H), 1.87 (m, -C*H*$_2$CH$_2$SH, 2H), 2.31 (t, *J* = 7.4 Hz, -C*H*$_2$C(O)OCH$_2$-, 2H), 2.50 (q, *J* = 7.4, -C*H*$_2$SH, 2H), 2.71 (d, *J* = 12.7 Hz, -CHC*H*$_2$S-, 1H), 2.91 (dd, *J* = 12.8 Hz, *J* = 5.0 Hz, -CHC*H*$_2$S-, 1H), 3.16 (m, -SC*H*-, 1H), 4.03 (t, *J* = 6.8 Hz, -OC*H*$_2$-, 2H), 4.30 (m, -NHC*H*CH$_2$-, 1H), 4.48 (m, -NHC*H*(CH-)$_2$, 1H), 5.44 (s, -N*H*CH(CH-)$_2$, 1H), 5.71 (s, -N*H*CHCH$_2$-, 1H); ^{13}C NMR (125 MHz, CD_2Cl_2, δ): 24.96 (-*C*H$_2$SH), 25.28, 26.33 28.71, 28.78 (2C), 29.08, 29.47, 29.66, 29.90 (3C), 34.32, 34.53, 41.04 (-*C*H$_2$S-), 55.90 (-S*C*H-), 60.54 (-N*C*CH2), 62.27 (-N*C*(CH-)$_2$), 64.82 (-C(O)O*C*-), 163.91 (-N*C*(O)N-), 173.95 (-*C*(O)O-); EI-MS *m*/*z* (relative intensity): (M + 1)$^{+}$ 431.2 (49), M^{+} 430.2 (13), 397.3 (26), 227.1 (76), 166.0 (83).

(3a*S*, 4*S*, 6a*R*) 11-{[3-(3-trifluoromethyl-3*H*-diazirin-3-yl)-phenylamino]-[1-(4-oxobutyl)-pyrrolidine-2,5-dioxo-3-yl]thio}undecyl 5-(hexahydro-2-oxo-1*H*-thieno [3,4-*d*]imidazol-4*t*-yl) pentanoate **(1)**

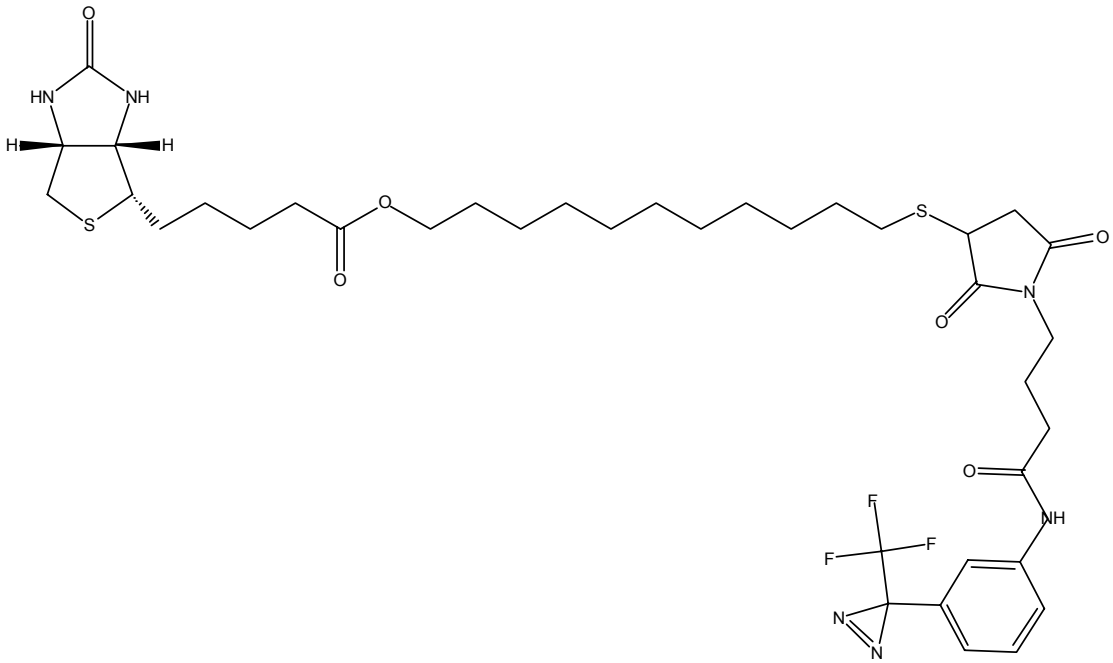

To a solution of thiol-biotin **2** (7.32 mg, 17 μmol) in CH_2Cl_2 (3 mL) at 0 ^oC, a solution of MAD (6.23 mg, 17 μmol) in 0.2 mL CH_2Cl_2 was added, followed by 5 drops of triethylamine. The mixture was allowed to reach room temperature and then was stirred for 7 h. The reaction was shielded from light in order to avoid photoinduced side reactions and was carried out under argon. The resulting mixture was concentrated under reduced pressure, and the residue was purified by chromatography on a silica glass plate (hexane/1,2-dichloroethane/acetonitrile/ethanol 40:30:24:6) to give the compound **1** as a diastereoisometric mixture in form of a white solid (11.1 mg, 82 % yield).

^{1}H NMR (200 MHz, $CDCl_3$, δ): 1.28 – 1.49 (m, 16H), 1.57 – 1.74 (m, 8H), 2.04 (m, -NCH$_2$C*H$_2$*CH$_2$CO-, 2H), 2.33 (m, -C*H$_2$*COOCH$_2$-, -NCH$_2$CH$_2$C*H$_2$*CO-, 4H), 2.50 (dd, *J* = 18.7 Hz, *J* = 3.3 Hz, -CH$_2$C*H$_2$*S-, 2H), 2.69 – 3.00 (m, -CHC*H$_2$*S-, -SCHC*H$_2$*CO-, 4H), 3.07 – 3.24 (m, -SC*H*CHNH, 1H), 3.58 – 3.76 (m, NC*H$_2$*-, -SC*H*CO, 3H), 4.07 (t, *J* = 6.6 Hz, -OC*H$_2$*-, 2H), 4.35 (m, -NHC*H*CH$_2$-, 1H), 4.53 (m, -NHC*H*(CH-)$_2$, 1H), 4.88 (s, -N*H*CH(CH-)$_2$, 1H), 5.06 (s, -N*H*CHCH$_2$-, 1H), 6.94 (d,

J = 7.1 Hz, Ar H, 1H), 7.34 (t, *J* = 7.9 Hz, Ar H, 1H), 7.48 (s, Ar H, 1H), 7.67 (d, *J* = 7.5 Hz, Ar H, 1H), 8.55 (d, *J* = 5.4 Hz, -N*H*-Ar, 1H); ESI-MS *m*/*z*: $(M + 1)^+$ 797, $(M + Na)^+$ 819, $(M + K)^+$ 835.

7.3 Preparation of Ion-Selective Electrodes

Membranes. ISE membranes were obtained by casting a solution of membrane components (see Table 7.1), dissolved in about 2.5 mL of THF, into a glass ring (40 mm or 60 mm i.d.) fixed on a glass plate covered with a Teflon foil. For each ISE, a disk of 7 mm diameter was punched from a membrane and glued to plasticized PVC tubing with THF.[6] The thickness of most membranes amounted to 300 μm.

The double membranes consisted of two disks of 13 mm diameter, which were punched from separate membranes, glued together using THF, and finally glued with THF onto the inner membrane holder of the transport cell.

Inner Fillings and Conditioning Solutions Used in Chapter 4. All ISEs were conditioned in a solution which had the same composition as the inner filling. The following internal fillings were used: 0.01 M NaCl and 0.1 M acetic acid/sodium acetate adjusted to pH 3.9 for ISEs made from membrane types 4A (H^+) and 4B (H^+); 0.1 M citric acid, 5 x 10^{-3} M NaCl and 0.25 M NaOH adjusted to pH 5.8 (4C (H^+) - 4G (H^+), 4L (H^+), 4M (H^+), 4N (H^+)); 0.1 M acetic acid, 5 x 10^{-3} M NaCl and 0.08 M NaOH adjusted to pH 5.7 (4H (H^+) - 4K (H^+)); 10^{-3} M NH_4Cl and HCl adjusted to pH 3.4 (4O (NH_4^+)); 0.01 M $MgCl_2$ (4P (NH_4^+)); 10^{-3} M NH_4Cl (4Q (NH_4^+)); 10^{-3} M NH_4Cl and 0.01 M acetic acid/sodium acetate adjusted to pH 4.0 (4R (H^+)); 0.05 M citric acid, 5 x 10^{-3} M NH_4Cl, and 0.13 M NaOH adjusted to pH 5.8 (4S (H^+)); 10^{-3} M KCl and H_2SO_4 adjusted to pH 3.0 (4T (H^+) - 4V (H^+)); 5 x 10^{-4} M K_2SO_4 and H_2SO_4 adjusted to pH 3.8 (4W (double)); 10^{-3} M NH_4Cl and HCl adjusted to pH 2.9 (4X (double)). The conditioning time amounted to 1 – 3 d. An exception were ISEs based on double membranes with a conditioning time of 10 d.

Table 7.1 Composition of ion-selective membranes studied.

membrane type (primary ion)	composition (in parentheses, concentration of the components in weight percent)
4A (H^+)	immobilized bis-2,6-hydroxymethyl pyridine (0.2) 14.0 mmol kg^{-1}, NaTFPB (0.6) 7.0 mmol kg^{-1}, PHB/PTHF 1:1 (99.2)
4B (H^+)	immobilized bis-2,6-hydroxymethyl pyridine (0.2) 12.0 mmol kg^{-1}, NaTFPB (0.5) 6.0 mmol kg^{-1}, PHB/PTHF 1:5 (99.3)
4C (H^+)	immobilized *N*-butyldiethanolamine (1.3) 80.1 mmol kg^{-1}, NaTFPB (0.7) 8.0 mmol kg^{-1}, PHB/PTHF 1:5 (98.0)
4D (H^+)	immobilized *N*-butyldiethanolamine (1.3) 80.4 mmol kg^{-1}, NaTFPB (0.7) 8.0 mmol kg^{-1}, immobilized *o*-NPOE (50.5), Tecoflex (47.5)
4E (H^+)	immobilized *N*-butyldiethanolamine (1.3) 80.1 mmol kg^{-1}, NaTFPB (0.1) 0.8 mmol kg^{-1}, *o*-NPOE (10.0), PHB/PTHF 1:5 (88.6)
4F (H^+)	immobilized *N*-butyldiethanolamine (1.3) 80.1 mmol kg^{-1}, NaTFPB (0.3) 3.2 mmol kg^{-1}, *o*-NPOE (9.8), PHB/PTHF 1:5 (88.6)
4G (H^+)	immobilized *N*-butyldiethanolamine (1.3) 79.4 mmol kg^{-1}, NaTFPB (0.7) 7.9 mmol kg^{-1}, *o*-NPOE (9.8), PHB/PTHF 1:5 (88.2)
4H (H^+)	immobilized *N*-butyldiethanolamine (1.3) 79.0 mmol kg^{-1}, DOS (67.1), PVC (31.6)
4I (H^+)	immobilized *N*-butyldiethanolamine (1.3) 79.0 mmol kg^{-1}, KTFPB (0.1) 0.8 mmol kg^{-1}, DOS (67.1), PVC (31.5)
4J (H^+)	immobilized *N*-butyldiethanolamine (1.3) 79.6 mmol kg^{-1}, KTFPB (0.4) 3.9 mmol kg^{-1}, DOS (66.5), PVC (31.8)
4K (H^+)	immobilized *N*-butyldiethanolamine (1.3) 80.3 mmol kg^{-1}, KTFPB (3.6) 40.2 mmol kg^{-1}, DOS (64.5), PVC (30.6)
4L (H^+)	immobilized *N*-butyldiethanolamine (1.3) 79.1 mmol kg^{-1}, NaTFPB (0.3) 3.2 mmol kg^{-1}, *o*-NPOE (10.0), Tecoflex (88.4)

4M (H^+)	immobilized *N*-butyldiethanolamine (1.3) 80.8 mmol kg^{-1}, NaTFPB (0.7) 8.1 mmol kg^{-1}, immobilized *o*-NPOE (21.2), Tecoflex (76.8)
4N (H^+)	immobilized *N*-butyldiethanolamine (1.3) 80.0 mmol kg^{-1}, NaTFPB (0.7) 8.0 mmol kg^{-1}, Tecoflex (98.0)
4O (NH_4^+)	nonactin/monactin (75:25) (1.0) 13.7 mmol kg^{-1}, NaTFPB (0.6) 6.9 mmol kg^{-1}, PHB/PTHF 1:5 (98.4)
4P (NH_4^+)	nonactin/monactin (75:25) (1.0) 13.1 mmol kg^{-1}, KTFPB (0.6) 6.6 mmol kg^{-1}, PHB/PTHF 1:1 (98.4)
4Q (NH_4^+)	nonactin/monactin (75:25) (1.0) 13.4 mmol kg^{-1}, KTFPB (0.6) 6.8 mmol kg^{-1}, DOS (65.3), PVC (33.1)
4R (H^+)	immobilized bis-2,6-hydroxymethyl pyridine (0.2) 14.0 mmol kg^{-1}, nonactin/monactin (75:25) (1.0) 13.8 mmol kg^{-1}, NaTFPB (0.6) 6.8 mmol kg^{-1}, PHB/PTHF 1:5 (98.2)
4S (H^+)	immobilized *N*-butyldiethanolamine (0.8) 50.0 mmol kg^{-1}, nonactin/monactin (75:25) (0.7) 10.0 mmol kg^{-1}, NaTFPB (0.4) 5.0 mmol kg^{-1}, PHB/PTHF 1:5 (98.1)
4T (H^+)	immobilized *N*-butyldiethanolamine (0.8) 50.0 mmol kg^{-1}, nonactin/monactin (75:25) (0.7) 10.0 mmol kg^{-1}, NaTFPB (0.4) 5.0 mmol kg^{-1}, PHB/PTHF 1:5 (98.1)
4U (H^+)	immobilized *N*-butyldiethanolamine (0.8) 50.0 mmol kg^{-1}, nonactin/monactin (75:25) (0.7) 10.0 mmol kg^{-1}, NaTFPB (0.4) 5.0 mmol kg^{-1}, ETH 500 (1.1) 10.0 mmol kg^{-1}, PHB/PTHF 1:5 (97.0)
4V (H^+)	immobilized *N*-butyldiethanolamine (0.8) 49.8 mmol kg^{-1}, NaTFPB (0.4) 5.0 mmol kg^{-1}, PHB/PTHF 1:5 (98.8)
4W1 (double)	nonactin/monactin (75:25) (0.7) 10.0 mmol kg^{-1}, NaTFPB (0.4) 5.0 mmol kg^{-1}, ETH 500 (1.1) 10.0 mmol kg^{-1}, PHB/PTHF 1:5 (97.8); The thickness of this membrane was 330 μm.
4W2 (double)	immobilized *N*-butyldiethanolamine (0.8) 50.0 mmol kg^{-1}, nonactin/monactin (75:25) (0.7) 10.0 mmol kg^{-1}, NaTFPB (0.4) 5.0 mmol kg^{-1}, ETH 500 (1.1) 10.0 mmol kg^{-1}, PHB/PTHF 1:5 (97.0); The thickness of this membrane was 330 μm.

4X1 (double)	nonactin/monactin (75:25) (1.0) 13.3 mmol kg^{-1}, NaTFPB (0.6) 6.7 mmol kg^{-1}, PHB/PTHF 1:5 (98.4); The thickness of this membrane was 400 μm.
4X2 (double)	immobilized bis-2,6-hydroxymethyl pyridine (0.2) 13.2 mmol kg^{-1}, nonactin/monactin (75:25) (1.0) 13.3 mmol kg^{-1}, NaTFPB (0.6) 6.6 mmol kg^{-1}, PHB/PTHF 1:5 (98.2); The thickness of this membrane was 400 μm.
5A (NH_4^+)	nonactin/monactin (75:25) (1.0) 13.2 mmol kg^{-1}, KTFPB (0.6) 6.5 mmol kg^{-1}, DOS (10.6), Tecoflex (87.8)
5B (NH_4^+)	nonactin/monactin (75:25) (0.7) 10.0 mmol kg^{-1}, NaTFPB (0.4) 5.0 mmol kg^{-1}, ETH 500 (1.1) 9.9 mmol kg^{-1}, DOS (32.7), Tecoflex (65.1)
5C (K^+)	valinomycin (1.2) 10.4 mmol kg^{-1}, NaTFPB (0.5) 5.2 mmol kg^{-1}, PTHF/PHB 1:5 (98.3)
5D (H^+)	tridodecylamine (0.5) 9.9 mmol kg^{-1}, NaTFPB (0.4) 5.0 mmol kg^{-1}, ETH 500 (1.1) 9.9 mmol kg^{-1}, DOS (65.7), PVC(32.3)
5E (NH_4^+)	nonactin/monactin (75:25) (0.7) 9.9 mmol kg^{-1}, NaTFPB (0.4) 5.0 mmol kg^{-1}, ETH 500 (1.1) 10.0 mmol kg^{-1}, DOS (66.8), PVC (31.0)
5F (H^+)	immobilized *N*-butyldiethanolamine (1.0) 62.3 mmol kg^{-1}, nonactin/monactin (75:25) (0.7) 9.9 mmol kg^{-1}, NaTFPB (0.4) 5.0 mmol kg^{-1}, ETH 500 (1.2) 10.2 mmol kg^{-1}, DOS (65.6), PVC (31.1)
5G1 (double)	nonactin/monactin (75:25) (0.7) 10.0 mmol kg^{-1}, NaTFPB (0.4) 5.0 mmol kg^{-1}, ETH 500 (1.1) 9.9 mmol kg^{-1}, DOS (32.7), Tecoflex (65.1)
5G2 (double)	immobilized *N*-butyldiethanolamine (1.0) 62.3 mmol kg^{-1}, nonactin/monactin (75:25) (0.7) 10.1 mmol kg^{-1}, NaTFPB (0.4) 5.1 mmol kg^{-1}, ETH 500 (1.2) 10.1 mmol kg^{-1}, DOS (34.5), Tecoflex (62.2)
5H1 (double)	nonactin/monactin (75:25) (0.7) 10.0 mmol kg^{-1}, NaTFPB (0.4) 5.0 mmol kg^{-1}, ETH 500 (1.1) 9.9 mmol kg^{-1}, DOS (32.7), Tecoflex (65.1)
5H2 (double)	immobilized bis-2,6-hydroxymethyl pyridine (0.1) 9.9 mmol kg^{-1}, nonactin/monactin (75:25) (0.7) 9.7 mmol kg^{-1}, NaTFPB (0.4) 5.0 mmol kg^{-1}, ETH 500 (1.1) 9.8 mmol kg^{-1}, DOS (33.6), Tecoflex (64.1)

6A ($N(CH_3)_4^+$)	NaTFPB (0.88) 9.9 mmol kg^{-1}, Tecoflex (99.12)
6B (Ca^{2+})	ETH 5234 (2.0) 24.8 mmol kg^{-1}, NaTFPB (1.0) 11.4 mmol kg^{-1}, Tecoflex (97.0); The thickness of this membrane was 70 µm.
6C (NH_4^+)	nonactin/monactin (75:25) (0.15) 2.0 mmol kg^{-1}, NaTFPB (0.09) 1.0 mmol kg^{-1}, Tecoflex (99.76)
6D (H^+)	ETH 2439 (0.14) 2.0 mmol kg^{-1}, NaTFPB (0.09) 1.0 mmol kg^{-1}, Tecoflex (99.77)
6E (Ca^{2+})	ETH 5234 (0.17) 2.1 mmol kg^{-1}, NaTFPB (0.06) 0.7 mmol kg^{-1}, Tecoflex (99.77)
6F (Ca^{2+})	ETH 5234 (2.0) 25.0 mmol kg^{-1}, NaTFPB (1.0) 11.2 mmol kg^{-1}, Tecoflex (97.0); The thickness of this membranes were 40, 75, or 100 µm.

Inner Fillings and Conditioning Solutions Used in Chapter 6. ISEs based on Tecoflex membranes (6A ($N(CH_3)_4^+$) - 6E (Ca^{2+})) with a classical response behavior were conditioned in a solution which had the same composition as the inner filling. The following internal solutions were used: $5 \cdot 10^{-3}$ M $N(CH_3)_4Cl$ for ISEs made from membrane (6A ($N(CH_3)_4^+$)); 10^{-3} M NH_4Cl (6C (NH_4^+)); 0.1 M citric acid, 10^{-3} M NaCl and 0.25 M NaOH adjusted to pH 5.8 (6D (H^+)); 10^{-3} M $CaCl_2$ (6E (Ca^{2+})).

The following inner fillings were used for ISEs made from membrane 6F (Ca^{2+}) with a super-Nernstian response behavior: 0.05 M Na_2EDTA, 10^{-3} M $CaCl_2$,, 0.06 M NaOH (pH 8.9), calculated ion activity $a_{Ca}{}^{2+} = 2.3 \times 10^{-12}$ M; 5 mM Na_2EDTA, 1 mM $CaCl_2$, 5 mM NaOH (pH 8.9), calculated $a_{Ca}{}^{2+} = 2.4 \times 10^{-11}$ M; 5 mM Na_2EDTA, 1 mM $CaCl_2$, 1.4 mM NaOH (pH 6.0), calculated $a_{Ca}{}^{2+} = 9.0 \times 10^{-8}$ M. For all these ISEs, the conditioning solution was either 10^{-3} M $CaCl_2$ or had the same composition as the inner filling. The conditioning time amounted to 1 – 3 d. A diaphragm separated the internal filling solutions containing EDTA from the reference half cell (Ag/AgCl in 0.1 M KCl) during the measurements.

7.4 Potentiometric Measurements

pH Buffered Solutions. The following solutions were used for the pH response measurements: A sample solution containing 10^{-4} M $MgCl_2$ and HCl was titrated with a solution of 10^{-4} M $Mg(OH)_2$ for the measurements with membrane type 4A (H^+) and 4B (H^+); sample solution 0.01 M Tris, titrated with 0.1 M HCl and 0.01 M Tris (4C (H^+), 4L (H^+), 4N (H^+), 4S (H^+)); sample solution 0.01 M HCl, 0.01 M NaCl, and 3 x 10^{-3} M Tris, titrated with 0.01 M NaOH and 3 x 10^{-3} M Tris (4C (H^+), 4D (H^+), 4F (H^+), 4L (H^+), 4M (H^+), 4N (H^+)); sample solution 0.01 M NaOH and 0.01 M Tris, titrated with 0.1 M HCl, 0.01 M NaCl, and 0.01 M Tris (4E (H^+), 4F (H^+), 4G (H^+), 4J (H^+), 4L (H^+), 6D (H^+)); sample solution 5 x 10^{-4} M NaOH and 5 x 10^{-4} M Tris, titrated with 0.1 M HCl, 5 x 10^{-4} M NaCl, and 5 x 10^{-4} M Tris (4H (H^+), 4I (H^+), 4J (H^+), 4K (H^+)); sample solution H_2SO_4, 5 x 10^{-3} M K_2SO_4, and 3 x 10^{-3} M Tris, titrated with 0.01 M KOH and 3 x 10^{-3} M Tris (4S (H^+)); sample solution H_2SO_4, 0.05 M K_2SO_4, and 0.03 M Tris adjusted to pH 8.1, diluted with H_2SO_4 and 0.03 M Tris at constant pH 8.1 (4T (H^+), 4U (H^+), 4V (H^+)); sample solution H_3PO_4 and 10^{-3} M K_2SO_4 adjusted to pH 2.9, titrated with 2 x 10^{-3} M KOH (4T (H^+), 4U (H^+), 4V (H^+)); sample solution H_2SO_4 and K_2SO_4 adjusted to pH 4.0 ,diluted with H_2SO_4 at constant pH 4.0 (4W (double)); inner solution 10^{-4} M NH_4Cl and HCl adjusted to pH 1.4, diluted with 10^{-4} M NH_4Cl (4X (double)).

Potentiometry. Measuring solutions were prepared by successive automatic dilution of stock solutions with a Liquino 711 and two Dosino 700 instruments (Metrohm AG, CH-9010 Herisau) equipped with 50 mL burettes. These experiments were performed under full computer control in a single 50 mL or 200 mL polyethylene beaker, where all ISEs were centered in the middle. Potentials were measured with a 16-channel electrode monitor EMF16 (Lawson Labs Inc., Malvern, PA 19355) at room temperature (20-21˚C) in stirred solutions during 10 - 60 min after sample changes. Reference electrodes (either double-junction free-flowing calomel or Metrohm Ag/AgCl type 6.0729.100) had 1 M KCl or 1 M LiOAc as bridge electrolyte. For activity coefficients, the Debye-Hückel approximation was used.[7] All EMF values, which were median of the potentials measured during 5 min, were corrected for the liquid-junction potential at the sample/bridge electrolyte interface using the Henderson equation.[8-10] Selectivity coefficients were determined by the separate solution method (SSM) or the fixed interference method (FIM).[11]

pH Titrations. The pH of the sample was continuously monitored with a pH glass electrode (Metrohm) against the same reference electrode as the solvent polymeric membrane electrodes. Hence, the liquid-junction potential was not corrected for these measurements. The titration solution was automatically added to the sample using a Dosimat 665 (Metrohm) and a custom made control software. The time of a continuous titration amounted to 5 h.

Measuring Cell. The calibrations with the double membranes were done using the measuring circuit and the symmetric cell described in Chapter 4.6.[12] The symmetric cell contained two identical half-cells based on Teflon and with a volume of 20 mL. The area of the double membrane in contact with the solution amounted to 20 mm^2.

7.5 CHEMFETs

Preparation of CHEMFETs. pH-ISFETs based on Al_2O_3 were obtained from our Institute of Microtechnology (IMT) in Neuchâtel.[13] All ISFETs displayed appropriate pH response using standard buffers (e.g., 48 – 57 mV dec^{-1}) were used in the subsequent studies. The deposition of the ion-sensitive polymer layer was made by solvent casting. 25 µL of a solution of the membrane (200 mg of the components, as shown in Table 7.1, dissolved in 2 mL of THF or 1,2-dichloroethane) were deposited by hand onto the gate oxide of each ISFET. The solvent was allowed to evaporate for 24 h before conditioning. The thickness of the deposited membrane on the ISFET was estimated with an optical light microscope and amounted to 50 µm.

For the deposition of the double membrane onto an ISFET, 2 µL of a solution of the inner membrane (200 mg of the components dissolved in 2 mL THF) was cast first onto the gate oxide resulting in a membrane with a diameter of 2 mm. The solvent was allowed to evaporate for 12 h. Secondly, a disk of the outer membrane with a diameter of 6 mm was glued with THF onto the CHEMFET covered with the inner membrane. The thickness of the double membrane on the ISFET amounted to about 100 µm.

In order to study the adhesion of the membranes, 100 mg of the polymeric membrane components (see Table 7.1) were dissolved in 1 mL THF. 5 µL of this membrane solution was cast onto each glass substrate or ISFET. Each series included

ten samples. Before conditioning the samples into 10^{-3} M NH_4Cl for four weeks, the solvent was allowed to evaporate for 24 h.

Conditioning Solutions. All CHEMFETs used for the NH_4^+-calibration curves were conditioned in 10^{-3} M NH_4Cl (membrane types: 4P (NH_4^+), 4O (NH_4^+), 5A (NH_4^+), 4Q (NH_4^+), and 5G (double)). The K^+-selective CHEMFETs were conditioned in 10^{-3} M KCl. H^+-selective CHEMFETs (membrane type 5D (H^+)) used to determine the pH measuring range were conditioned in H_2SO_4 at pH 5.0.

For the studies of the interference of carbon dioxide and organic acids on the response signal (Chapter 5.3 - 5.5), the NH_4^+-selective CHEMFETs were conditioned in a solution which had the same composition as the conditioning solution of the CHEMFETs containing an H^+-selective ionophore. Conditioning solution of the CHEMFETs described in Chapter 5.3 (membrane types 5D (H^+) and 5E (NH_4^+)): H_2SO_4 (pH 4.5), 76 mM NaCl, and 1 mM NH_4Cl. Conditioning solution of the CHEMFETs described in Chapter 5.4 (membrane types 5E (NH_4^+) and 5F (H^+)): H_2SO_4 (pH 4.5) and 1 mM K_2SO_4. Conditioning solutions of the CHEMFETs described in Chapter 5.5: Membrane types 5B (NH_4^+) and 5G (double), H_2SO_4 (pH 5.0) and 1 mM NH_4Cl; Membrane types 5B (NH_4^+) and 5H (double), H_2SO_4 (pH 3.5) and 1 mM NH_4Cl. The conditioning time for all CHEMFETs was at least 12 h.

CHEMFET Measuring Circuit. Measurements were made in a constant drain-current mode (I_D = 100 μA). The drain-source voltage was maintained constant (V_{DS} = 0.5 V). This was achieved with a custom-made ISFET amplifier. Four ISFETs were simultaneously monitored, and the measured data were collected using a personal computer with a program written in LabVIEW (National Instruments, Austin, Texas). All measurements were made in conjunction with a separate double junction reference electrode (Metrohm) in which the outer chamber was filled with 1 M LiOAc. The potential values of the calibration curves were corrected using the Henderson equation, as described in Chapter 7.4.

Addition of Interferents into the Sample Solution. Prior to testing the response to carbon dioxide, benzoic acid, and acetic acid, the integrity of the polymer membranes cast onto the gate region was evaluated. Firstly, each CHEMFET was evaluated to the response to ammonium ions. This was carried out at concentrations of 0.1 and 1 mM NH_4^+ at constant pH 3.0 (H_2SO_4). Secondly, the response to pH changes was tested at appreciate pH. No significant response towards H^+ indicated that the polymeric membrane was intact, i.e. there was no leaks or pinholes enables

hydrogen ions in the sample solution to approach the pH-sensitive gate or inner membrane. For the evaluation of the measuring range of the H^+-selective CHEMFETs based on membrane type 5D (H^+), the sample solution (0.01 M Tris) was titrated with a 0.1 M HCl solution containing 0.01 M Tris.

In order to study the response towards acidic interferents, four CHEMFETs were set into the measuring solution. For comparison, two CHEMFETs containing an H^+-selective ionophore were simultaneously measured with two CHEMFETs based on a simple NH_4^+-selective membrane containing only one ionophore (nonactin). After 3-5 min, when the output signal was stable, the sample solution was purged with CO_2 using an aeration tube. Removal of the carbon dioxide was accomplished by purging with nitrogen. To test the influence of organic acids and $NaHCO_3$ on the response signal, benzoic acid (stock solution: 0.06 M sodium benzoate and 0.05 M citric acid (pH 4.5)), acetic acid (stock solution: 1 M sodium acetate and H_2SO_4 (pH 4.5)), or carbonic acid (1 M $NaHCO_3$) were added to the buffered sample solution. In all experiments, the pH of the sample solution was monitored separately using a convential glass pH electrode.

The following measuring solutions were used in order to test the response towards the acidic interferents. Measuring solution of the CHEMFETs described in Chapter 5.3 (membrane types 5D (H^+) and 5E (NH_4^+)): 50 mM citric acid (pH 4.5), 76 mM NaOH, and 1 mM NH_4Cl. Measuring solution of the CHEMFETs described in Chapter 5.4 (membrane types 5E (NH_4^+) and 5F (H^+)): For carbon dioxide, 0.05 M NH_4Cl; For benzoate, 100 mM citric acid (pH 4.5), 167 mM NaOH, and 1 mM NH_4Cl. Measuring solution of the CHEMFETs described in Chapter 5.5 (membrane types 5B (NH_4^+), 5G (double), and 5H (double)): For carbon dioxide, 0.05 M NH_4Cl; For benzoate, 100 mM citric acid (pH 4.5), 167 mM NaOH, and 1 mM NH_4Cl. All equipment was placed in a dark and grounded metal box in order to eliminate any effects from static electricity and photosensitivity of the CHEMFETs.

7.6 Surface Immobilization

Immobilization of MAD. ISEs with membrane type 6A ($N(CH_3)_4^+$) or solid substrates covered with pure Tecoflex were washed in ethanol and dried for 1 h at room temperature under high vacuum (10^{-2} mbar). Then 25 µL of a MAD solution

(0.027 mM, 0.27 mM, or 2.7 mM in ethanol) were deposited on each membrane. The samples were dried under a vacuum of 20 mbar for 1 h at room temperature. For photobinding, the samples were irradiated for 20 min using a Stragene UV Stratalinker 350 nm light source with an irradiance of 0.95 mW cm^{-2} and washed in hexane and in ethanol.[4, 14] Photolyses were done at ambient temperature (20 - 25 ^{o}C).

Immobilization of MAD-biotin. ISEs with membrane type 6F (Ca^{2+}) were washed in deionized water and dried under vacuum (20 mbar) for 1 h at room temperature. Then 40 µL of a MAD-biotin solution (0.28 mM in acetonitrile) were deposited on each membrane. The samples were dried for 1 h under a vacuum of 20 mbar at room temperature. For photobinding, the ISEs were irradiated for 20 min using a Stragene UV Stratalinker 350 nm light source with an irradiance of 0.95 mW cm^{-2} and washed in acetonitrile. Photolyses were done at ambient temperature (20 - 25 ^{o}C).

Immobilization of Streptavidin. The conditioned ISEs were set, before the streptavidin incubation, into a solution of 0.02 % Tween (w/w) 20 for 20 min. A 0.1 M MES buffer of pH 6.1 (with NaOH) was used for the streptavidin binding experiments. The concentration of streptavidin in the MES buffer was 42 µg mL^{-1} (0.7 µM), and binding of this solution to the surface was allowed to proceed for 1 h. The samples were rinsed with buffer in order to remove unbound streptavidin, set back into the conditioning solution for 1 h, and followed immediately by potentiometric measurement.

7.7 Methods of Surface Analysis

Sample Preparation. Glass microscope slides covered with an Au layer were used as substrate for the AFM, FT-IRAS, and XPS-measurements. These substrates were prepared according to a standard procedure for self-assembled monolayers.[15] Solution aliquots of pure Tecoflex were cast onto the gold substrate resulting in a membrane of 200 µm thickness. For AFM and XPS experiments, gold substrates with a size of (1.0 x 1.0 cm^2) were used, and the size of the substrate for FT-IRAS was 2.5 x 2.5 cm^2. 50 µL of a 2.7 mM MAD solution were cast onto the small membrane (AFM and XPS), whereas 300 µL 2.7 mM MAD were cast onto the big membrane (FT-IRAS). The immobilization processes of MAD are described in Chapter 7.5.

Atomic Force Microscopy (AFM). An Autoprob CP from Park Scientific Instruments was used to image a pure Tecoflex membrane. The images were collected in intermittent-contact mode, in room atmosphere, and at ambient temperature. Commercially available silicon cantilevers with high aspect ratio tips were used.

X-ray Photoelectron Spectroscopy (XPS). The surface of dry membrane films was analyzed *via* XPS under an ultra high vacuum of 10^{-9} mbar. Spectra were collected with a Perkin-Elmer 5700 spectrometer (Perkin Elmer, Norwak, CT) using an Al K_α X-ray source ($h\nu$ = 1486.7 eV) with an emission power of 350 W to stimulate photoelectron emission. A spherical analyzer with an investigation area of 0.80 mm^2 was used, and the hydrocarbon C1s peak was referenced at 285 eV. Samples were analyzed at 45° take-off angle, which is the angle between the surface normal and the analyzer lens axes. An average of three measurements was obtained. Data were collected and stored on a Perkin-Elmer computer, which also controlled the spectrometer. Software provided with the instrument was used to interpret the data.[16]

Fourier Transformation Infrared Reflection Absorption Spectroscopy (FT-IRAS). IR spectra were recorded on a Bruker IFS 66 v spectrometer equipped with a Hg-Cd-Te detector. The measurements were performed at an incidence angle of 80° with a fixed angle set. To minimize atmospheric bands of water and carbon dioxide, the pressure in the sample chamber was reduced to 100 Pa. A gold surface was used as reference.

Radiochemistry. Glass slides (0.8 x 0.8 cm^2) were covered with a membrane of type 6B (Ca^{2+}). The samples were washed in acetonitrile and dried under vacuum (10^{-2} mbar) for 1 h at room temperature. Samples of series A and B: deposition of 25 µL of a MAD-biotin solution (2.3 mM in acetonitrile (ACN)), drying for 10 min under high vacuum of 0.05 mbar at room temperature, UV-irradiation, washing in ACN. Samples of series C: deposition of 25 µL MAD-biotin (2.3 mM in ACN), drying for 20 min under 0.05 mbar at r.t., UV-irradiation, washing in ACN. Samples of series D, E and F: deposition of 25 µL MAD-biotin (2.3 mM in ACN), drying for 80 min under 0.05 mbar at r.t., UV-irradiation, washing in ACN. Samples of series H: deposition of a pure ACN drop, drying for 80 min under 0.05 mbar at r.t., UV-irradiation, washing in ACN. Samples of series G and I: only washing in ACN. All photobinding experiments were carried out employing a high pressure mercury lamp (Osram HBO 350 W) mounted in a SUSS LH 1000 lamp house equipped with a shutter to control exposure times. The samples were irradiated for 200 s with an

irradiance of 1.14 W cm^{-2} at 365 nm and washed in acetonitrile. Photolyses were done at ambient temperature (20 - 25 ^{o}C). Besides, some blank samples had no treatment at all.

After the photoimmobilization, most of the glass-slides with the membrane were conditioned in water for 2 d. A 0.1 M MES buffer of pH 6.1 (with NaOH) was used for the streptavidin-binding. The protein concentrations in the MES buffer were 21 µg mL^{-1} (0.35 µM) streptavidin (not radiolabeled) and 3.1 ng mL^{-1} (52 pM) [^{35}S]-streptavidin with an activity of 15.4 x 10^3 Bq mL^{-1}. After rinsing with water in order to remove unbound streptavidin, the samples were set back into the conditioning solution for 1 h, and dried at room temperature for 15 h. As shown in Table 6.2, some sample series were set before or after the streptavidin incubation into a solution of 0.02 % Tween (w/w) 20 for 20 min. Autoradiography of the dried glass slides with the membranes was done with storage screens from Molecular Dynamics (Sunnyvale, CA), which were exposed for 12 h. For quantification, a PhosphorImager from Molecular Dynamics and an external one-point calibration (n = 5) with [^{35}S]-streptavidin was used. All work with radioactivity was performed in a C-type laboratory.

References

(1) Bakker, E.; Lerchi, M.; Rosatzin, T.; Rusterholz, B.; Simon, W. Synthesis and Characterization of Neutral Hydrogen Ion-Selective Chromoionophores for Use in Bulk Optodes. *Anal. Chim. Acta* **1993,** *278*, 211-225.

(2) Schöning-Hammer, A., Personal Communication, Zurich, 1998.

(3) Püntener, M., Doctoral Dissertation in Preparation, ETH, Zurich.

(4) Collioud, A.; Clémence, J. F.; Sänger, M.; Sigrist, H. Oriented and Covalent Immobilization of Target Molecules to Solid Supports: Synthesis and Application of a Light-Activatable and Thiol-Reactive Cross-Linking Reagent. *Bioconjugate Chem.* **1993,** *4*, 528-536.

(5) Ikura, M.; Kunio, H. Application of Two-Dimensional NMR Spectroscopy to the Complete Analysis of the 1H and 13C NMR Spectra of d-Biotin in Aqueous Solution. *Org. Magn. Reson.* **1982,** *20*, 266-273.

(6) Jenny, H. B. Entwicklung von Elektroden und Messsystemen für die direktpotentiometrische Bestimmung von Natrium- und Kalium-Konzentrationen in Urin, Doctoral Dissertation No. 7411, ETH, Zurich, 1983.

(7) Meier, P. C. Two-Parameter Debye-Hückel Approximation for the Evaluation of Mean Activity Coefficients of 109 Electrolytes. *Anal. Chim. Acta* **1982,** *136*, 363-368.

(8) Hamman, C.; Vielstich, W. *Elektrochemie*; Wiley-VCH: Weinheim, 1998.

(9) Morf, W. E. *The Principles of Ion-Selective Electrodes and of Membrane Transport*; Elsevier Science: New York, 1981.

(10) Marcus, Y. *Ion Properties*; Marcel Dekker: New York, 1997.

(11) Bakker, E.; Pretsch, E.; Bühlmann, P. Selectivity of Potentiometric Ion Sensors. *Anal. Chem.* **2000,** *72*, 1127 -1133.

(12) Haase, E. A. Untersuchung der Wechselwirkungen zwischen ionenselektiven Flüssigmembranen und Messgut im Hinblick auf die kontinuierliche Erfassung von Kationen im Vollblut, Doctoral Dissertation No. 10453, ETH, Zurich, 1993.

(13) Smith, R. L.; Scott, D. C. An Integrated Sensor for Electrochemical Measurements. *IEEE Trans. Biomed. Eng., BME-33* **1986**, 83.

(14) Leonard, D.; Chevolot, Y.; Bucher, O.; Sigrist, H.; Mathieu, H. J. ToF-SIMS and XPS Study of Photoactivatable Reagents Designed for Surface Glycoengineering - Part I. N-(m-(3-(trifluoromethyl)diazirine-3-yl)phenyl)-4-maleimido-butyramide (MAD) on Silicon, Silicon Nitride and Diamond. *Surf. Interface Anal.* **1998,** *26*, 783-792.

(15) Fibbioli, M. New Types of Ion-Selective Electrodes: Hydrophilic Anions and Solid-Contacted Membranes, Doctoral Dissertation No. 13789, ETH, Zurich, 2000.

(16) Moulder, J. F.; Stickle, W. F.; Sobol, P. E.; Bomben, K. D. *Handbook of X-Ray Photoelectron Spectroscopy*; Perkin-Elmer Corporation: Minnesota, USA, 1982.

Glossary

a'_{i}	activity of the primary ion in the sample solution [mol L^{-1}]
a''_{H}	hydrogen ion activity in the inner solution [mol L^{-1}]
a''_{i}	activity of the primary ion in the inner solution [mol L^{-1}]
ACN	acetonitrile
AFM	atomic force microscopy
C	unprotonated covalently bound H^+-selective ionophore
c'_{aq}	initial concentration of CO_2 in the sample solution [mol L^{-1}]
c''_{aq}	concentration of CO_2 in the water film between membrane and gate [mol L^{-1}]
$\Delta c'_{aq}$	change of the CO_2 concentration in the sample solution [mol L^{-1}]
CH^+	protonated covalently bound H^+-selective ionophore
CHEMFET	chemically modified field-effect transistor
$c_{\mathrm{i,T}}$	total concentration of the free ion I^{z_i} and of all its positively charged complexes [mol L^{-1}]
c_{L}	concentration of the free ionophore L in the membrane [mol L^{-1}]
CWE	coated-wire electrode
d	thickness of the membrane [m]
D	diffusion coefficient [cm^2 s^{-1}]
DOS	bis(2-ethylhexyl) sebacate
E	electromotive force [mV]
E^0	reference potential summarizing all potential contributions in addition to the membrane potential E_M [mV]
E_{I}^0	sum of all constant potential contributions of the ISE measuring cell [mV]

EDTA	ethylenediaminetetraacetic acid
E_i^0	standard reference potential of the measuring cell for the primary ion [mV]
$E_{J(inner-solution)}$	liquid-junction potential of the reference electrode in the inner solution [mV]
$E_{J(sample)}$	liquid-junction potential of the reference electrode in the sample [mV]
E_M	membrane potential [mV]
EMF	electromotive force [mV]
$E_{reference}$	potential of the reference electrode [mV]
ETH 500	tetradodecylammonium tetrakis-(4-chlorophenyl)borate
ETH 2439	4-{[9-(dimethylamino)-5*H*-benzo[a]phenoxin-5-ylidene]amino}phenyl-acetic acid 11-[(1-butylpentyl)oxy]-11-oxoundecyl ester
ETH 5234	*N*,*N*-dicyclohexyl-*N'*,*N'*-dioctadecyl-3-oxapentanediamide
F	Faraday constant (96487 C mol^{-1})
FIM	fixed interference method
FT-IRAS	Fourier transformation infrared reflection absorption spectroscopy
i	primary ion
I^+	primary ion
I_D	drain current [A]
IR	infrared spectroscopy
ISE	ion-selective electrode
ISFET	ion-selective field-effect transistor
J^+	interfering ion
K_{Hj}^{pot}	selectivity coefficient of the inner membrane
$\overline{K}_{Hj}^{pot}$	selectivity coefficient of the pH electrode
K_i	overall partition coefficient of the indicated ion I^{zi}

K_{ij}^{pot}	Nicolskii selectivity coefficient for the interfering ion relative to the primary ion
KTPB	potassium tetraphenylborate (KTPB)
L	ionophore
MAD	*N*-{3-[3-(trifluoromethyl)diazirine-3-yl]phenyl}-4-maleimido-butyramide
MES	3-(*N*-morpholino)ethanesulfonic acid
MISFET	metal-insulator-semiconductor transistor
mp	melting point [degree Celsius]
MS	mass spectroscopy
n	stoichiometric factor of the complex formed or number of samples/sensors
NaTFPB	sodium tetrakis[3,5-bis(trifluoromethyl)phenyl]borate
NMR	nuclear magnetic resonance
o-NPOE	2-nitrophenyl octyl ether
PHB	poly[3-(R)-hydroxybutyric acid] diol
p*K*a	acid dissociation constant
p-Si	p-type semiconductor
PTHF	poly(tetrahydrofurane) diol
PVC	poly(vinyl chloride)
R	molar gas constant (8.314 J K^{-1} mol^{-1})
R^-	lipophilic anionic site
R_T	total concentration of anionic sites [mol L^{-1}]
SSM	separate solution method
STDEV	standard deviation
T	absolute temperature [K]
t	time [s]

TBAF	tetrabutylammonium fluoride
THF	tetrahydrofuran
TMDI	2,2,4-trimethylhexamethylene diisocyanate
Tris	tris(hydroxymethyl)aminomethane
Tween 20	polyoxyethylenesorbitan monolaurate
ΔV	voltage drop: parallel shift of the I_{DS} - V_{GS} curve [mV]
V_D	drain voltage [mV]
V_G	gate voltage [mV]
V_{GS}	gate-source voltage [mV]
V_{SS}	potential contributions originating from the solid-state part of the CHEMFET [mV]
V_T	threshold voltage [mV]
x	space coordinate measured perpendicular to the section [m]
X^-	counterion
XPS	X-ray photoelectron spectroscopy
zi	charge of the ion i
z_m	charge of the ion in the membrane
$\beta_{iL,n}$	stability constant of a given 1:n complex IL_n^{zi}
$\gamma_{i(x)}$	activity coefficient of the uncomplexed ion I^{zi} in the membrane
δ_{aq}	thickness of the aqueous boundary layer between sample and membrane [m]
ϕ	boundary electric potential [mV]
Ψ	function of the boundary electric potential ϕ
Ψ_0	potential difference between the insulator and the thin water film [mV]
′	membrane/sample phase boundary
″	membrane/inner solution phase boundary

Acknowledgements

I would like to express my gratitude to Prof. Nico F. de Rooij from the Institute of Microtechnology (IMT) in Neuchâtel for the opportunity to conduct my PhD thesis in his group. He supervised my dissertation and provided a well equipped work place. I acknowledge with thanks PD Dr. Werner E. Morf for his ideas, helpful comments, and valuable guidance of my thesis. Dr. Peter van der Wal was an outstanding advisor. I have appreciated his beneficial hints and enormous helpfulness. He imparted some of his scientific knowledge, instinct, and enthusiasm to me. I owe thanks to Sylviane Pochon for the encapsulation of the ISFETs. I also thank Prof. M. Koudelka-Hep for kindly agreeing to be co-examiner of my thesis. Furthermore, I want to acknowledge the good working atmosphere provided by all my colleagues at the IMT.

I am most thankful to Prof. Ernö Pretsch from the Laboratory of Organic Chemistry of the ETH Zurich for his continuous support throughout the whole work and that he agreed to act as co-examiner of this thesis. I gratefully acknowledge Angela Schöning-Hammer for introducing me to polyurethane membranes and for her helpful advice. She provided me with the "self-plasticizing" polyurethanes and the immobilized ionophore. I greatly appreciate all the trouble André Müller took on my behalf for the organic syntheses, and his help with the problems encountered in the everyday life of a chemical laboratory. Martin Püntener was also a great help with his synthesis of the covalently bound ionophore and during my own syntheses. Thanks are due to Andrea Rainelli for his valuable assistance while he carried out his diploma thesis research with me. I acknowledge the excellent support of the radiochemistry team of Dr. Martin Badertscher and Klaus Girgenrath. I would like to thank Dr. Markus Schildenberger for the AFM measurements and Prof. A. Rossi-Elsener for the XPS measurements.

Finally, I would like to express my gratitude to Dr. Hans Sigrist from the Swiss Center for Electronics and Microtechnology (CSEM) in Neuchâtel. He gave me very valuable suggestions in the biochemistry part of my work, provided me with the photo-cross-linker compound MAD, and agreed to be co-examiner.

This doctoral dissertation was financially supported by the Swiss National Science Foundation under project numbers 2000-059390 and 2100-051001.

Biography

Patrick Reichmuth was born on July 7, 1971, in Lucerne, Switzerland. In 1991, he received his university entrance qualification (Maturity type C – mathematics and science) at the cantonal grammar school of Reussbühl near Lucerne. He earned his diploma in environmental science with specialization in chemistry at the Swiss Federal Institute of Technology in Zurich (ETHZ) in October 1997. His master thesis dealt with the development of a solid-phase extraction method coupled with liquid chromatography. From October 1995 – February 1996 he held an industrial internship at F. Hoffmann – La Roche AG in Basle. He was research chemist at the Swiss Federal Institute of Environmental Science and Technology from November 1997 to February 1998. In March 1998, he started his PhD work at the Institute of Microtechnology (IMT) at the University of Neuchâtel in Switzerland in the field of ionophore-based chemical sensors. This dissertation was carried out in collaboration with the Laboratory of Organic Chemistry of the ETHZ, where he performed the first part of his thesis from March 1998 to August 2000. Simultaneously with his PhD research activities, he was teaching assistant at the Chemistry Department of the ETHZ. The second part of his dissertation was carried out at the IMT in Neuchâtel from September 2000 to July 2001. He may contacted at his e-mail address, patrick.reichmuth@alumni.ethz.ch, which will be valid for the remainder of his life.